H_2O

H_2O

CO_2
H_2O

O_3

O_3

H_2O

CO_2

CO_2

2007

Annual Report
Jahresbericht

Remote Sensing
Technology Institute

Department
Atmospheric Processors

DLR

Contents

1. Foreword

The 7th edition of the annual report for the past year 2007 presents results from scientific research and development work which has been accomplished by the Department *Atmospheric Processors* (IMF-AP) at DLR's Remote Sensing Technology Institute (IMF).

Contrary to the previous reports 2000-2006, for the first time we are now presenting a completely English edition. Owing to our international collaborations with ESA, EUMETSAT and industrial and academic partners, the English version may address a much wider readership.

After the successful launch of MetOp in October 2006, a considerable part of our work dealt with the GOME-2 processor in EUMETSAT's distributed ground segment for MetOp. Beginning of March 2007 EUMETSAT started the regular delivery of GOME-2 level 1 products via EUMETCast. Only two weeks later IMF and DFD were able to commence with the operations test-phase for the complete UPAS processing chain under the control of DIMS. Important GOME-2 goals reached during 2007 were: The dissemination of demonstrational GOME-2 near-real-time total ozone and NO_2 products by end of March 2007, and in October 2007 EUMETSAT's announcement that the status of these products is pre-operational.

For SCIAMACHY on ENVISAT, another of our 'in-orbit workhorses', the previous year was important in several aspects. Firstly, ESA installed the *SCIAMACHY Quality Working Group (SQWG)*, a consortium of the leading European SCIAMACHY institutions. The goal of the *SQWG* for the coming years is to intensify and to condense all activities around the evolution of the operational processing of SCIAMACHY data within one single entity of experts. This entity is responsible for the evolution and improvement of the operational data processing chain from instrument to product level including the delivery of new advanced SCIAMACHY products. Secondly, in March 2007 the first part of the ENVISAT mission extension – lasting until 2010 – started with the platform and the SCIAMACHY instrument still being in very good condition. Meanwhile ESA has developed ideas how to extend ENVISAT operations even further until the year 2013/2014 timeframe. Via the *SCIAMACHY Operations Support Team (SOST)* we are involved in the studies required to prepare SCIAMACHY instrument operations for this period. In 2008 it is expected to finish these investigations and to establish an instrument configuration well suited for successful operations and measurements in the entire extended in-orbit lifetime.

The editorial team wishes to thank all authors and co-authors for their contributions.

Prof. Dr. Thomas Trautmann   Dr. Manfred Gottwald

2. Highlights of the Year 2007 – The First Year of O3M-SAF Operations

D. Loyola, P. Valks, W. Zimmer, S. Kiemle (DFD-IT), N. Hao, S. Emmadi, T. Ruppert (DFD-MM), K.-H. Seitz (DFD-BI)

The *Satellite Application Facility on Ozone and Atmospheric Chemistry Monitoring (O3M-SAF)* is a key component of EUMETSAT's Polar System (EPS) ground segment. The EPS mission comprises three MetOp satellites that will supply operational products during the next 14 years. The commissioning phase of the GOME-2 sensor was started after the MetOp launch in October 2006. Beginning of March 2007 EUMETSAT initiated the regular delivery of GOME-2 level 1 products via EUMETCast. Only two weeks later DLR was able to start the operations test-phase after finishing the initial checks of the retrieval algorithms, the GOME-2 reading interfaces in the UPAS system, and the complete processing chain controlled by DIMS. By end of March 2007 DLR started the dissemination of demonstrational GOME-2 near-real-time total ozone and NO_2 products via *EUMETCast* and in October 2007 these products were declared pre-operational shortly after the validation teams from the University of Thessaloniki (AUTH) and the Belgian Institute for Space Aeronomy (BIRA) in Brussels confirmed the high quality reached by the total ozone and NO_2 products.

The level 2 near-real-time products are processed and delivered to the users in less than 15 min, that means that products are available 2:30 minutes after sensing (2:15 minutes are needed for the delivery of level 1) outperforming the EPS requirements of 3 hours. DLR was able to surpass the expectations on GOME-2 and the O3M-SAF, and at the same time we reinforced the DLR role as key player in atmospheric remote sensing providing accurate and unique products for the future GMES atmospheric service.

GOME-2 on MetOp
The main improvements for GOME-2 compared with GOME are the enhanced spatial coverage, the smaller ground pixel size, and more extensive polarization measurements in two perpendicular planes with better spectral resolution. The GOME-2 field of view may be varied in size from 5 km × 40 km to 80 km × 40 km (default) for a readout time of 0.1875 sec. The mode with the largest footprint (i.e. 24 forward steps with a total coverage of 1920 km × 40 km) provides almost daily global coverage at the equator.

O3M-SAF Ground Segment
A schematic representation of the O3M-SAF ground segment at DLR is given in fig. 2-1. An ensemble of two *EUMETCast* terminals (top right) receives the GOME-2 level 1 PDU products which are available 2:15 hours after sensing. The arrival of a new PDU triggers the DIMS controlled near-real-time and off-line processing.

The UPAS high availability cluster (top left) processes the PDU and generates total column products in HDF5 and BUFR in less than 10 minutes. The NRT level 2 products are transmitted to Usingen, the European uplink site for *EUMETCast*. Finally the GOME-2 level 2 products are broadcast to the users using a commercial satellite. The NRT products are additionally distributed via FTP to selected users. The GOME-2 total ozone and NO_2 near-real-time products are available at the user's desk in less than 2:30 hours after sensing.

The GOME-2 level 1 PDUs are bundled into consolidated orbits used for the off-line processing. These orbit products are archived in the product library after the operator runs the QA processing. The GOME-2 off-line products are disseminated to the users via FTP and will be accessible via DLR's EOWEB. Metadata are transmitted to UMARF using the SAF-Client from EUMETSAT.

Trace Gases Retrieval
The GOME Data Processor (GDP) is the baseline algorithm for the operational trace gas column retrievals from GOME-2 *(Spurr et al. 2005, Van Roozendael et al., 2006)*. The GDP 4.2 *(Van Roozendael et al., 2006)* uses the Differential Optical Absorption Spectroscopy (DOAS) technique for the generation of total column amounts of ozone, NO_2, BrO, SO_2, H_2O, HCHO, and OClO.

This algorithm has two major steps: a DOAS least-squares fitting for the trace gas slant column, followed by the computation of a suitable Air Mass Factor (AMF) to convert the slant column into a vertical column density (VCD). GOME cloud information, namely fractional cover, cloud-top height and cloud albedo, is derived directly with the OCRA and ROCINN algorithms *(Loyola et al. 2007)*.
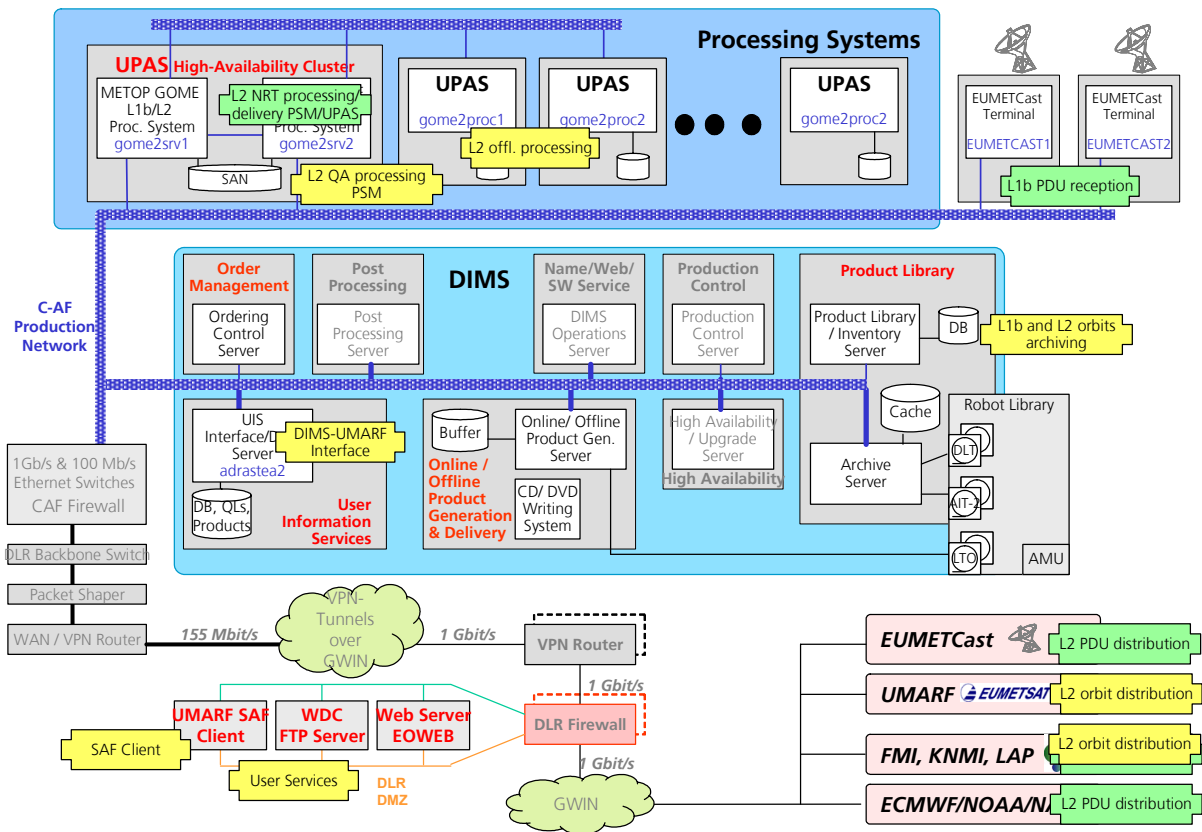
Fig. 2-1: O3M-SAF ground segment at DLR. The near-real-time components are indicated in green, the off-line components in yellow. See the text for more details.

<u>*Validation*</u>

Quality assessment of the GOME-2 products is carried out with a continuous geophysical validation using correlative measurements from ground-based networks. The O3M-SAF partners AUTH and BIRA, responsible for validating the GOME-2 total columns products, performed an initial validation of ozone *(Balis et al. 2007)* and NO_2 *(Lambert et al. 2007).*

The average agreement of GOME-2 total ozone products with ground-based and other satellite ozone column measurements reached the 'percent level'. GOME-2 generally underestimates the total ozone column by 0.5-2%, and the total ozone columns show a scan angle dependency. Present quality of these products makes them suitable for a wide variety of geophysical applications including assimilation in NWP models, ozone trend monitoring and polar process studies.
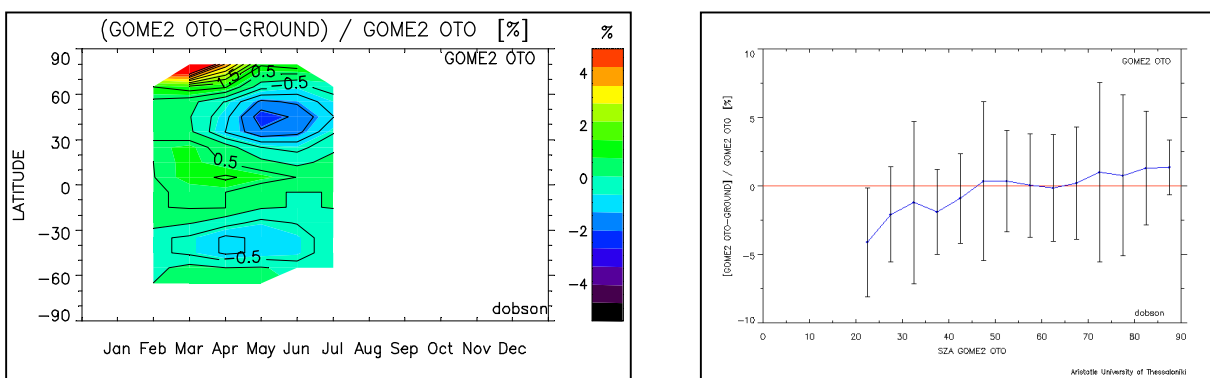
Fig. 2-2: Differences between GOME-2 total ozone and ground-based measurements. Latitude dependence on the left panel and sun zenith angle (SZA) dependence on the right panel. Images courtesy D. Balis (AUTH).

GOME total nitrogen dioxide products are in excellent qualitative agreement with ground-based and other satellite observations of the NO_2 field and of its temporal variations at scales from day to months. The overall accuracy is estimated to fall within the 10% to 20% range, provided that the contribution of

6

tropospheric NO_2 to the vertical column remains low. GOME-2 reports systematically smaller NO_2 column values by 4-6 10^{14} molec/cm^2 (10-20%), see fig. 2-3.
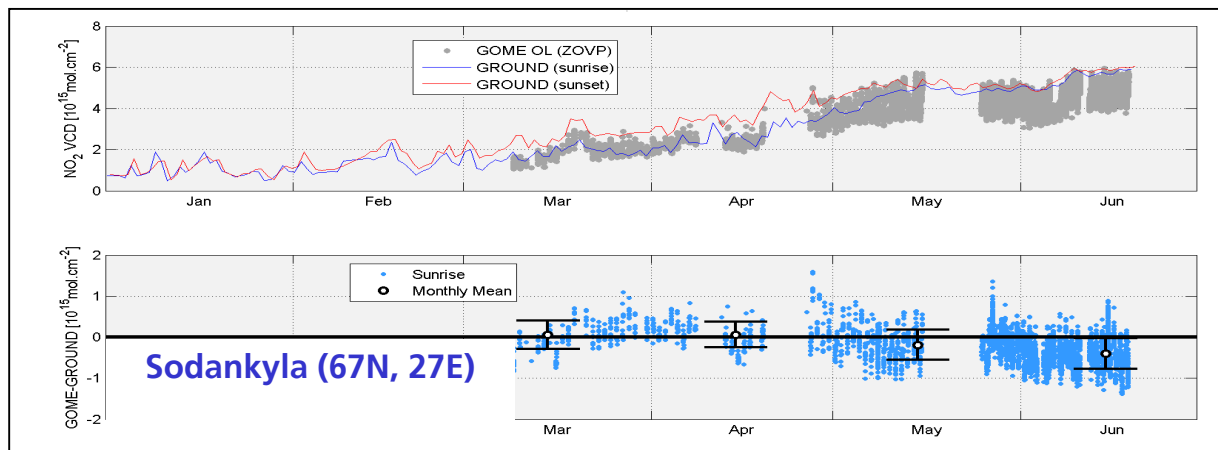
Fig. 2-3: Comparison of GOME-2 total NO_2 with measurements in the Sodankyla station. Image courtesy J.-C. Lambert (BIRA).

Highlights

During 2007 we participated in a number of public events featuring the GOME-2 O3M-SAF products from DLR. A joint EUMETSAT/DLR press release on March 6 showed the first total ozone and NO_2 images from GOME-2

http://www.eumetsat.int/Home/Main/Media/Press_Releases/029529?l=en
http://www.dlr.de/desktopdefault.aspx/tabid-4530/3681_read-7925/3681_page-7/

A GOME-2 NO_2 image from DLR was selected for an EU poster presented during the GMES conference in Munich on April 17. The first GOME-2 SO_2 product displaying the eruption of Mount Piton de la Fournaise, Reunion Island, was published as EUMETSAT image of the month May

http://oiswww.eumetsat.org/WEBOPS/iotm/iotm/20070407_piton/20070407_piton.html

GOME-2 ozone results were presented on September 26 during the symposium celebrating the 20th anniversary of the Montreal protocol (following the invitation of UNEP, WMO, EESC, IO3C, the Academy of Athens, and the National Observatory of Athens). On October 5 a joint EUMETSAT/DLR press release described the first ozone hole measurements from GOME-2.

http://www.eumetsat.int/Home/Main/Media/Press_Releases/030269?l=en
http://www.dlr.de/DesktopDefault.aspx/tabid-1/86_read-10593/
http://www.terradaily.com/reports/Initial_Measurements_From_GOME_2_Show_No_Substantial_Recovery_In_The_Ozone_Hole_999.html

Another very important achievement is the usage of GOME-2 WDC-RSAT products in the WMO Ozone Bulletin from November 2007 (see fig. 2-5).
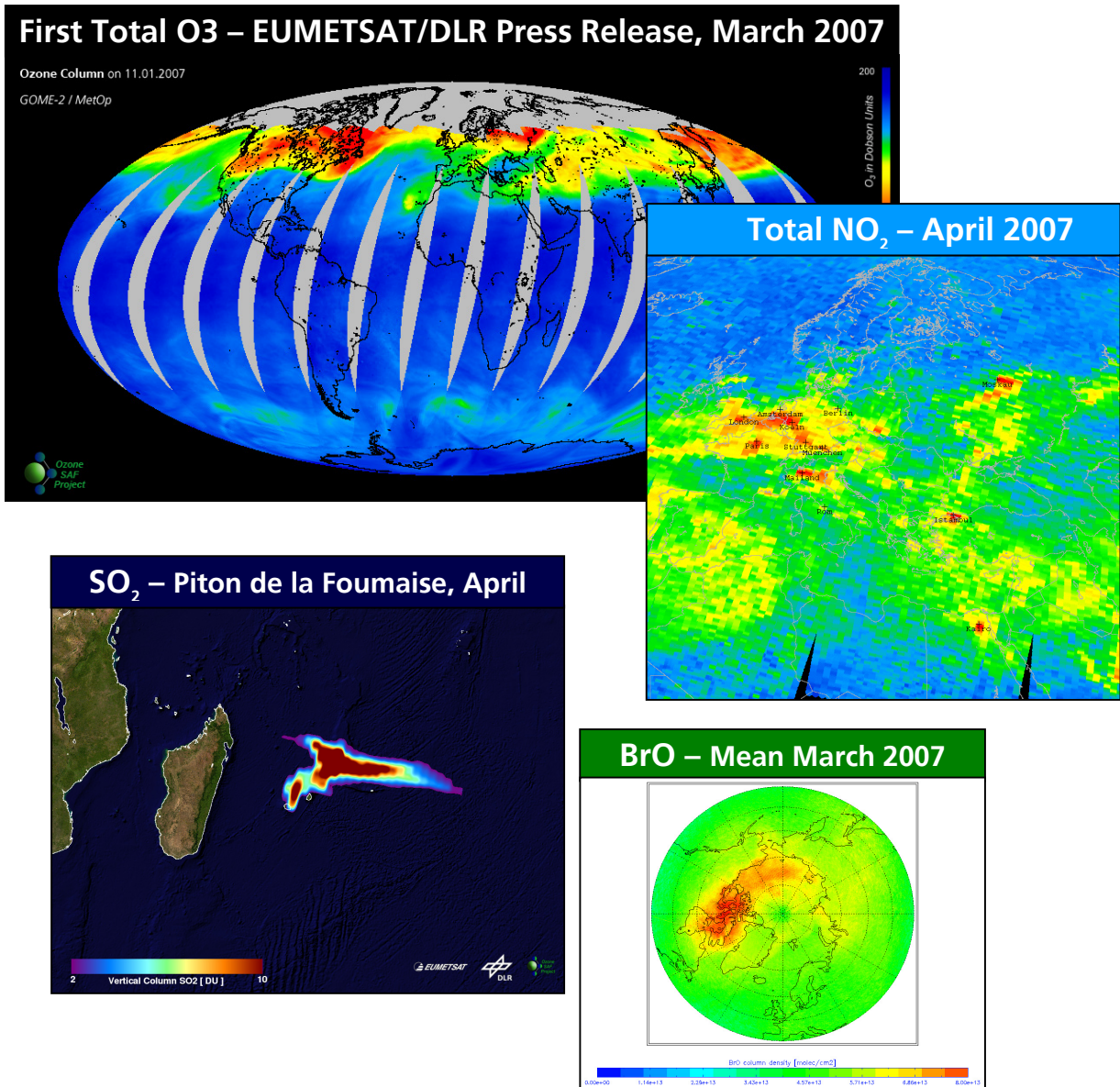
Fig. 2-4: GOME-2 highlights 2007 showing first total ozone, NO_2, SO_2 and BrO products.

Product Distribution

The O3M-SAF near-real-time products are disseminated via *EUMETCast* and FTP. The off-line products are available on FTP. User access through DLR's EOWEB and EUMETSAT's UMARF are foreseen for early 2008. GOME-2 level 3 and level 4 products generated by DFD-KA and animations from DFD-MM are accessible via a dedicated site in WDC-RSAT (http://wdc.dlr.de/sensors/gome2).

Modelled ozone loss rates

Figure 16 shows the rate of ozone change in the Southern Hemisphere for the same three dates as in the three previous figures. One can see that the dark blue region, which represents the fastest ozone loss covers the largest area on 10 September and that by 10 October the ozone depletion has almost come to a halt.

Sep 10, 2007   Sep 25, 200

Ozone change [ppb/day]   Ozone change [pp
-3 -2 -1 0 1 2 3   -3 -2 -1 0 1

*Figure 16. Chemical ozone depletion, at the isobaric level of 56 hPa,
Aerospace Center. Input ozone data comes from GOME-2 on the Me*

Ozone observations

Figure 9 shows total ozone averaged over the month of September for the years 1995-2007. The measurements are carried out with the satellite instruments GOME, SCIA-MACHY and GOME-2. One can see that the 2007 ozone hole is somewhat weaker than the ones of 2000, 2005 and 2006 and stronger than ones of 2002 and 2004. Otherwise, it looks very similar, both in terms of depth and extent, to most ozone holes of the previous twelve years.

Monitoring the Antarctic Ozone Hole by GOME, SCIAMACHY and GOME-2

Total Ozone Monthly Mean, September 1995 - 2007

1995 1996 1997 1998 1999
2000 2001 2002 2003 2004
2005 2006 2007

Total Ozone [Dobson Units]
100 200 300 400 500

Figure 9. September monthly mean total ozone as measured with the satellite instruments GOME (1995-2002), SCIA-MACHY (2003-2006) and GOME-2 (2007). The plot has been provided by the World Data Centre for Remote Sensing of the Atmosphere, hosted by the German Aerospace Centre (DLR).

Fig. 2-5: Extract from the WMO Ozone Bulletin 4/2007 showing the history of ozone satellite products from DLR (front panel) and the modelled ozone loss rates (back panel) using as input GOME-2 total ozone.

References

Spurr, R., D. Loyola, W. Thomas, W. Balzer, E. Mikusch, B. Aberle, S. Slijkhuis, T. Ruppert, M. Van Roozendael, J.-C. Lambert, and T. Soebijanta: GOME level 1-to-2 data processor version 3.0: a major upgrade of the GOME/ERS-2 total ozone retrieval algorithm, Applied Optics, *44 (33)*, 7196-7207, 2005

Van Roozendael, M., D. Loyola, R. Spurr, D. Balis, J.-C. Lambert, Y. Livschitz, P. Valks, T. Ruppert, T. Kenter, C. Fayt, and C. Zehner: Ten years of GOME/ERS-2 total ozone data: the new GOME Data Processor (GDP) Version 4: I. Algorithm Description, J. Geophys. Res., *111*, D14311, DOI 10.1029/2005JD006375, 2006

Loyola, D., W. Thomas, Y. Livschitz, T. Ruppert, P. Albert, and R. Hollmann: Cloud properties derived from GOME/ERS-2 backscatter data for trace gas retrieval, IEEE Transactions on Geoscience and Remote Sensing, *4 (9)*, 2747-2758, 2007

Balis, D., M. Koukouli, D. Loyola, P. Valks, and N. Hao: Validation of GOME-2 total ozone products (OTO/O3, NTO/O3) processed with GDP 4.2, AF/O3M/AUTH/GOME-2VAL/RP/01. Retrieved from http://wdc.dlr.de/sensors/gome2/SAF-O3M-AUTH-GOME-2VAL-RP-01.pdf, 2007

Lambert, J.-C., I. De Smedt, J. Granville, and P. Valks: Initial Validation of GOME-2 Nitrogen Dioxide Columns (GDP 4.2 OTO/NO2 and NTO/NO2): March - June 2007, TN-IASB-GOME2-O3MSAF-NO2-01. Retrieved from http://wdc.dlr.de/sensors/gome2/TN-IASB-GOME2-O3MSAF-NO2-01_1_B.pdf, 2007

3. Current Projects

3.1 Sulfur Dioxide Monitoring for Volcanic Hazards using GOME-2

P. Valks, N. Hao, M. Rix, W. Zimmer, T. Erbertseder (DFD-KA)

Volcanic eruptions are a major natural hazard, not only to the local population near large volcanoes but also to aviation. Space based atmospheric sensors like GOME and SCIAMACHY, make it possible to detect the emissions of volcanic gases (sulfur dioxide), and monitor volcanic activity and eruptions on a global scale. Atmospheric sulfur dioxide (SO_2) is retrieved from solar backscatter measurements in the ultra-violet (UV) spectral range around 320 nm, applying the Differential Optical Absorption Spectroscopy (DOAS) method. This retrieval technique uses the high spectral resolution of these instruments to determine the total column density of SO_2.

IMF-AP´s expertise on retrieval of volcanic SO_2 from space is used in several national and international projects, such as the *Aviation Control Support* service of the ESA GMES Service Element for Atmospheric Monitoring (PROMOTE), and the BMBF Geotechnology project for the development of a *Volcano Fast Response System (Exupéry)*.

PROMOTE Aviation Control Support Service
The *Aviation Control Support* service of PROMOTE is a cooperation between the Belgian Institute for Space Aeronomy (BIRA), the Royal Netherlands Meteorological Institute (KNMI), Carlo Gavazzi Space (CGS) in Italy, and DLR. Its purpose is to monitor the extension and movement of volcanic plumes over Europe, Africa and Asia by using satellite measurements in an analysis and warning system. Volcanic SO_2 and ash plumes are a major hazard to aviation: volcanic ash can melt in the engines resulting in engine failures and it can limit the view of pilots.

IMF-AP's contribution to this PROMOTE service concentrates on the provision of NRT SO_2 columns from the GOME-2 instrument on MetOp. With GOME-2, it is possible to detect and track the volcanic SO_2 and aerosols plumes in near-real time (NRT) and on a global scale, a fact particularly important for volcano early warning services. GOME-2 measures the SO_2 column with a spatial resolution of 80×40 km^2, and provides a global coverage within about one day. A recent potential volcanic aviation hazard that illustrates the importance of this service was the major eruption of the Jebel al-Tair volcano (Yemen) in October 2007. This was the first eruption of this Red Sea volcano since 1883. Fig. 3-1 shows the long range transport of the volcanic SO_2 plume by the sub-tropical jet stream, as measured with GOME-2. Maximum SO_2 column densities of more than 20 Dobson Units were measured, and the volcanic plume reached altitudes of 15-17 km in the stratosphere.

Another IMF-AP activity for *Aviation Control Support* service was the calculation of volcanic SO_2 air mass factors, which are needed for the conversion of the measured SO_2 slant column density into the vertical column density. An accurate retrieval of the vertical SO_2 column is important for a reliable volcanic warning service. The SO_2 air mass factors are derived with the multiple scattering radiative transfer model LIDORT, and take the volcanic plume height into account.

Exupéry – The Volcano Fast Response System
The BMBF Geotechnology project for the development of a *Volcano Fast Response System (Exupéry)* started in October 2007. The Exupéry project is a cooperation between 10 institutes, including IMF and DFD, and is coordinated by the University of Hamburg. The mobile *Volcano Fast Response System* that can be quickly deployed in case of a volcanic crises or volcanic unrest, builds on established volcanic monitoring techniques, such as seismicity, ground deformation, and volcanic gas measurements. A major novelty of this mobile system is the direct inclusion of satellite based observations to deduce ground deformation, to detect hazardous gas emissions and to monitor thermal activity.

Within Exupéry, IMF-AP and DFD-KA will develop a volcanic monitoring and warning service using GOME-2 SO_2 data. Near-real time GOME-2 SO_2 measurements and ground-based observations will be combined with state-of-art particle-dispersion models and global meteorological models to monitor and forecast the dispersion of volcanic plumes up to 3 days in advance (Fig. 3-2). An important milestone for the Exupéry project will be a prototype installation of the *Volcano Fast Response System* at the Fogo volcano on the Azore Island Sao Miguel, scheduled for early 2009.
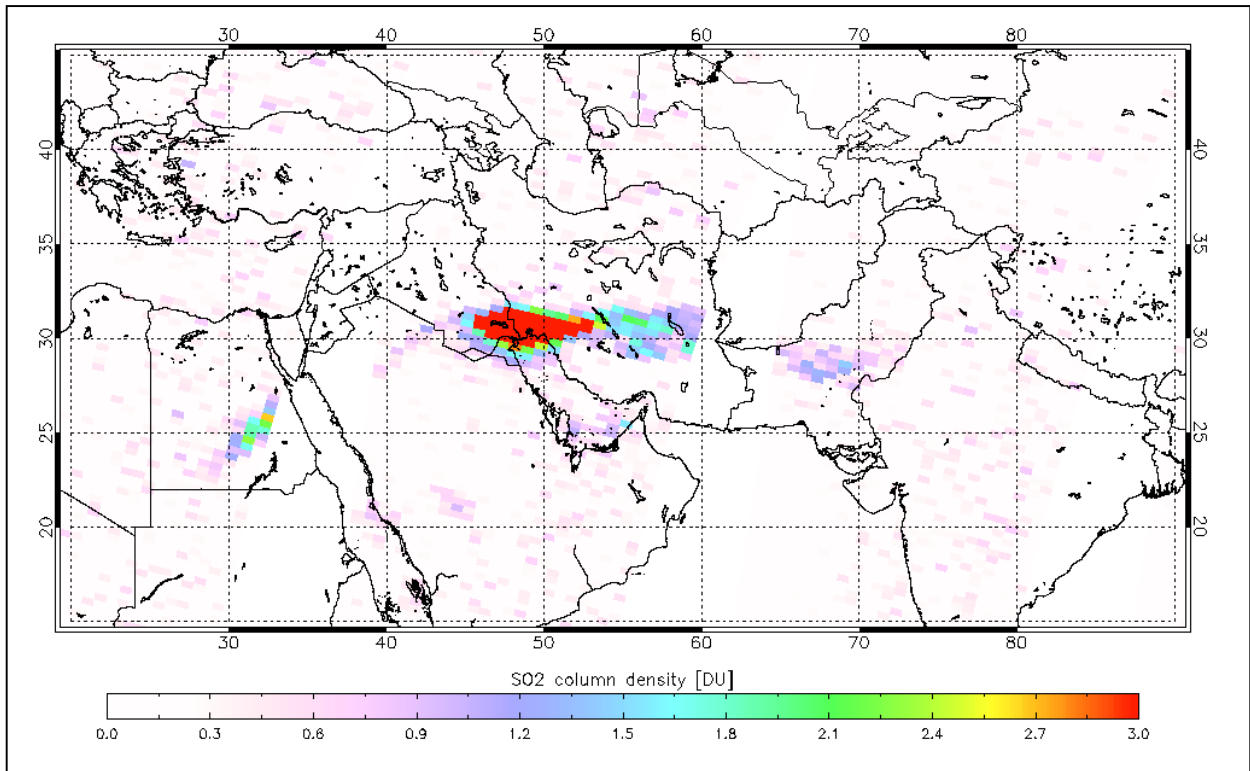
Fig. 3-1: Volcanic SO$_2$ from the Jebel al-Tair volcano (Yemen) as measured by GOME-2 on 3 October 2007. The Jebel al-Tair volcano erupted on 1 October, the first eruption of this Red Sea volcano since 1883. The volcanic plume reached altitudes of 15-17 km in the stratosphere, and was transported over large distances by the sub-tropical jet stream.

SO$_2$ retrieval and satellite imagery	Trajectory Matching	Validation
SO$_2$ columns from GOME-2; imagery from MODIS	3D trajectory matching for attribution of SO$_2$ source to particular volcano and plume height determination	Coupling ground-based measurements and a particle-dispersion model for SO$_2$ plume validation
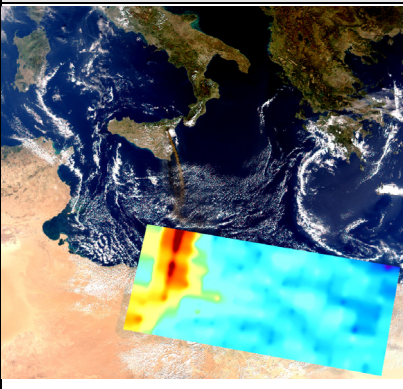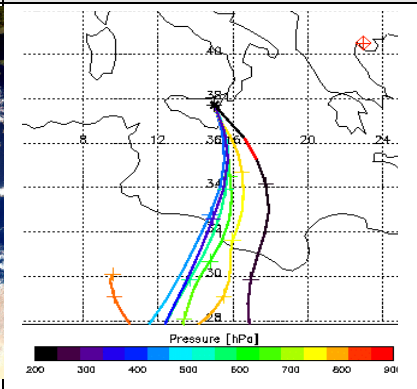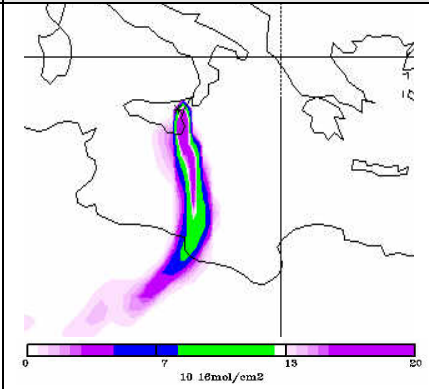
Fig. 3-2: Overview of the GOME-2 based volcanic SO$_2$ monitoring and warning service: a space-based component of the Exupéry volcano fast response system

3.2   SCIAMACHY Level 0-1 Improvements

G. Lichtenberg, S. Slijkhuis, B. Aberle, D. Scherbakov, A. von Bargen

The Level 0-1 data processing converts spectra from binary units per detector pixel into intensity per wavelength. In the previous year the focus was on the improvement in the spectral stray light correction, the *Dynamical Bad & Dead Pixel Mask* (DBPM) and the inclusion of the degradation correction in the user tool *Scial1c*. The improved spectral stray light correction is described below in chapter 3.4. Additionally IMF provided expert support in solving an anomaly in the level 0-1b processor IPF (not to be confused with the DLR developed prototype, which did not display this anomaly) and in the optimisation of the angle offsets for the correct calculation of the tangent height. The latter is critically important for limb profile products. All the issues were solved and in July the new IPF version 6.03 became operational.

Dynamical Bad & Dead Pixel Mask
The DBPM contains detector pixels that are rendered useless for scientific purposes, most likely by proton impact during passage of the satellite through the *Southern Atlantic Anomaly (SAA)*. Various effects make these pixels useless:

- total loss of response due to disconnection
- random telegraph noise, the unpredictable jump in time between (several) dark signal levels
- excessive amount of noise
- high leakage current leading to saturation of the detector already at short exposure times

All pixels marked as bad in the DBPM are not used in any retrieval. Bad pixels are mostly a problem of the IR channels 6-8; these have different detector material more susceptible to particle damage. SRON has developed a correction based on level 0 dark measurements and several channel wide thresholds to determine if a pixel is still useful. An experimental scheme using data available in level 1 products[1] was implemented already in 2006. In 2007 this scheme was improved and brought into alignment with the SRON approach. Additionally, a change to thresholds for individual pixels instead of channel thresholds is in preparation.

Improvements of the SciaL1c tool
The *SciaL1c* tool, developed and released by IMF in 2006, was improved and expanded to contain new functionality. The purpose of the tool is to give users the opportunity to generate calibrated data from SCIAMACHY level 1b files. The user can choose which calibration(s) have to be applied. Additionally, in 2007 the new functionality of degradation correction with the so-called *m-factors* was implemented. The *m-factors* are calculated by the IUP/IFE, University Bremen as part of the SOST activities. A first, preliminary set became available for the first time this year. *M-factors* are delivered for every month for the whole mission as individual files. In order to let the user take advantage of the *m-factors* the *SciaL1c* tool had to be changed to accept external input, since the original philosophy of ESA's level 1b format is to provide all calibration data within one file without the need of any external data. The tool was adjusted to automatically select the appropriate *m-factor* file for the level 1 data to be processed. In addition the user has also the option to specify an *m-factor* file of own choice.

As a preparation to ease future releases, a cross compilation environment was developed permitting to produce binaries for different architectures (the tool is delivered for Linux, HP/UX , Solaris and Linux DEC Alpha) under Linux (see chapter 3.3).

---

[1] The individual dark measurements are not part of the level 1 product, only the average of the dark measurements

3.3 SCIAMACHY SciaL1c Tool

D. Scherbakov, B. Aberle, G. Lichtenberg, A. von Bargen

The *SciaL1c* s/w package is a command-line tool permitting users to extract from SCIAMACHY level 1b products data in the level 1c format, i.e. fully calibrated spectra from the SCIAMACHY detector channels. In order to increase the range of applications for the user, *SciaL1c* was designed so that users can select from a list of calibration routines those they would like to apply. Additionally, the extraction can be combined with several filters allowing an extraction of special scenes or sub-sets of measurement data, e.g. Nadir observation only.

In the past, the development of *SciaL1c* was totally separated from the development of the Level 0-1b and Level 1b-2 data processing development. Thus, for every upgrade of the Level 1b-1c data processing a specific project had to be initiated for modification of the tool. This caused a delay between data processing and tool development due to the additional effort involved. Therefore it was decided to derive *SciaL1c* calibration applications from the data processor kernel. The selected approach ensured that, within days, an upgrade of the data processor software could be followed by a corresponding upgrade of *SciaL1c*. Since development and maintenance of the tool and the data processor remains in one hand it ensures that both software packages are compatible.

The *SciaL1c* version 1.23 replaced the Java-based tool from the *EnviView* package maintained by ESA. This was the first version of the tool released to the public and it was available as precompiled binaries for two platforms – Linux x86 and Sun Solaris. Since the release of version 1.23 the development of the tool continued including bug fixes and implementation of new functionalities from the main processor as well as some additional features:

- support of monitoring factors
- dark correction switching between GADS and LIMB darks implemented due to different views at dark correction among several science groups
- complete re-writing of help system and command-line argument parsing
- processing of monitoring states and dump of data into ASCII files
- development of new test complex permitting comparison of binaries produced on different platforms in order to ensure that the tool produces the same results on all platforms
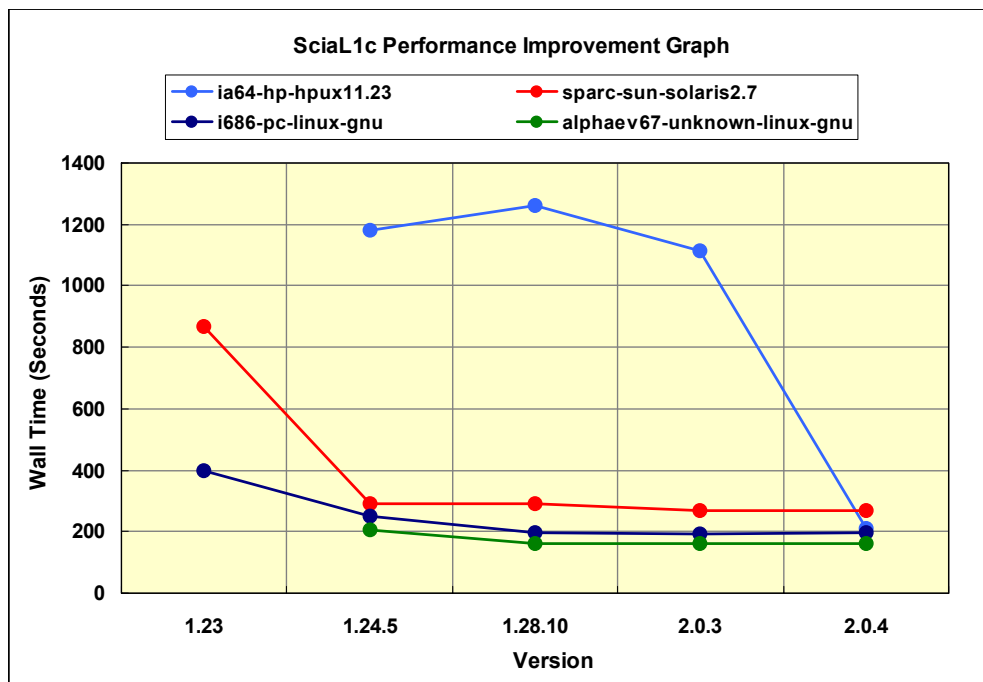

Fig. 3-3: Improvement of SciaL1C performance starting with version 1.23. The *Wall Time* is the time required for a complete run of the tool.

The performance of the *SciaL1c* tool is tested with each release on all target platforms in order to ensure quality of the final product. The biggest achievements were speed gains of more than a factor of

3× on Sun Solaris in version 1.24.5 using cross-compilation and 2× on Linux in version 1.28.10 and 2.0.3. Currently the tool is available for the following platforms (note that in 2008 ESA plans to fund development of the binary for MS Windows):

- Linux on x86 processors (i686-unknown-linux-gnu)
- Linux on DEC-Alpha (alphaev67-unknown-linux-gnu)
- Sun Solaris (sparc-sun-solaris2.7)
- HP-UX on IA64 (ia64-hp-hpux11.23)

3.4   SCIAMACHY Straylight Correction

S. Slijkhuis, B. Aberle, G. Lichtenberg, M. Gottwald, E. Krieg (TwIG), A. von Bargen

SCIAMACHY has been designed with stringent requirements on straylight in mind. Nevertheless, straylight needs to be corrected, to reach the very high signal-to-noise ratios required for the retrieval of weak trace gas absorbers in the Earth's atmosphere. We discern two types of straylight: spectral straylight and spatial straylight. Spectral straylight is a redistribution of input light, at any wavelength, to all detector pixels in the instrument. It has been calibrated on-ground, and is routinely corrected in SCIAMACHY Level-0-1b processing. Spatial straylight is light from outside the instrument's field of view, which is somehow scattered into the instrument. The prime mechanism is thought to be scattering by surface roughness of the first scan mirror. This type of straylight was considered uncritical, because of SCIAMACHY's ultra-smooth mirrors, and was not characterised on-ground. However, a non-negligible amount of spatial straylight appears to be present in the Limb measurements. This is due to the high contrast between the very weak signal at high altitudes, and the strong signal from the ground and lower altitudes.

Spectral straylight
Ideally, a complete description of spectral straylight would be given by a matrix which describes the signal transfer from each input wavelength to all $8 \times 1024 = 8192$ detector pixels. Early in the design phase for instrument calibration, it was considered to deliver the full 8192×8192 straylight matrix as input to Level 0-1b processing. However, it quickly became clear that evaluating such big matrices for each measurement (typically 4-8 spectra per second) is not feasible in operational processing because of processing time.

The initial straylight calibration concept of SCIAMACHY uses a simplified approach with two components:

- uniform straylight, independent of the shape of the input spectrum
- a set of ghosts, where the straylight onto a pixel is derived from a limited number of input wavelengths

Re-analysis of the on-ground calibration data, by R. Snel from SRON, confirms that in the current *Calibration Keydata* the level of uniform straylight was specified near the lowest straylight level in a channel (this to prevent negative signals after straylight correction). From another side, independent DOAS trace gas retrievals in the framework of the operational Level 1b-2 verification, indicated that residual straylight levels up to a few percent may be present in calibrated SCIAMACHY data in channel 2 (*C. Lerot, BIRA-IASB, private communication*, *2006*).

A new straylight algorithm has been developed, which is based on the much more accurate concept of the full straylight matrix. However, to keep processing time reasonable, this matrix has been compressed to about 300 input points per channel, and even less output points. This compressed matrix can only represent a smooth straylight function, and therefore cannot handle the sharply focussed ghosts which are present in channels 3-8 (see fig. 3-4). Ghosts are handled separately, as before.
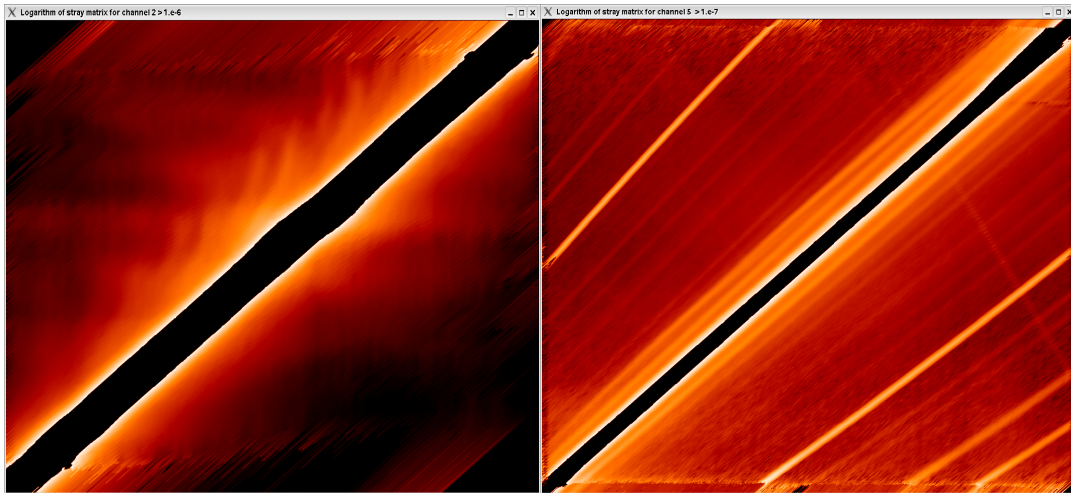
Fig. 3-4: Straylight in channel 2 (left panel) and channel 5 (right panel), based on data from R. Snel (SRON). The plot shows on a logarithmic scale the 1024 x 1024 matrix for straylight within each channel. Each row (*,y) shows the stray-light spectrum due to unit input in pixel y. The region around the diagonal is defined as being free from straylight: this is light contained in the instrument slit function. The lines parallel and normal to the diagonal in the plot for channel 5 are reflected and refocused ghosts. These are absent in channel 2, which has a holographic instead of a classically ruled grating.

Fig. 3-5: Straylight-corrected and sun-normalised spectra at the very end of channel 2, for two measurements where the Sun is observed through the atmosphere. Upper panel: strong UV cut-off (Sun low in atmosphere), lower panel: moderate UV cut-off). The red curve shows data using the old algorithm, the black line using the new straylight correction algorithm. The dots indicate the expected signal level, based on channel 1 measurements.
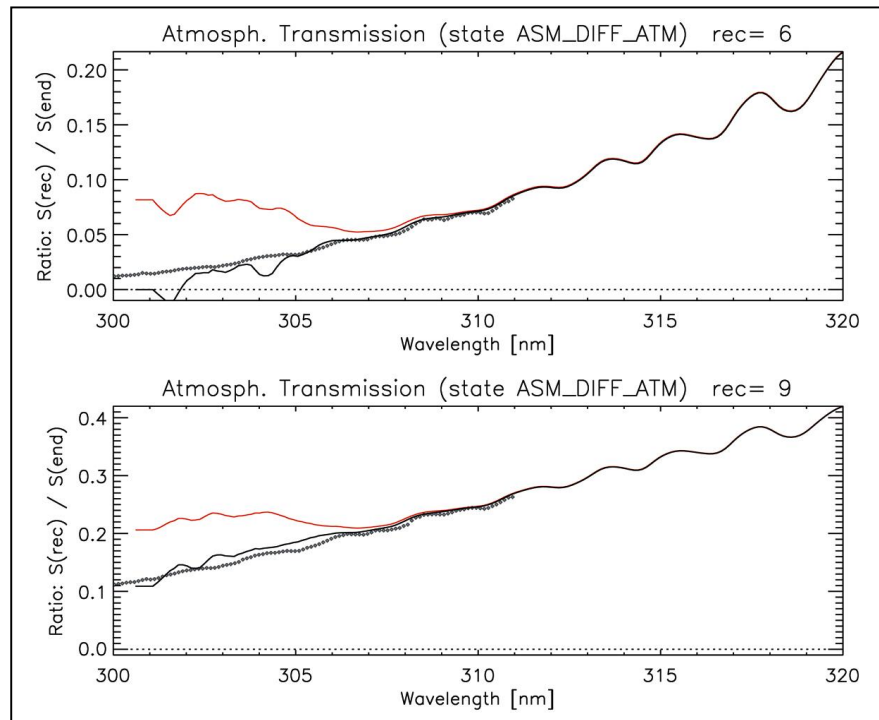
Presently, the new algorithm has been implemented in the DLR-IMF Level 0-1b prototype processor, and has been verified for channel 2 (fig. 3-5). In this channel the straylight problem appears most severe.

Implementation and verification/validation of the other channels is foreseen for 2008.

Spatial straylight

Spatial straylight was not calibrated on-ground. Special limb measurements, carried out in the Commissioning (SODAP) Phase, were analysed for this purpose. While they show the rough magnitude of the straylight, these measurements do not contain sufficient information to derive a correction algorithm for spatial straylight. An OCR (Operational Change Request, see chapter 3-9) has been submitted to carry out dedicated straylight measurements with SCIAMACHY. These measurements are made in the time window for solar measurements. The field of view is positioned at a given distance to the Sun, and then a limb-type scan is performed while the Sun slowly drifts away. The first set of measurements has been performed, at close distance to the Sun, using the small aperture. More measurements, at larger distances, using the full aperture, are scheduled for 2008.

3.5   SCIAMACHY Level 2 Processor Versions 3.01 and 4

G. Lichtenberg, A. Doicu, S. Gimeno-Garcia, S. Hrechanyy, K. Kretschel, M. Meringer,
F. Schreier, A. von Bargen

The Level 2 off-line processor generates geophysical products from level 1b data. Major activities in the previous year were the verification and the release of version 3.01 of the processor and the preparation of version 4 with new products.

Version 3.01 of the Level 1b-2 offline processor
Version 3.0 of the processor was updated to incorporate the recommendations of the validation as presented during the ACVE-3 (*Atmospheric Chemistry Validation of ENVISAT*) meeting. The recommendations resulted in the following algorithm changes:

- Extension of cloud parameter calculation: The original algorithm SACURA by IUP/IFE to calculate cloud top height (CTH) and cloud optical thickness (COT) was limited to cloud fractions of above 20%. A new version of SACURA (version 2.1) was delivered by IUP/IFE and incorporated in the data processor. The new version calculates CTH and CTO down to 5% cloud fraction. Since the cloud parameters are also used in the retrieval of O_3 and NO_2 an extensive testing was done not only for the cloud parameters but for the NO_2 and O_3 products as well. The agreement was within the expected range.
- Increase of number of limb profiles: SCIAMACHY obtains atmospheric profile values for various heights. At each height an horizontal scan is executed. In version 3.0 only one profile value per height was provided to increase the signal to noise. Following a request of the users, in version 3.01 a maximum of 4 profiles is obtained per height.
- Removal of NO_2 post-processing: In the verification of the NO_2 nadir vertical column a bias was found with respect to other algorithms. Thus a corrective offset was added to the retrieved column. However, testing on a larger dataset showed that the bias was period specific. The adding of the offset was removed from the retrieval in version 3.01.

Additional changes following user requests and bug fixes included:

- changing the filling of the records in the Cloud and Aerosol datasets
- correcting the content of the quality flag of the Cloud and Aerosol Products
- updating the pressure and temperature values in the Limb products to reflect changes made in version 3.0 profile retrievals
- adding the Ring effect correction to the slant column density (SCD) entry of O_3 (before, the entry contained the pure SCD and the Ring effect correction was applied in an intermediate step of the total column retrieval)

All changes were extensively verified on a large dataset of 109 orbits. After the required *Factory Acceptance Test (FAT)* the offline processor was delivered to ESA. The switch-on of the operational processing of Level 1b data occurred on October 9th.

Re-processing campaign
Since both processors (Level 0-1b and Level 1b-2) now contain major improvements compared to the previous versions, ESA decided to re-process all mission data from August 2002 through September 2007. For this large amount of data one cannot apply the normal scheme used in day-to-day processing of the incoming data (also called *forward processing)*. Usually re-processed data shall be of highest quality achievable. Thus the optimal calibration data have to be used. In the *forward processing* only the most recent *available* calibration data can be used for two reasons: (1) calibration data are not as frequently measured as science data; there are daily, weekly and monthly calibrations and (2) the data have to be first processed before they can be used for calibration purposes, introducing a time delay in the availability of the data. In order to ensure that level 1b data contain a full complement of calibration data, even if calibration data were not measured in the time that is covered by the Level 1b product, the ESA developed *Instrument and Engineering Calibration Facility (IECF)* copies calibration data that were generated by *SciCal* to the level 1b product (see also fig. 3-6). For an optimal calibration, the re-processing is done in 3 steps:

- Calibration data are re-processed to generate the necessary *Auxiliary Data Files (ADF)* needed for the calibration during level 0-1b processing. This was done by IMF using the *SciCal* tool and the prototype.

- Consolidated level 0 data are processed to level 1b. Since all ADFs are already at hand this can be done in parallel on several cluster nodes.
- A soon as level 1b data become available, they are processed to level 2, again parallel on several cluster nodes.

Both, the processing from level 0 from 1b and further to level 2 were executed by D-PAC under a contract issued by ESA. The new level 2 products will be validated and the first results will be presented at a meeting early 2008.

Next version (V4) of the Level 2 offline processor
The next version of the processor is currently in development and will be released in 2008. It features basic software changes that apply to all products and several new geophysical products that were not available previously.
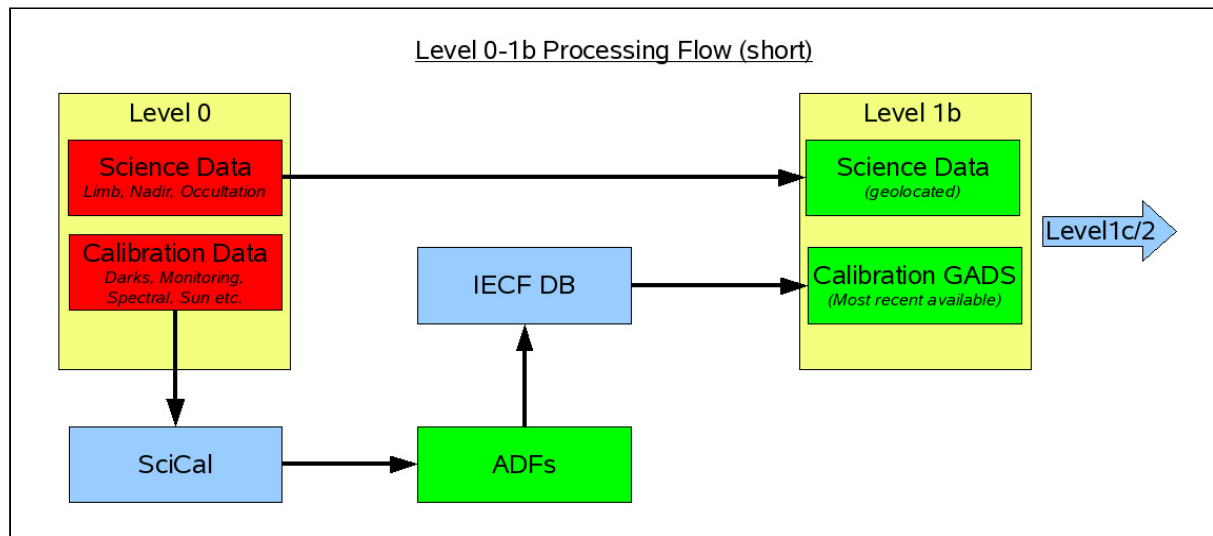

Fig. 3-6: Simplified scheme of level 0-1b processing. level 0 data contain science data and less frequently measured calibration data. From the calibration data, SciCal generates ADFs that are copied to a database. The IECF then copies the appropriate calibration data to the level 1b product, which then can be further processed to level 1c or level 2.

With the coming version of the level 2 processor it will be possible to choose calibration options that should be applied to the Earth shine spectra. This feature can be useful in cases where retrievals do not require fully calibrated spectra. One example is the DOAS retrieval of atmospheric trace gases. Since DOAS makes only use of differential structures in the spectrum, it is not sensitive to absolute intensity values. Thus the radiometric calibration is not needed for DOAS trace gas retrieval. Experience has shown that the radiometric calibration of SCIAMACHY introduces small scale spectral features that harm some DOAS retrievals. Thus it was decided not to apply the radiometric calibration in such cases. In order to be flexible for future applications, e.g. improvement of the radiometric calibration permitting its full usage in all retrievals, the software was changed to allow for any calibration to be switched on or off individually. Another fundamental change to level 2 processing is the introduction of the *m-factor* correction in the level 1b-2 processing. The new version of the processor can now correct the degradation for the products when considered appropriate. The *m-factor* correction can be individually switched on or off for each product just as the other calibration options (see above). This is particularly important for the *Absorbing Aerosol Index (AAI)*.

AAI
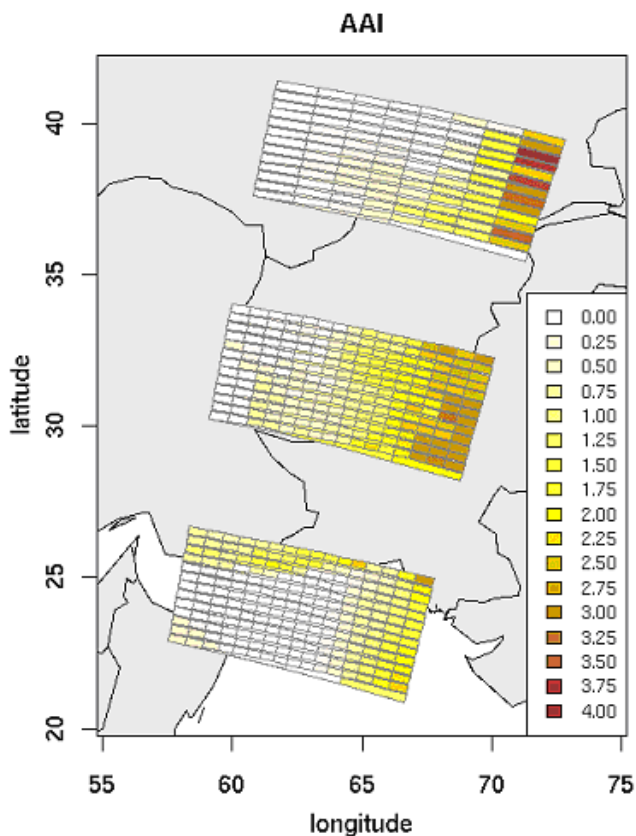
Fig. 3-7: First example of retrieved aerosol values for an orbit that passes over Afghanistan and Pakistan.

The new processor will have two new nadir products: Slant column densities of SO_2 and of BrO. The SO_2 retrieval is based on an algorithm of A. Richter from IUP/IFE, University of Bremen and uses background subtraction of a reference sector over the Pacific Ocean. For the operational processing a new database will be added to the database server of the processor, which is continuously updated with new background data as they become available in the forward processing. Along with the background values themselves also various quantities like cloud coverage and statistical error are placed in the database enabling to judge the quality of the SO_2 column. The BrO algorithm was developed by BIRA. Here, as well as in the SO_2 retrieval the Earth shine spectra will not be radiometrically calibrated to avoid corrupting effects of the small spectral features introduced by the correction. The implementation of the SCDs is the first step to implement the retrieval of total columns for both species planned to be operational for 2009. Finally, in the coming version of the processor also a new algorithm, developed by KNMI (see e.g. *de Graaf and Stammes, 2005*), to retrieve the AAI will be implemented. A first example of the AAI retrieved values is shown in fig. 3-7. The implementation is currently under verification.

Limb verification and validation campaign 2007/2008

Apart from the implementation and development of the Nadir products, IMF's own development of limb profile retrievals of O_3 and NO_2 continued in 2007. Several refinements of the retrieval were successfully achieved. Currently investigations are ongoing if these should be included in the next version of the data processor. The refinements include:

- increase of the number of atmospheric layers from 24 to 33
- introduction of *Picard iteration* (see chapter 3.6)
- inclusion of ECMWF temperature and pressure profiles
- increase of the polynomial order for the fit from 3 to 4 to be able to model finer structures for O_3
- extension of the spectral retrieval window for NO_2.

A detailed study comparing the results when using different combinations of the above parameters as well as comparing the IMF results with results from other algorithms was started at the end of the year together with IUP/IFE. An extended validation of the results using a complete data set of 2003 is also planned. Results of these studies are expected in 2008.

References

de Graaf, M. and P. Stammes: SCIAMACHY Absorbing Aerosol Index – calibration issues and global results from 2002-2004, Atmos. Chem. Phys., Vol. 5, 2385-2394, 2005

3.6 Updates of the SCIAMACHY Limb Processor

A. Doicu, K. Kretschel, M. Meringer, A. von Bargen, G. Lichtenberg

The operational SCIAMACHY processor developed at the IMF-AP uses a single-scattering model, while the multiple scattering effect is taken into account by using look-up table corrections. The multiple scattering correction factor is defined as the ratio of the total scattered light (calculated with a multiple scattering model) to the single scattered light, and is computed for a set of solar zenith angles, relative azimuth angles, surface albedo, tangent heights and wavelengths. In some situations the interpolation error of the correction factor among the five parameters of the look-up table may becomes extremely large. For this reason, we replaced the single-scattering model by a multiple-scattering model and compute the correction factors for the 'exact' limb viewing geometry. The correction factors are then only interpolated in the wavelength domain. This technique improves substantially the retrieval results.

Because the scattering problem is axi-symmetric, the multiple-scattering model uses a two-dimensional *Picard iteration* and computes the radiances at a set of discrete points in the zero azimuth plane. The domain of analysis has an angular extent of 94° and is bounded by the vertical Z-axis and the shadow region. At each iteration step, the radiance at a generic grid point and in a specific discrete ordinate direction is computed by using the integral form of the radiative transfer equation. The discrete ordinate is specified in the local coordinate system attached to the generic point, and the integration is carried out along a characteristic passing through the generic point and intersecting the cell face at a reference point. The reference value of the radiance is computed using linear interpolation of the two grid point values of the face pierced by the ray. Due to the sphericity of the atmosphere a further interpolation in the discrete ordinate space is required. Along the vertical radial line we consider axi-symmetric boundary conditions, while along the cylinder line bounding the shadow region, we assume homogeneous boundary conditions.

The *Picard Iteration* involves the following steps:

1) Consider a two-dimensional discretization of the domain of analysis.
2) Initialize the discrete radiance values to zero or compute the initial estimate by using the pseudospherical model (at each radial line).
3) Beginning downward, for each layer, compute the source function (in fact, the multiple scattering term) at the top of the layer and then, for each cell of the layer, compute the radiances at the lower nodes for the discrete ordinates in the third and fourth quadrant.
4) Compute the upward radiances at the bottom of the domain by using the boundary conditions for a Lambertian surface.
5) Working upwards, repeat the calculations of step 3, but compute the radiances at the upper nodes for the discrete ordinates in the first and second quadrant.
6) Interpolate the radiances at each point situated on the line of sight and for all discrete ordinates using the grid radiance values of the cell containing the point.
7) Compute the multiple scattering terms at all points situated on the line of sight.

Repeat steps 3-6 until the maximum change in the multiple scattering terms is smaller than some pre-assigned error values at all points.

Steps 3, 4 and 5 represent one *Picard iteration*. A specific feature of the above method is that the source function is updated at each layer calculation. Note that in order to reduce the computational effort, one may compute the source function at the beginning of each *Picard iteration*.

In order to reduce the computer time, we may solve the scattering problem on a reduced domain of analysis, which is bounded by the end-points of the line of sight. The values of the diffuse radiance pointing into the domain are computed by using the pseudospherical model. They remain unchanged during the iterative process. Thus, the boundary lines become independent of the interior cells and the radiance at their grid points serves as the boundary radiance for the interior points. This type of boundary conditions is known as open boundaries. For this reason, this method is referred to as the *Picard iteration* method with open boundaries.

The numerical results presented in fig. 3-8 illustrate the relative errors of the multiple scattering correction factor obtained by using the *Picard iteration* method with open boundaries and the CDI approach developed by *Rozanov et al. (2002)*. Both models were found to agree to less than 2%, and

this agreement proves the accuracy of the multiple-scattering model with *Picard iteration* and open boundaries.
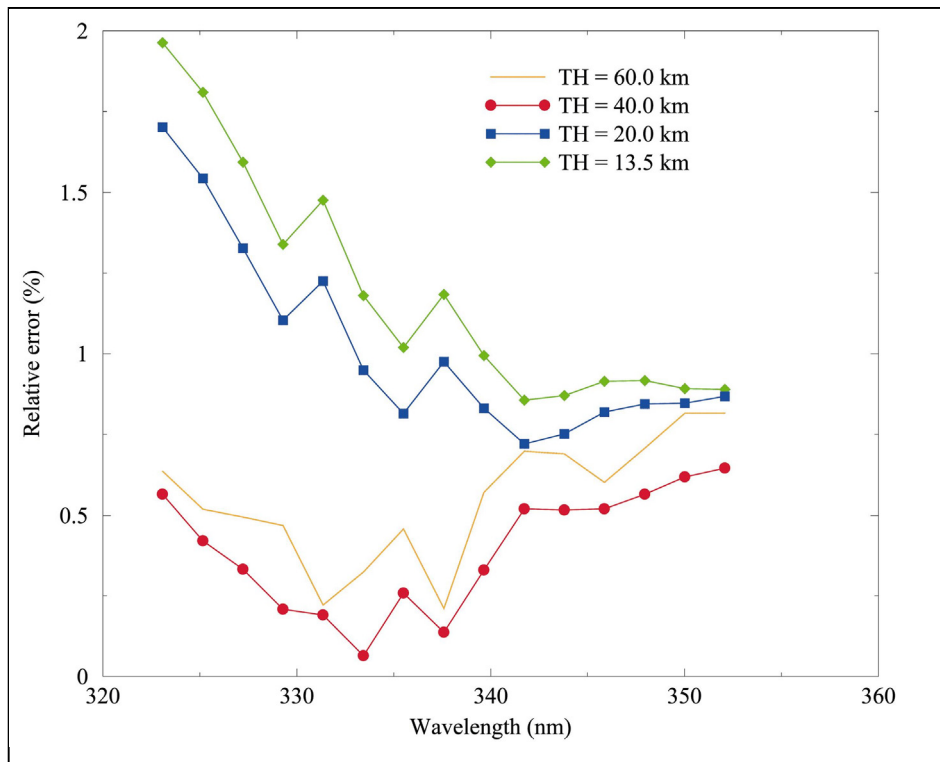

Fig. 3-8: Relative errors between the multiple scattering correction factors computed with the *Picard iteration* with open boundaries and the CDI approach.

References

Rozanov, A.V., V. V. Rozanov, and J.P. Burrows: Combined differential-integral approach for the radiation field computation in a spherical shell atmosphere: Nonlimb geometry, J. Geophys. Res. 105, 22 937-942, 2007

3.7 SCIAMACHY Nadir-Infrared Retrieval

F. Schreier, S. Gimeno-Garcia

In addition to the 'classical' UV channels of the GOME and GOME-2 instruments onboard ERS-2 and MetOp, respectively, SCIAMACHY on ENVISAT is equipped with near infrared channels (971 – 1773 nm, 1934 – 2044 nm, and 2259 – 2386 nm) permitting the nadir sounding of column densities of trace gases such as CO, CH_4, N_2O, CO_2 and H_2O. For UV instruments such as SCIAMACHY *(Bovensmann et al., 1999)*, the analysis is traditionally based on a DOAS-type methodology. This approach has also been successfully applied for analysis of SCIAMACHY's near infrared channels *(Buchwitz et al., 2007; Frankenberg et al., 2005)* and was the basis of the BIAS (Basic Infrared Absorption Spectroscopy) nonlinear least squares algorithm developed for the operational level 2 data processor *(Spurr, 1998)*. In order to gain greater flexibility in the forward modelling and a more efficient and robust least squares inversion, a 'Better InfraRed Retrieval Algorithm' (BIRRA) has been recently prototyped at IMF-AP.

Carbon monoxide retrieval from SCIAMACHY nadir observations is rather challenging: Only channel 8 from 2259 to 2386 nm features CO absorption signatures, albeit very weak and superposed by stronger absorption lines of concurrent gases, i.e. H_2O and CH_4. Additionally, an ice layer on the detector modifies the measured signal. Even worse, degradation of the detector increasingly reduces the number of reliable pixels, i.e. only about 50 of 1024 pixels in channels 8 are useful for CO retrieval, when using the WFM-DOAS bad/dead pixel mask.

The BIRRA algorithm

The forward model is based on the MIRART (Modular InfraRed Atmospheric Radiative Transfer) line-by-line code, developed for arbitrary observation geometry, instrumental field-of-view and spectral response functions *(Schreier and Schimpf, 2001)*. Molecular absorption cross sections are calculated using spectroscopic line parameters from the Hitran, Geisa and other databases, together with optional continuum corrections (continuum corrections to the absorption coefficient are supported). Derivatives of transmission and/or radiance spectra are obtained by means of automatic differentiation. MIRART has been extensively verified by intercomparisons with other codes, e.g. in the framework of the EU study AMIL2DA.

The relation between forward model *F* and measured signal *I* is

$$F(x) = I(\nu) = r\, I_{sun}(\nu) \exp\left(-\sum x_m \tau_m(\nu)\right) \otimes S(\nu, \gamma) + b$$

where τ_m is the optical depth along the entire line-of-sight (Sun-ground-satellite) for the reference atmosphere, ν is the wavenumber and $S(\nu, \gamma)$ is the spectral response function. The state vector x to be retrieved comprises the column density scaling factors x_m, the slit function half width γ, the surface reflectivity (albedo) r and the baseline correction b. Note that the reflectivity r and the baseline b enter the forward model linearly and the least squares problem can be reduced to a separable nonlinear least squares problem. For the solution of the least squares problem, BIRRA uses solvers provided in the PORT Optimization Library based on a scaled trust region strategy. BIRRA provides the option to use a least squares with simple bounds (e.g., non-negativity) to avoid unphysical results.

Intercomparison of BIRRA and WFM-DOAS Carbon Monoxide for Orbit 8663

Carbon monoxide is an important atmospheric trace gas, highly variable in space and time, that affects air quality and climate. About half of the CO emissions come from anthropogenic sources (e.g. fossil fuel combustion), and further significant contributions are due to biomass burning. Our intercomparison of BIRRA and WFM-DOAS is based on SCIAMACHY Level 1c data of orbit 8663 (October 27, 2003) covering Russia, the Arabic peninsula, and Eastern Africa. In this observation period large biomass fires occurred, particularly in Mozambique, which should be clearly visible in CO column densities derived from nadir sounding instruments.

Contrary to what has been presented in the IMF-AP annual report of 2006, the new intercomparison is based on the same Level 1c dataset (spectra) provided by IUP/IFE Bremen. In fig. 3-9 we compare the 'xCO' data products, i.e., the retrieved CO column densities (averaged in 1° latitude bins) after correcting the effects of the ice layer formed in channel 8. Enhanced CO emissions over Southern Africa are found in both retrievals. The low signal measured over the ocean leads to a large scatter of the retrieval results in both approaches. These outliers are obviously removed. The averaging includes only data passing the quality checks (e.g., *physical* lower and upper bounds, *good* residuals, cloud free pixel). The plot shows a good correlation over the African continent, and – albeit different absolute numbers – similar trends over the northern hemisphere.

Response of the retrieved CO column to radiance perturbations

As mentioned before, channel 8 shows detector degradation making individual pixels unusable or at least unpredictable over time. Any CO retrieval is very sensitive to changes of the relative signal of individual pixels because of the weak signal. In order to identify pixels critical to the retrieval, a study of the response of the CO total column to individual pixel radiance perturbations has been performed. We used a synthetic spectrum as reference and made systematic individual pixel perturbations on it. Some pixels show a random behaviour with time, some cause systematic bias, and others have no effect at all *(Gloudemanns et al., 2005)*. Therefore the definition of a good bad/dead pixel mask is not trivial. As a consequence, it may occur that incorrect pixels, assumed to be reliable, are used in the retrieval model leading to a wrong fit.
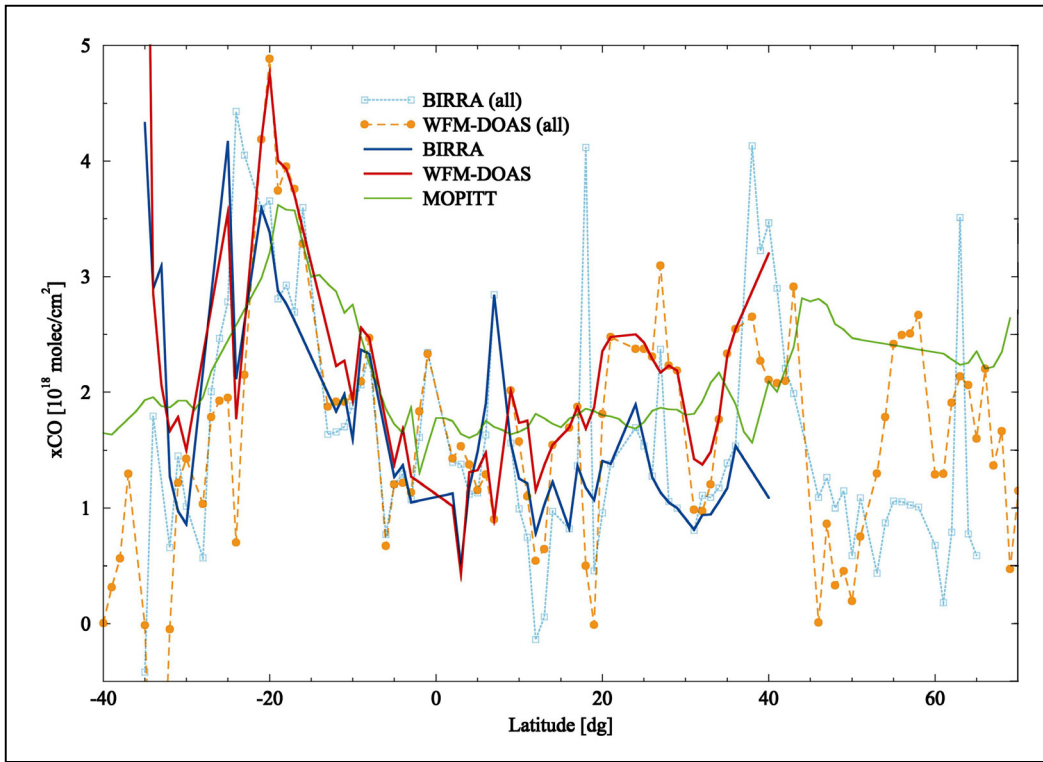
Fig. 3-9: Comparison between CO column densities derived with the BIRRA and the WFM-DOAS algorithms for SCIAMACHY orbit 8663 (October 27, 2003).

Figure 3-10 displays the response of the CO total column to individual perturbations on the spectral pixels, i.e. the synthetic spectrum is left unchanged except for one pixel in which we apply the modifications. The WFM-DOAS bad/dead pixel mask only leaves 51 pixels for the CO-retrieval. The location of these pixels is represented as small blue squares on the vertical axis of the left plot. The CO absorption cross section within this spectral window is also shown. As we fitted the spectrum using the WFM-DOAS pixel mask, the radiance modifications were only applied to the aforementioned 51 pixels. The CO column response to the perturbed spectra is shown in the right plot. The horizontal axis represents the 20 perturbations labelled from 0 to 2, and the vertical axis the wavenumber interval. In total, 1020 simulations (51 pixels x 20 perturbations) were carried out. The pixel perturbations can be labelled as

$$\widetilde{I}_{ij} = a_i \times I_j^{syn}, \quad a_i = 0.1 \cdot i, \quad i = 0,1,...,19,20 \ / \ j = 1,2,...,51$$

where $\widetilde{I}_{ij}$ represents the radiance of pixel j perturbed by a factor α_i, and I_j^{syn} is the radiance of the reference spectrum.

The left plot indicates that only 6 CO spectral lines are present within this spectral window. Further, there are only useful detector pixels at the centre of 3 of these lines (centred at 4285 cm⁻¹, 4292 cm⁻¹, 4301 cm⁻¹, respectively), and some useful pixel at the right wing of a forth line at 4288 cm⁻¹. This means that the available CO information is not only weak but also scarce. As we can see in the righthand picture, the retrieval of the CO column including a wrong signal in one of the important pixels (those around the centre of the aforementioned lines), would lead to enormous errors, whereas modifications at the other pixels would have a small or no effect at all on the retrieval of the CO column. Note that the colour scale displays "times the reference CO column", so modifications in specially sensitive pixels may cause a retrieval of the CO column 40 times larger than its real value!

Outlook
The new intercomparison has shown that the use of a different Level 1 dataset has a significant influence on the retrieved CO columns. Furthermore, the selection of a good pixel mask for the CO retrieval turns out to be at least as important as the forward model itself. In order to obtain a high

quality CO product, it is not only important to have accurate forward models and inversion algorithms, but it is crucial to use accurately calibrated Level1 data.
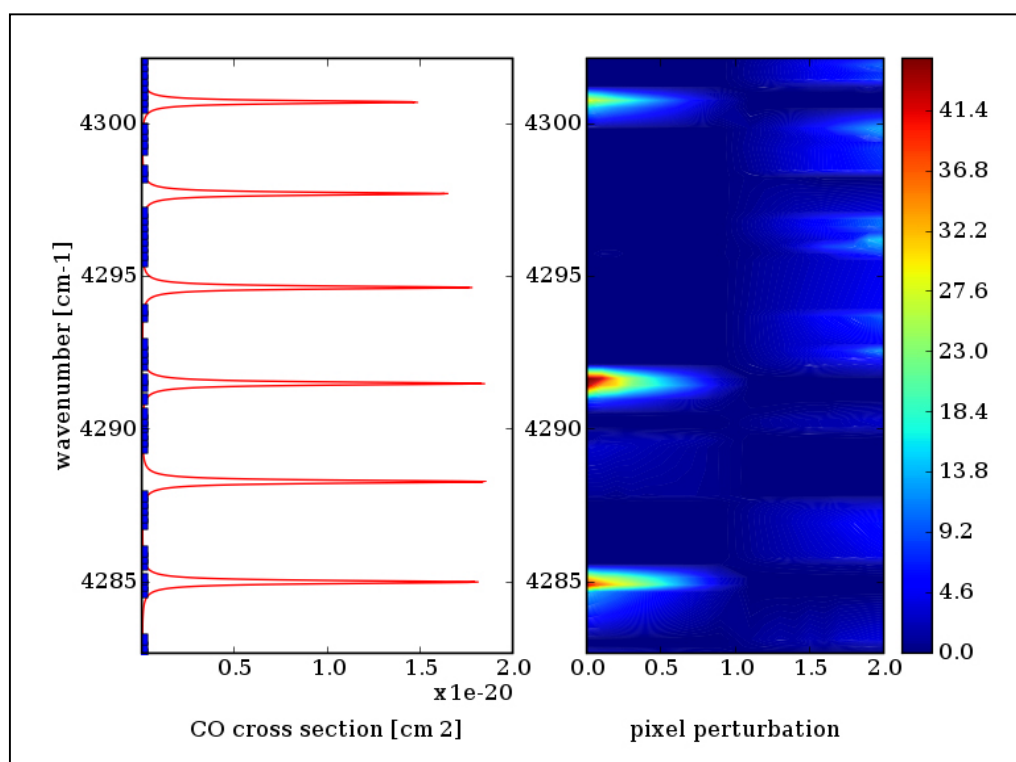

Fig. 3-10: Left: CO absorption cross section in WFM-DOAS fitting window. The blue squares on the vertical axis represent the locations of the pixels surviving the bad/dead pixel mask. Right: CO total column as a function of individual pixel perturbations. The CO columns are in units of the absolute reference value CO_{ref} =2.385E+18 cm^{-2}.

References

Bovensmann, H., J.P. Burrows, M. Buchwitz, J. Frerick, S. Noël, V.V. Rozanov, K.V. Chance, and A.P.H. Goede: SCIAMACHY: Mission objectives and measurement mode, J. Atmos. Sci., 56, 127-150,1999

Buchwitz, M., I. Khlystova, H. Bovensmann, and J. P. Burrows: Three years of global carbon monoxide from SCIAMACHY: comparison with MOPITT and first results related to the detection of enhanced CO over cities, Atm. Chem. Phys. Disc., 7, 405-428, 2007

Frankenberg, C., U. Platt, and T. Wagner: Retrieval of CO from SCIAMACHY onboard ENVISAT: detection of strongly polluted areas and seasonal patterns in global CO abundances, Atm. Chem. Phys., 5, 1639-1644, 2005

Gloudemanns, A.M.S, *H. Schrijver, Q. Kleipool, M.M.P. van den Broek, A.G. Straume, G. Lichtenberg, R.M. van Hees, I. Aben, and J.F. Meirink*: The impact of SCIAMACHY instrument calibration on CH4 and CO total columns, Atmos. Chem. Phys., 5, 2369-2383, 2005

Schreier, F., and B. Schimpf: A new efficient line-by-line code for high resolution atmospheric radiation computations incl. derivatives. In W.L. Smith and Y. Timofeyev, editors, IRS 2000: Current Problems in Atmospheric Radiation, p. 381-384. A. Deepak Publishing, 2001

Spurr, R.: SCIAMACHY level 1b to 2 off-line processing. Algorithm Theoretical Basis Document, ENV-ATB-SAO-SCIA-2200-0003, DLR-DFD and Harvard-CfA-SAO, 1998

3.8   SCIAMACHY Quality Working Group

G. Lichtenberg, M. Gottwald, A. von Bargen

The goal of the SCIAMACHY Quality Working Group (SQWG) is to intensify and to condense all activities around the evolution of the operational processing of SCIAMACHY data into one group being responsible for the evolution and improvements of the operational data processing chain from level 0 to level 2. The formation of such a group for SCIAMACHY follows the exercise successfully applied to the evolution of data processing of other instruments onboard ENVISAT. For the SQWG prime IUP/IFE, University of Bremen was selected. The focus of the SQWG is the so-called *Algorithm Baseline* which includes the processor prototypes of the operational processors, calibration tools, the user application *SciaL1c,* test data and procedures and all documentation needed to go from the prototypes to the operational processors. Clear procedures were defined in order to streamline the evolution of the processor and thus minimise the time needed for the implementation of new algorithms and the correction of errors in the processor.

Processor evolution approach
The approach follows the typical lifetime cycle for the operational processing. After finishing a version of an operational processor and integration into the ground segment, the products are subject to validation. The identification of deficits of the operational products during validation has to be taken into account in the evolution and improvement cycle – either in case of severe deficits before releasing the final version of the processor (then at least a verification of the improved algorithms is required), or for the next evolution step. The results of the algorithm evolutions and improvements are subject to the implementation in the prototype environment of the operational data processors. The activities can be broken down in three main tasks:

1) *Algorithm Baseline Maintenance and Evolution:* DLR-IMF is responsible for the prototype development and documentation of the prototypes and the operational implementation of the Level 2 offline processor as well as for the user tool *SciaL1c* and the calibration tool *SciCal.*
2) *Level 0-1c Algorithm and Calibration Evolution:* SRON has the lead on the evolution and development of the calibration algorithms for SCIAMACHY.
3) *Level 2 Algorithm and Data Quality Evolution:* IUP/IFE has the lead on the overall development and improvement of level 2 products.

Note that each main task is further divided into subtasks, which are not necessarily covered by the task lead. Apart from the Algorithm Baseline Maintenance, IMF has several work packages in the development of level 0-1 algorithms and level 1b-2 algorithms (notably Limb profile retrievals and retrieval in the IR wavelength range). The Belgian Institute for Aeronomy (BIRA) is also part of the SQWG and develops operational Nadir trace gas retrievals within the third task. The overall coordination is done by a steering group that consists of the project leads of the participating institutes.

The ESA change procedures relevant to the SQWG are distinguished in two categories: the *Software Change Request (SCR)* and the *Software Problem Report (SPR).* A SPR is a problem report with respect to the implementation of current algorithm baseline. Contrary to SCRs, SPRs can only be opened by ESA. A SPR obliges the SQWG to resolve an inconsistency within the current algorithm baseline. SCRs comprise all reasonable changes and evolutions which are proposed for implementation to improve the algorithm baseline. SCRs can be initialised by ESA, SQWG members and experienced users via the change request (CR) procedure outlined below.

The logical flow to handle the CRs is captured in fig. 3-11. The CR mechanism starts with the opening of a CR. Since the SQWG core task is to improve the prototype algorithms, this is provided as a pre-step in the logical flow. In general, the CR is opened by a suggestion brought up to the SQWG coordinator and/or via ESA to the SQWG, the agencies themselves or the SCIAMACHY Science Advisory Group (SSAG) and its sub-groups or the interested data users. This includes SQWG internal generation of CR for example from level 2 feedback on potential level 1 data quality improvements. The suggestions are checked by the SQWG and – if necessary – by additional experts for inclusion in the processor.
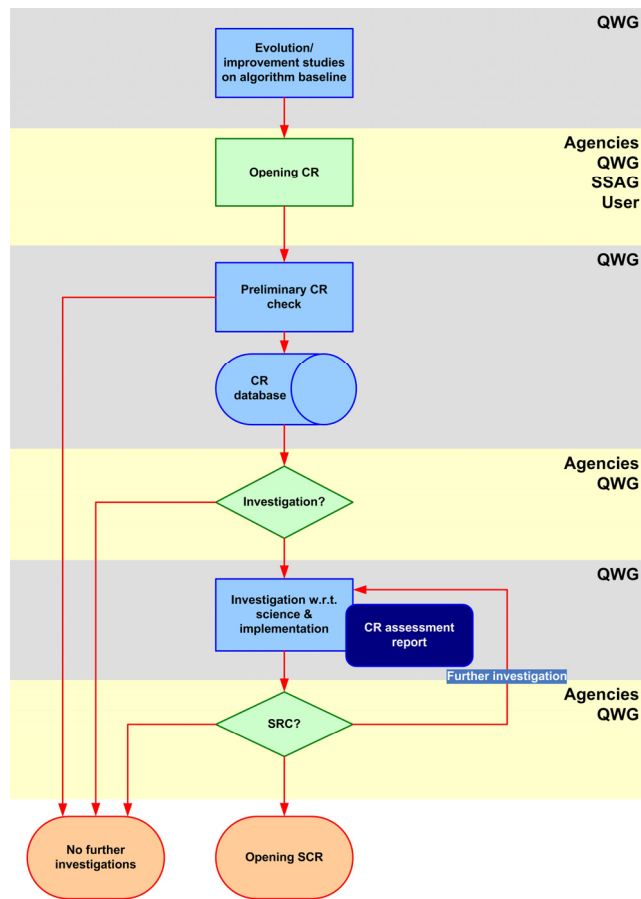
Fig. 3-11: Logical flow of a CR. Steps which are accomplished by SQWG only are highlighted while steps which are carried out in cooperation with agencies or others are not. Additionally, the parties involved are provided for each phase.

The decision criteria are user needs, affordability of change, and feasibility of operational implementation and availability of resources. Note that three different decisions are possible

- opening a SCR, which implies an implementation in the processor
- denial of the CR
- recommendation for further investigation.

In case a CR is recommended to become an SCR, the prioritisation with respect to the already approved SCR's needs to be agreed by SQWG and ESA, taking also into account user needs. Note that the above outlined description of CR handling implies SCR as a logical consequence of this handling, but it shall be noted that ESA can open directly a SCR, if they are convinced of its justification.

The logical handling of a SCR is illustrated in fig. 3-12. The processing of the SCR is straightforward. The first step is the implementation which requires a technical description of the algorithm (ATBD), test data for the verification and also external data (e.g. climatological databases) where required.
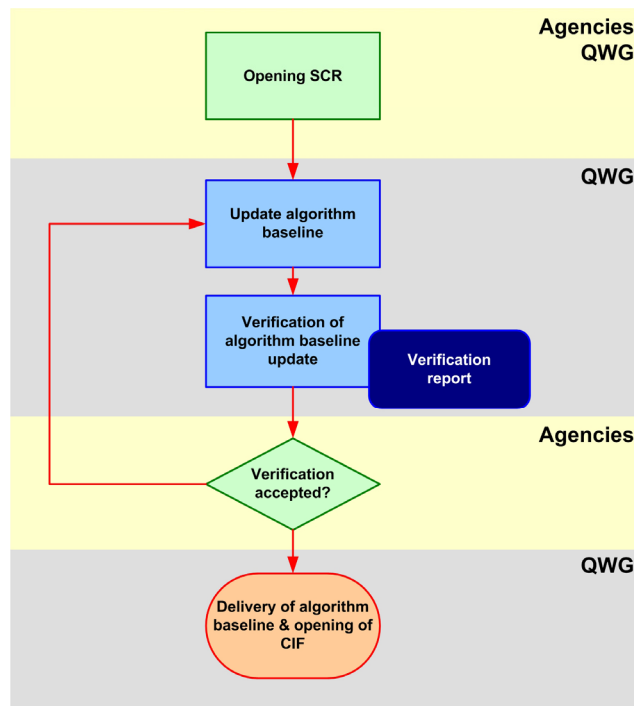
Fig. 3-12: The logical flow of the SCR handling. Activities under SQWG response are highlighted. Also shown are the entities which are in charge in each single phase.

After implementation, the verification of the algorithm baseline is prepared. The SQWG carries out the verification of an algorithm baseline and summarizes the verification results into a verification report. ESA will decide about acceptance of the implementation on the basis of the verification report and a presentation to ESA representatives. After acceptance of the algorithm baseline the documents will be finalised, proposed changes will be implemented, and the algorithm baseline will be delivered to ESA for implementation into the operational processing chain.

Anomaly handling of already operational processors is handled by opening a *Software Problem Report*. A SPR will be opened towards the currently implemented algorithm baseline if an anomaly investigation leads to the observation of an inconsistency. The SPR is exclusively opened by ESA. Since an inconsistency in the algorithm baseline needs to be removed to preserve the data quality, the SPR has high priority. The first step is to assess where the problem in the algorithm baseline is located. This is carried out in addition to the known assessment attached to the SPR. With the assessment the SQWG provides a solution scheme to ESA and will implement this solution scheme on ESA request. The SPR then becomes an SCR and the above described procedure is followed. At the end an updated algorithm baseline will be provided.

3.9   SCIAMACHY Operations Support

M. Gottwald, E. Krieg (TwIG), K. Reissig (IBR), J. How (TwIG)

The year 2007 was special for ENVISAT and SCIAMACHY since on March 1st, when the orbit 26138 had been finished, the nominal mission duration of 5 years was accomplished and the agreed extension until 2010 began. With the start of the routine phase in January 2003 the SCIAMACHY Operations Support Team (SOST), consisting of personnel from DLR/IMF-AP and IUP/IFE at the University of Bremen, became responsible for SCIAMACHY's measurement operations. In the past years we have contributed to the successful execution of the mission in close collaboration with representatives from the Quality Working Group (SQWG) and ESA (flight operations at ESOC, post launch support at ESTEC and payload data segment at ESRIN).

Our goal in 2007 was to maintain the high duty cycle and to satisfy the scientific requirements as good as possible. Both objectives have been achieved.

Operations Statistics

Fig. 3-13 displays the availability of the instrument. Of in total 5224 orbits only 175 could not be used since SCIAMACHY had been transferred to a mode lower than MEASUREMENT TIMELINE. Thus measurements were executed in 97% of all possible orbits. Within each orbit more than 90% of the orbital period were covered with states (scientific or calibration & monitoring).

Instrument anomalies were mainly failures triggered by Single Event Upsets (SEU). They originate in high energy particles, e.g. protons impinging onto instrument electronic components. In one case an incorrect on-board configuration was commanded leading to a brief interrupt of measurements. On platform level the service module (SM) unexpectedly switched off all instruments. For several orbits in May/June the subsolar observations were corrupted because the dish of the Ka-band antenna was blocking the Nadir Calibration Window (NCWM) due to a non-optimized parking position. Usually recovery from anomaly phases occurred fast such that data losses could be kept to a minimum. Slightly less orbits than those missed by failures were unavailable because of scheduled SM or orbit maintenance. The procedure for out-of-plane orbit control manoeuvres (OCM) had been modified by ESA at the beginning of 2007 in support of radar observations for the Internal Polar Year (IPY). Currently every 3 cycles (3 × 501 orbits) an OCM is planned where SCIAMACHY operates in MEASUREMENT IDLE mode only. Each OCM lasts for about 7 orbits. On a monthly basis only September and December exhibit availabilities below 90%. Even then one of the major contributors was always an OCM combined with SM maintenance activities.


Fig. 3-13: Instrument availability since launch
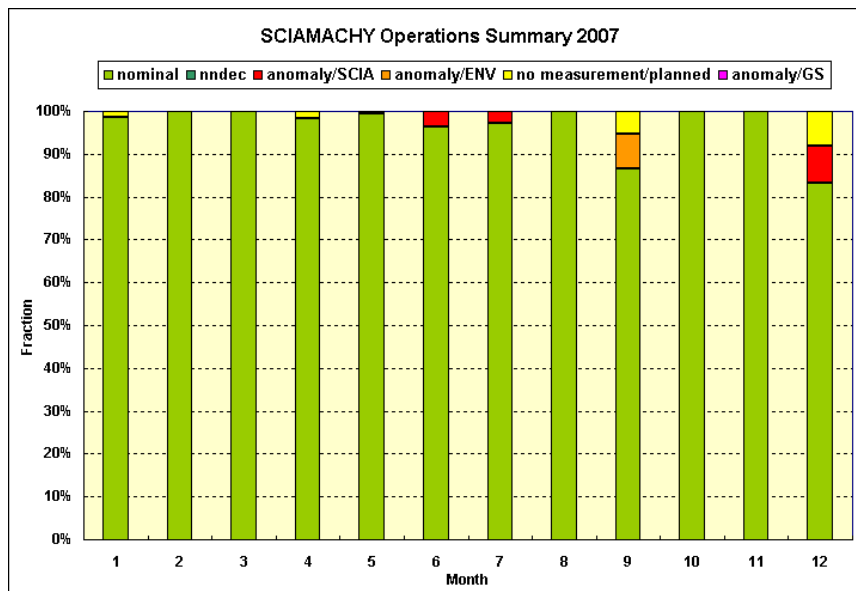
Abb. 3-14: Availability in 2007 on a monthly basis

Routine Operations

All routine operation tasks were executed as required. This concerns measurement planning, on-board configuration and long-term monitoring. The latter was adapted to the growing needs of the first mission extension. Components as e.g. the scanners – which were not considered critical during the nominal lifetime – are now regularly monitored. Particular attention required the *Operation Change Requests (OCR)* which transferred the routine final flight status in a temporary non-nominal configuration in support of specific test measurements. No permanent modification of the final flight settings occurred in 2007. In total 4 OCRs had been successfully implemented.

SCIAMACHY operations information was made publicly available via the SOST webpages (http://atmos.af.op.dlr.de/projects/scops/). The extent of the website has grown considerably such that ideas for a major re-configuration are being developed taking also the second mission extension (see chapter 3-12) into account.

3.10   SCIAMACHY Consolidated Level 0 Data

M. Gottwald, E. Krieg (TwIG), K. Reissig (IBR), J. How (TwIG)

By the end of 2007, SCIAMACHY onboard ENVISAT has executed more than 30000 orbits. Because of SCIAMACHY's high duty cycle the data archives host a large amount of high quality measurement data. This dataset is widely used in the Atmospheric Chemistry community. A complete and quality controlled level 0 dataset is the basis for further processing to level 1b and 2. Thus monitoring of the level 0 consolidation is a pre-requisite ensuring that the operational performance of the instrument is reflected in the data products generated by the ENVISAT ground segment. The task of monitoring the consolidated level 0 (cL0) products was an activity initiated by SOST at IMF-AP several years ago. Since 2007 it is partially supported by the ENVISAT PDS as an extension of the DPQC contract. Thus the status of cL0 verification became robust because it changed from a *best effort* basis to an operational function.

The delivery of SCIAMACHY consolidated data to the AOP is one of the AOP specific data interfaces in the PDS. For cL0 data, this interface has been technically implemented via an electronic link between D-PAC and the Data Information Management System (DIMS) of the German Remote Sensing Data Center (DFD) at DLR. The transfer from D-PAC to DIMS shall generate, over the mission lifetime, a complete data set of SCIAMACHY cL0 products. This data set shall serve as the cL0 master data set.

It is one of the basic properties of consolidated products that they represent the planned and executed measurements as precisely as possible. This is due to the fact that consolidation also refers to absolute

orbits in the same way as planning. Each consolidated product starts at the time when ENVISAT crossed a particular ANX and ends when this occurs for ANX+1. Therefore, the consolidated products are expected to contain all measurements for a specific orbit. Since SCIAMACHY executes timelines almost continuously from several minutes before sunrise to shortly before the end of eclipse, consolidated products must usually cover a complete orbital period. Only in cases of instrument unavailability, either triggered by a planned switch-off or an unexpected platform or instrument anomaly, the consolidated product does not exist or may deviate from planning.

Consolidated Product Consistency Checking

Consolidated products have been generated at LRAC and delivered to D-PAC for a period starting mid 2002. With the beginning of cL0 delivery, several inconsistencies had been observed. They included:

- orbits are not covered by cL0 products although SCIAMACHY was operational.
- orbits are covered by cL0 products but the product duration does not comply with the actually planned and executed instrument operations in that particular orbit.
- for one orbit there can be more than one cL0 product. These products may be identical or different in content.
- cL0 products exhibit corrupt data (e.g. exceeding Reed Solomon correction threshold, sync bit errors). The occurrence of such products is non-uniform.

A pre-condition for a cL0 master data set is to identify and reject cL0 files transferred from LRAC to D-PAC containing any of the above listed inconsistencies. Therefore, prior to sending a data file from D-PAC to DIMS, a filter mechanism ensures the consistency of each product. A sequence of error checks is performed. Only files passing each check are finally transferred to DIMS. All others are rejected. The consistency check is based on information retrieved from filename, Main Product Header (MPH), Specific Product Header (SPH) and data format.

If a cL0 product does not contain all measurement data from the corresponding unconsolidated level 0 products, its product duration will be different from what is expected from planning. SOST maintains a database of measurement states with scheduled elapsed times for each orbit, based on the reference orbit. From this database, expected product durations can be determined and compared with the duration in the cL0 files. As long as the durations are within a margin of 80 sec (= duration of the longest state which might be executed close to ANX), the product is accepted. The reference orbit deviates from the predicted/restituted orbit by a few seconds. For states starting close to ANX this may lead to reference product durations which differ by a few hundred seconds from the actual durations. Such products are also rejected by the filtering mechanism. They must be manually inspected and transferred in a second step, if found acceptable.

Usually two parallel quality monitoring processes are operational. The first transfers current[2] cL0 products from D-PAC to DIMS. It maintains a continuous cL0 status for those orbits which had been executed rather recently. The second requires interactions between SOST and ESRIN and processes historic[3] cL0 data as these stem from past years. At the end of both processes the final cL0 statistics for a each year, starting mid 2002, can be elaborated.

Our goal is to establish a cL0 master archive which contains more than 95% of all orbits of a year meeting the specified quality criteria described above. The remaining few % can usually be attributed to one of the above listed inconsistencies.

Current Consolidated Level 0 Status

At the end of 2007 cL0 products of more than 25000 orbits have been successfully quality checked and transferred to DIMS. The status of individual years can be seen in fig. 3-14. It is also described in much more detail on single orbit level at the SOST website (http://atmos.caf.dlr.de/projects/scops/). For the level 0-1b and level 1b-2 re-processing in 2007 the information of quality checked cL0 files had been extracted from DIMS and used by the PDS to ensure consistency in the re-processed data sets. This PDS activity was the first 'operational' test where the cL0 master archive idea proved to be rather useful.

---

[2] Current cL0 products are those which are continuously transferred from LRAC to D-PAC
[3] Historic cL0 products are those which result from re- or backlog generation.

cL0 Availability - 2002 (Cycle 8-12)

cL0 Availability - 2003

cL0 Availability - 2004

cL0 Availability - 2005
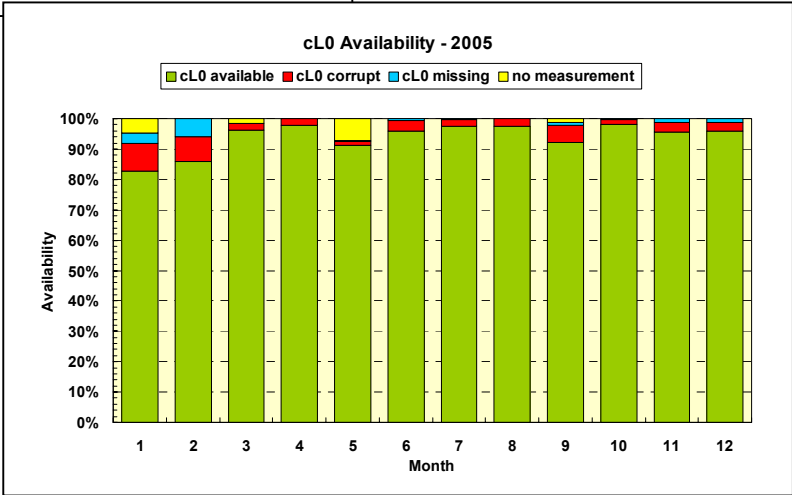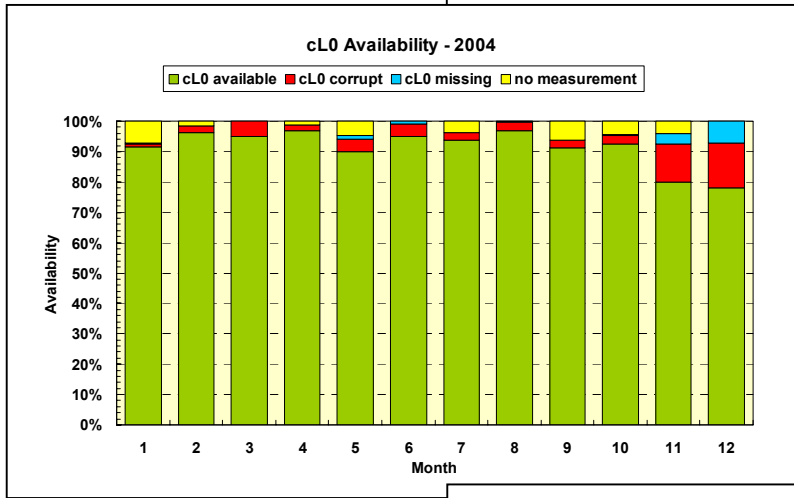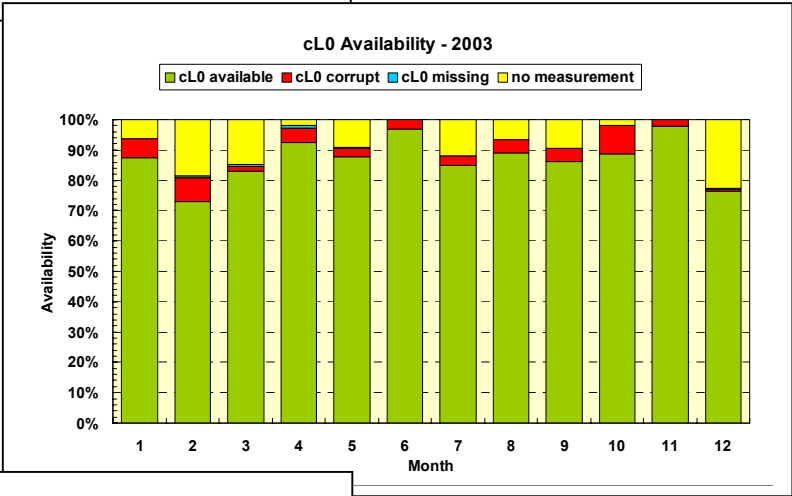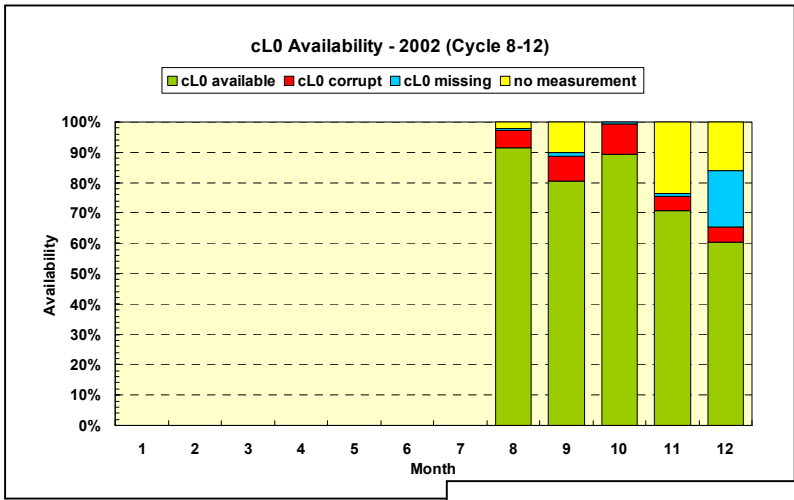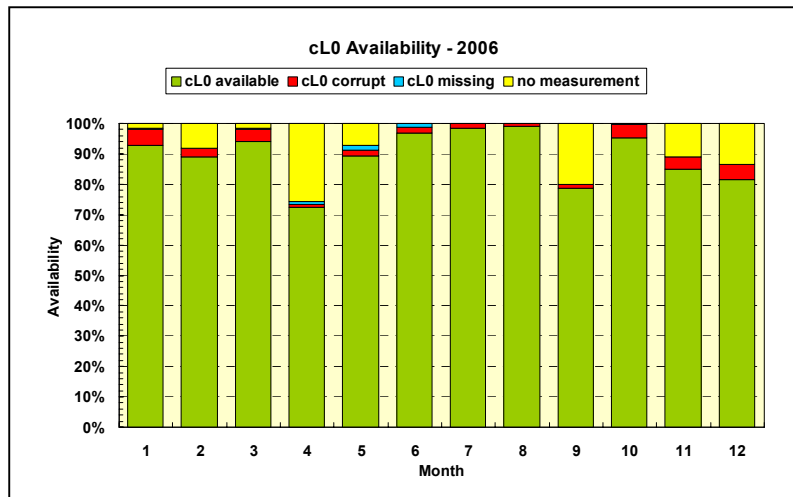
Fig. 3-14 (continued from previous page): cL0 statistics for the years 2002-2006 (from top to bottom).

3.11 SCIAMACHY Extra Misalignment Model

M. Gottwald, E. Krieg (TwlG)

Certain geolocation parameters derived in the early analyses of SCIAMACHY's limb measurements deviated from the expected values. After a corrective action in the ENVISAT flight operation segment concerning state vector parameters the situation improved significantly. However small inconsistencies persisted. These included a still existing bias and a left-right asymmetry in the limb tangent heights. Since the quality of limb results was severely hampered by those effects an explanation together with a quantitative correction was required. We tackled the problem by assuming that the inconsistencies originate in additional small line-of-sight misalignments. This view was triggered by the known azimuth/elevation features observed in solar occultation and sub-solar measurements around times when scanner control is switched from prediction to Sun Follower. In a model approach these specific measurements of SCIAMACHY were used to quantitatively determine extra misalignments in pitch, roll and yaw.

Observed Line-of-Sight Anomalies
SCIAMACHY's line of sight exhibits small inconsistencies in certain solar measurements (see fig. 3-15). These include in the

- Sun Occultation & Calibration (SO&C) window
  - an elevation jump of about -0.04 deg when acquiring the Sun with the Sun Follower (SF) in elevation above the atmosphere
  - an azimuth jump of +0.1 deg when acquiring the Sun with the SF in azimuth at an altitude of 17.2 km
- subsolar window
  - an elevation jump of about -0.02 deg when acquiring the Sun with the SF in elevation above the atmosphere
  - a time shift of the maximum signal of the Sun w.r.t. the subsolar state centre

The SO&C state 49 is executed each orbit except when in a daily calibration state 47 is scheduled. State 53 is the subsolar pointing state which was, until October 2006, only run as part of the monthly calibration.
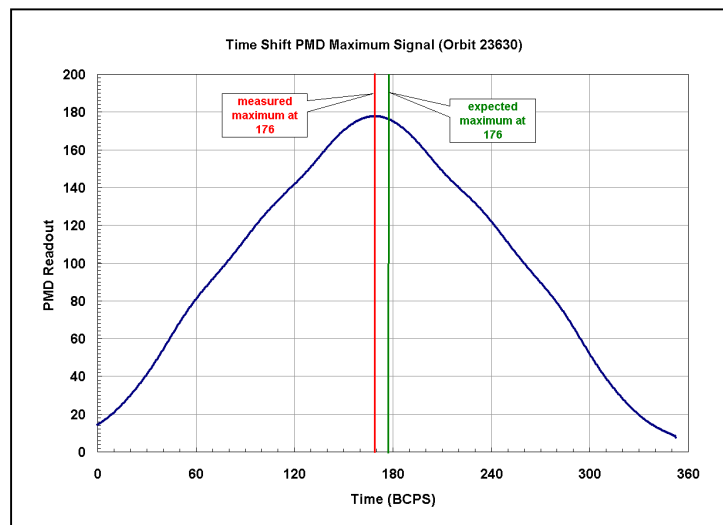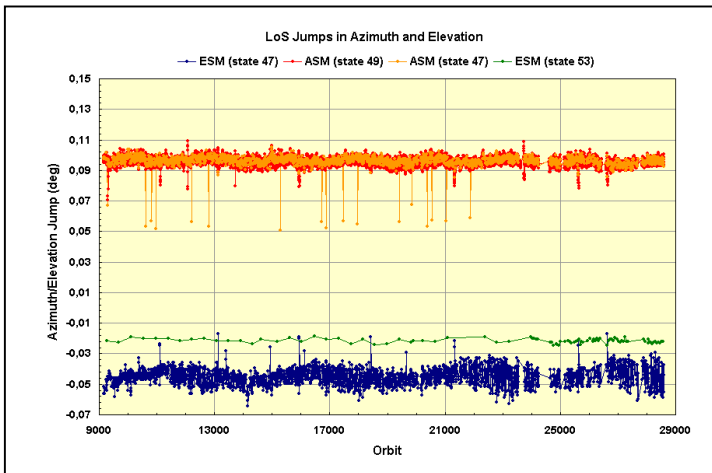
Fig. 3-15: Measured ESM & ASM jumps as derived from scanner readings in solar measurements (top) and an example for a shifted subsolar signal (bottom). Here the maximum is obtained slightly earlier than expected, indicating a deviation of the actual from the predicted LoS.

Extra Misalignment Model

The Extra Misalignment Model (EMM) assumes that the cause for the LoS anomalies in the SO&C (the azimuth jump of state 47 is excluded because it does not manifest in the subsolar measurements – specific test measurements in April have indeed shown that the azimuth jump might be attributed to an additional offset of the ASM) and subsolar measurements is also responsible for the tangent height inconsistencies. In general, the origin of the LoS anomalies could be related to

- extra instrument misalignment (pitch, roll, yaw)
- ESM/ASM offset
- extra platform mispointing (pitch, roll, yaw)
- mission planning and scheduling s/w (CFI, SCIACAL)
- scanner control s/w
- Sun Follower control loop

The EMM describes the discrepancies by small extra misalignments. These might mainly result from an extra instrument mispointing but as long as contributions from other sources could be split into pitch, roll and yaw components, these are included as well (note that the platform mispointing is described in the AUX_FRA files). The EMM approach has the advantage that it can be implemented in operational processing via the pitch, roll, and yaw mispointing angles in the TARGET routine of the ENVISAT CFIs. How small pitch, roll and yaw extra misalignments impact the elevation and azimuth scanner readings, i.e. potential jumps, depends on the selected viewing geometry.

The EMM simulates the observed scanner jumps or signal time shifts by modeling azimuth and elevation with the ENVISAT CFIs (see fig. 3-16). Various misalignment configurations are necessary since measurement execution is controlled differently in states 53 and 47 or 49.

Since some axes are not independent, a full 3D approach was not feasible. Instead the best fit extra misalignments were derived using an iterative method by sequentially fixing two extra misalignments while the third was varied to find the best fit value. Known boundary conditions limit the possible ranges of the extra misalignment (e.g. the elevation jump in the subsolar measurement limits the extra misalignment in roll to about -0.020 deg). With a minimum step size of 0.001 deg the best fit extra misalignments were found to be

pitch = -0.026 ± 0.003 deg, roll = -0.020 ± 0.001 deg, yaw = +0.009 ± 0.008 deg

Verification

The EMM results were verified using the findings from tangent height investigations of SO&C scanning measurements which yielded a mean offset of -2 km for a nominal solar tangent altitude of 25 km. Our best fit extra misalignments produced in the SO&C window a solar centre tangent height offset of -2.02 ± 0.08 km (at 25 km) and -1.92 ± 0.08 km (at 100 km) in good agreement with what was derived independently in the solar scanning analysis. Without the platform contribution the expected limb tangent height offset from the extra misalignments amounts to 1.4-1.5 km over the entire orbit with an estimated accuracy of 0.003 deg, i.e. approx. 150-200 m.

All three mispointing angles were implemented in the geolocation routines of the operational processor and used for the re-processing activities in 2007. This improved the retrieved limb tangent heights such that the value of the operational limb products increased significantly.
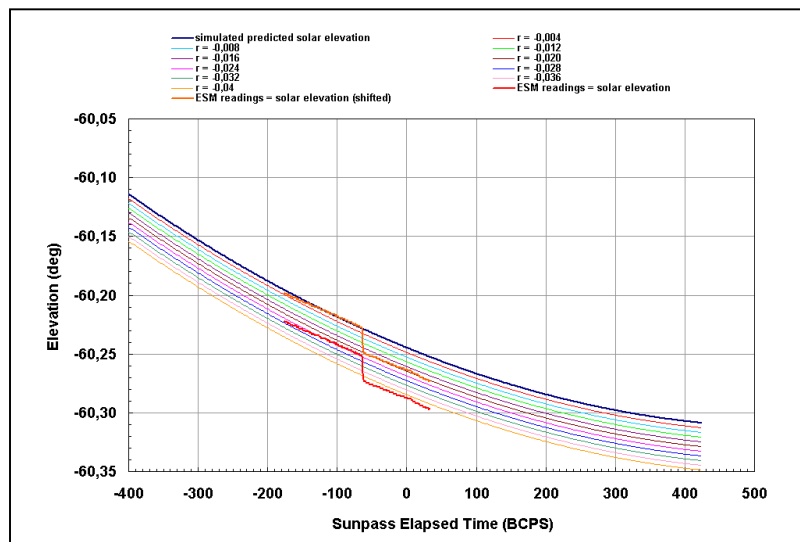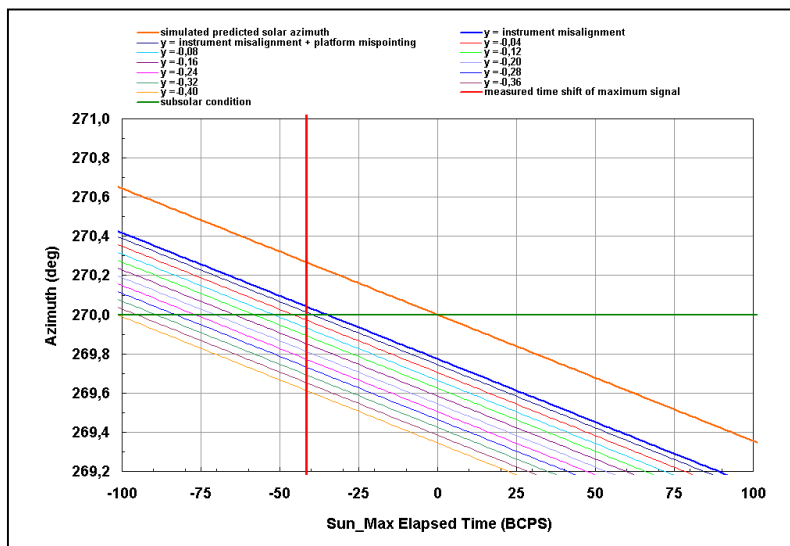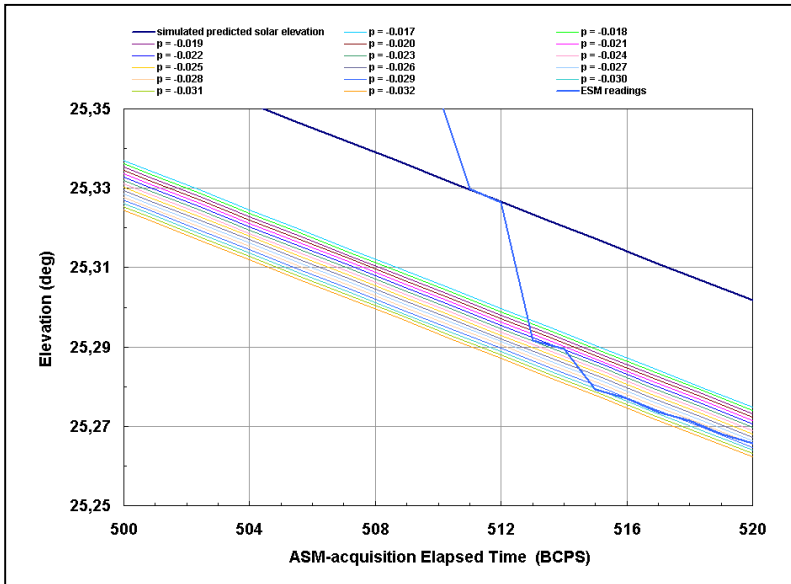
Fig. 3-16 (continued from previous page): Example EMM simulations for orbit 19822 with subsolar time-shift (top left, yaw variation), subsolar elevation (top right, roll variation) and SO&C elevation (bottom, pitch variation). The parallel lines represent different extra misalignment for a single axis while the other two extra misalignments were fixed at the most likely value.

3.12 SCIAMACHY Mission Extension

M. Gottwald, E. Krieg (TwIG)

In March 2007 ENVISAT has entered the first phase of its mission extension lasting until 2010. Because of the excellent status of the mission ESA has started to derive a concept allowing a further extension beyond 2010 until about 2014. This second phase of mission extension shall start October 2010 by decreasing the altitude of ENVISAT and adjusting to a new repeat cycle (table 3-1). The altitude lowering manoeuvre disposes ENVISAT from its current orbit as required by rule. It consumes most of the remaining fuel but leaves sufficient margin for further altitude manoeuvres, although a slight altitude drift is considered acceptable. However no more inclination manoeuvres shall occur. Thus the inclination and Mean Local Solar Time will drift slightly.

Modified Orbit Parameter	
Geodetic altitude at ANX	769.84 km* with altitude drift = -74 m/year
Orbital period	6014.06 sec* with orbital period drift = -0.087 sec/year
Inclination	98.55°* with inclination drift = -46 mdeg/year
Repeat cycle	30 days / 431 orbits
MLST	22:00 ± 10 min (22:10 in June 2012, 21:50 in August 2014)

* at start of extension in October 2010

Table 3-1: Parameters of modified ENVISAT orbit in second mission extension phase

The proposed scenario requires to show that SCIAMACHY is in good condition when the extension starts in 2010 and still delivering useful results at the end of the extended lifetime in 2014. The in-orbit performance is driven by two parameters

- Time: With evolving time the subsystems of the instrument degrade. Thus *Begin of Life (BOL)* properties cannot always be maintained. When reaching the *End of Life (EOL)* milestone the

scientific requirements are usually still met but beyond this date the in-orbit performance has to be extrapolated from what has been observed during nominal mission lifetime.

- Orbit: SCIAMACHY as an instrument with multi-viewing capabilities is strongly dependent on the status of the LoS during measurements. Since LoS control is based on the current ENVISAT orbit, the instrument settings (e.g. scanner control) have to be analysed and items needing reconfigurations must be identified.

In 2007 SOST has started investigations to assess both time/degradation and orbit aspects of those items falling under our responsibility. This work forms the basis for SQWG to analyse the impacts on retrieval algorithms and data products. In addition we established an interface to industrial support in those areas where industry is still the leading entity, e.g. on-board s/w maintenance. Goal of these activities is to obtain a good understanding of the expected instrument performance and to specify modifications to instrument settings.

Mean Local Solar Time Variations
It was of main interest how far the MLST is allowed to drift until instrument operations become severely affected. SCIAMACHY has been designed for a specified MLST of 22:00 ± 5 min at ANX. Thus modifications exceeding this range are expected to affect SCIAMACHY operations in various ways. The change in orbital parameters alters the LoS to the Sun and the moon, i.e. solar and lunar events along the orbit occur at times different from the reference orbit. Also angular relations, e.g. azimuth and elevation, between the platform and the Sun or the moon will not remain stable. Since SCIAMACHY operations are entirely linked to solar and lunar events a careful analysis was required to study these effect. As an additional consequence of the modified angular relations the external thermal environment, depending on solar illumination, needed further attention.

For the full implementation of SCIAMACHY's operations concept about 100 parameters are usually derived from operation simulations over a full year. This number was reduced in our analyses due to time constraints. We investigated the seasonal behaviour of the following parameters:

- Duration of
    - SO&C window: from sunrise (including refraction) to when the Sun leaves the limb TCFoV
    - MO&C window: from moonrise (including refraction) to when the moon leaves the limb TCFoV
    - SO&C end to eclipse start: from when the Sun leaves the TCFoV to sunset (including refraction)
    - SO&C end to center of subsolar window: from when the Sun leaves the TCFoV to when the Sun crosses the center of the subsolar window
    - SO&C end to start of MO&C window: from when the Sun leaves the TCFoV to moonrise (including refraction) in each monthly lunar visibility window
    - Subsolar center to eclipse start: from when the Sun crosses the center of the subsolar window to sunset (including refraction)
    - Subsolar center to MO&C start: from when the Sun crosses the center of the subsolar window to moonrise (including refraction) in each monthly lunar visibility window
    - MO&C end to eclipse start: from when the moon leaves the TCFoV to sunset (including refraction)
    - Eclipse: from sunset to sunrise (both including refraction)
- Solar azimuth at SO&C start
- Solar elevation at subsolar center
- Lunar phase at MO&C start.

These 12 parameters are representative for illustrating the impact of MLST variations. The final three parameters are particularly interesting for calibration & monitoring measurements as they define the seasonal visibility of the Sun and the moon. All other parameter indicate possible changes to timeline definitions.

The results obtained showed that overall the current SCIAMACHY operations concept is capable of handling the proposed MLST variations. Potentially some states and timelines might require modifications. Only at the extreme excursions from 22:00, i.e. 22:10 and 21:50 gaps of about 40 days duration will occur in subsolar measurements due to the annual variability of the solar elevation (fig. 3-17). However SQWG has already stated that this does not endanger the quality of calibration & monitoring parameters.
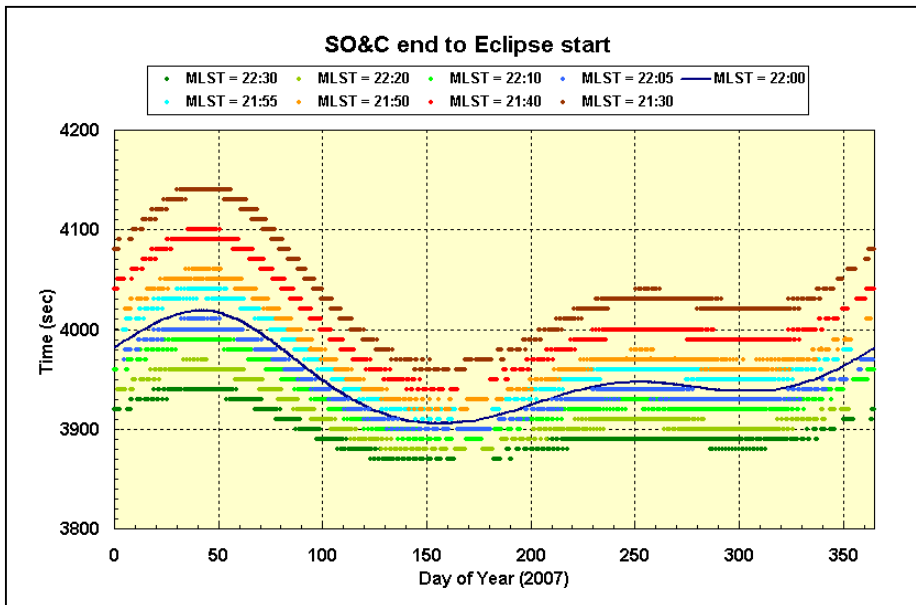
Fig. 3-17: Duration of orbit phase from end of SO&C window to start if eclipse for various MLST settings.
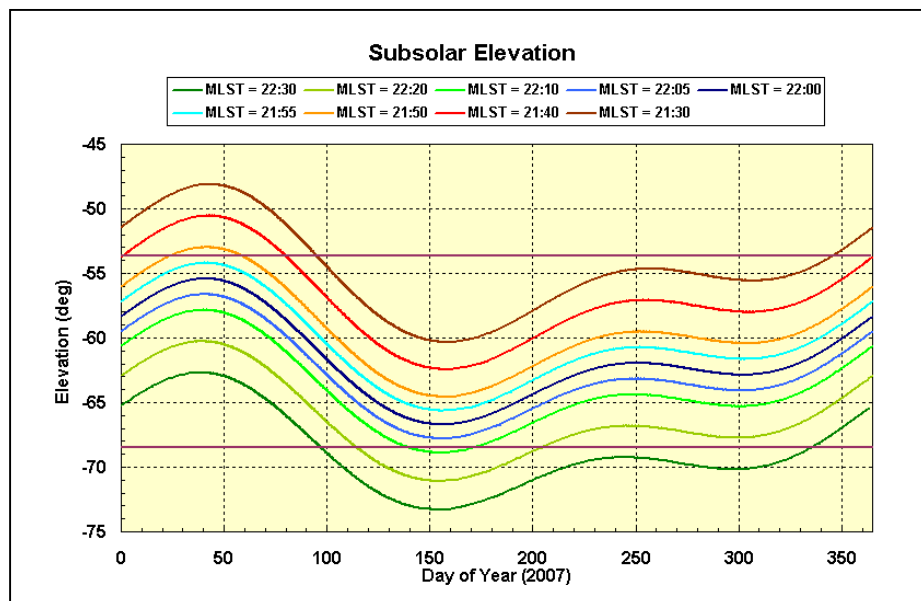
Fig. 3-18: Elevation of the Sun in the subsolar window for various MLST settings. The horizontal lines represent the elevation limits of the subsolar TCFoV.

In-orbit Instrument Performance
The quality of SCIAMACHY measurements is determined by the performance of the instrument's

- Optics: The optical throughput typically decreases with time as a consequence of degradation of optical components. In addition detector parameters, e.g. dark current, pixel quality, exhibit ageing effects.
- Thermal systems: Both thermal systems (ATC and TC) degrade at a rate much smaller than predicted. While the ATC controlling the OBM temperature is expected to have sufficient margin to stay within limits, at least one of the detectors may not as the heaters of the TC system could reach their lower limit of 0 W.
- Line-of-Sight: Scanner control will require update of on-board settings due to the modified orbit. This is industry's task with support from SOST. Both scanner motors show no signs of degradation.
- Life Limited Items: In-flight activations of the defined LLIs are regularly monitored to stay within the allocated in-flight budgets. No violations are predicted until 2014.

36

- Operations: All orbit related changes to states and timelines can be implemented using the current operational interfaces. This is also true in case mission scenarios have to be changed, e.g. due to new calibration & monitoring requirements.

A TN has been produced which describes all currently available performance aspects of these items. The results presented therein are to a large extent based on regularly executed instrument monitoring activities illustrating mainly degradation effects. The TN shows particularly that the extrapolated behaviour of optical components and the thermal subsystems still ensures high quality measurements. No showstoppers for a mission extension were identified such that the proposed mission extension scenario is fully supported by SCIAMACHY.
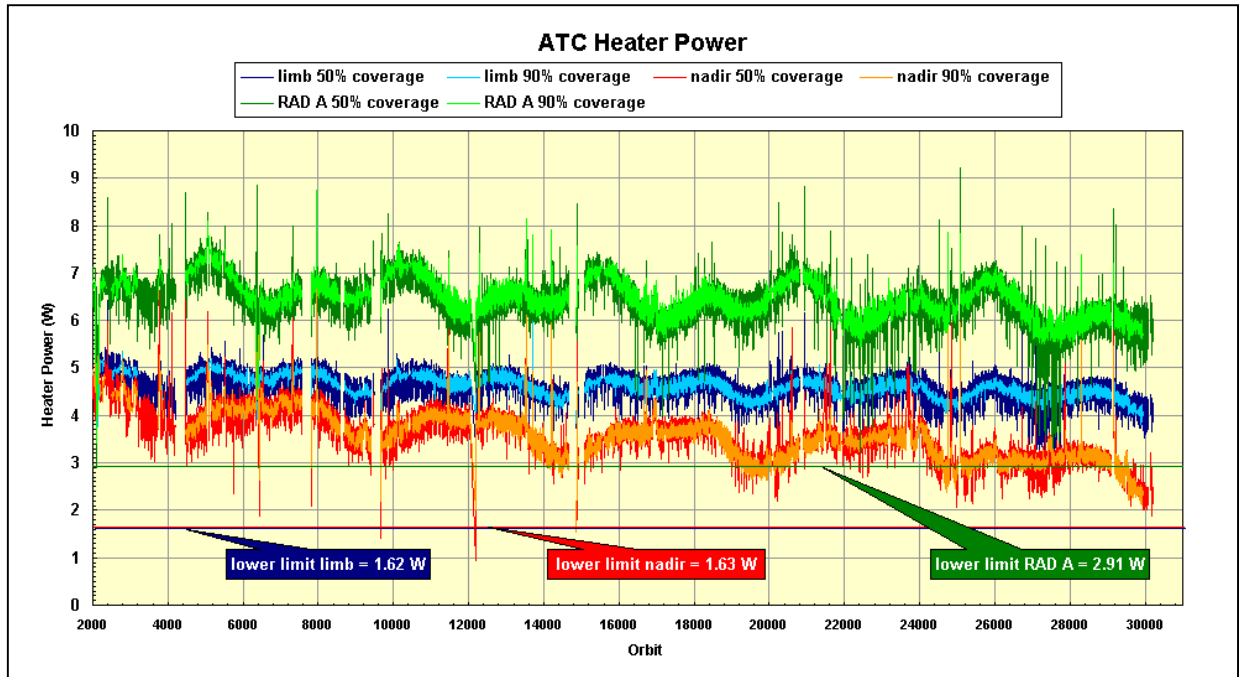
Fig. 3-19: Average ATC heater powers per orbit over 5 years of routine operations. For each heater two curves display orbits with 50% and 90% HK telemetry coverage. The degradation of the nadir heater (red) is most obvious.
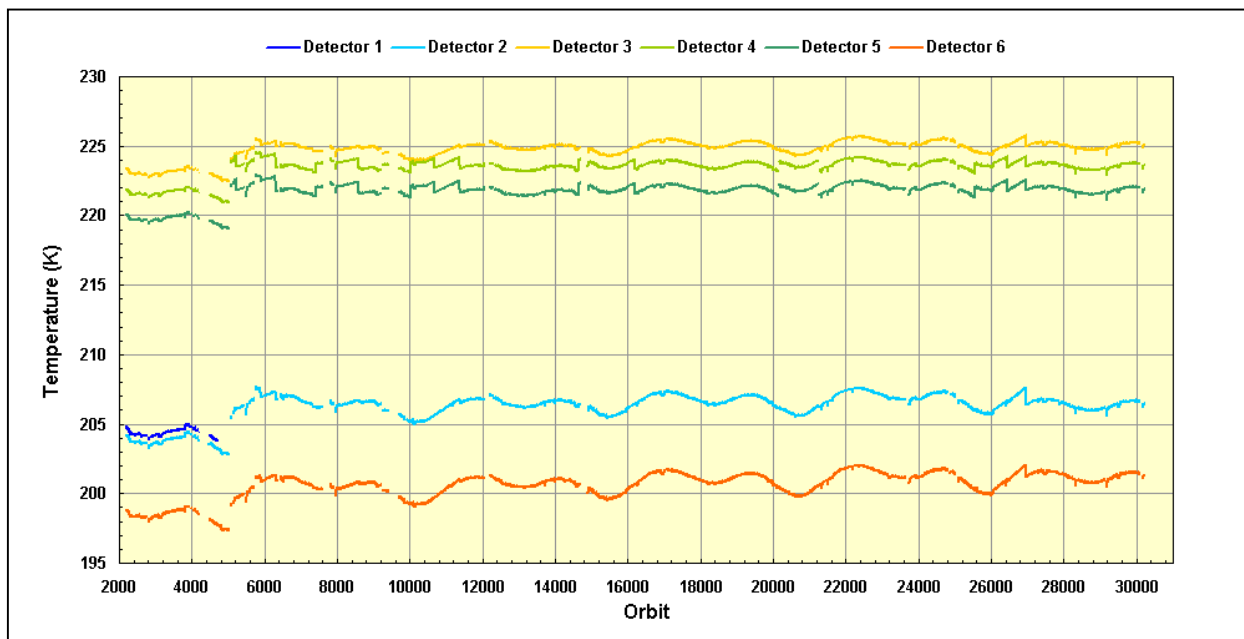

Fig. 3-20: Average detector temperatures (channels 1-6) per orbit over 5 years of routine operations. Periods with decontaminations or recovery after transitions to modes lower than MEASUREMENT are excluded.
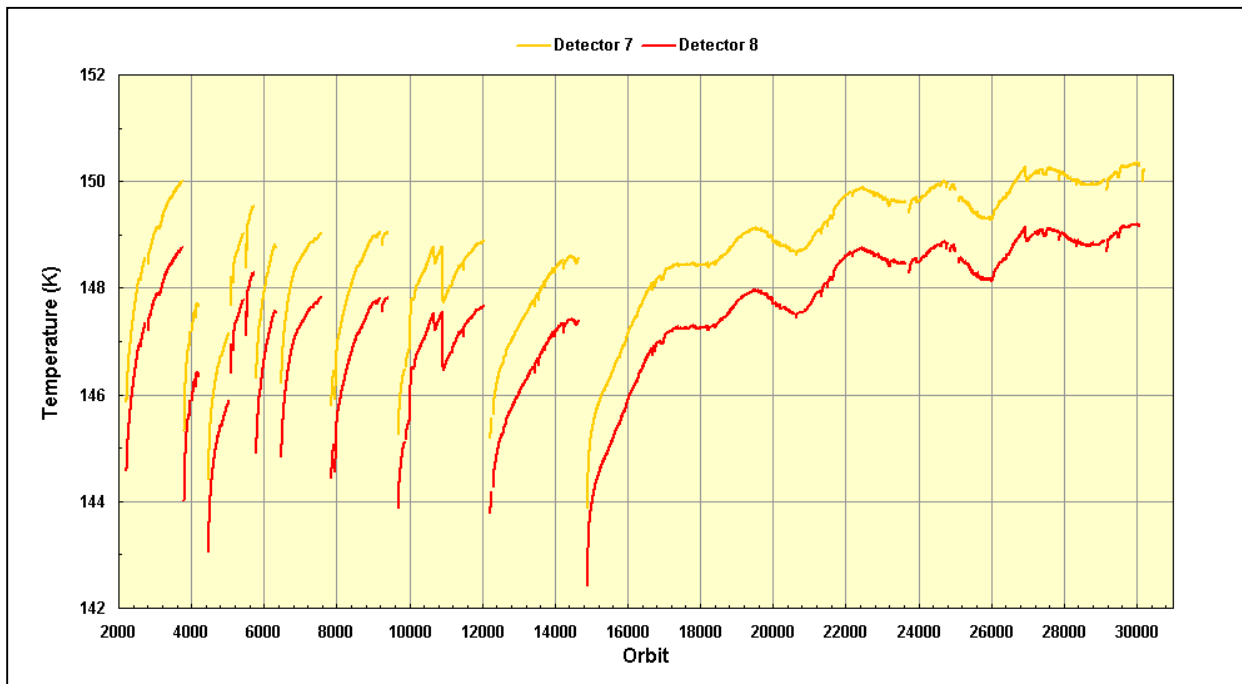
Fig. 3-21: Average detector temperatures (channels 7 & 8) per orbit over 5 years of routine operations. Periods with decontaminations or recovery after transitions to modes lower than MEASUREMENT are excluded.

3.13 PFUI and CLUMP – Interfaces to Atmospheric Radiative Transfer Codes

F. Schreier

Atmospheric radiative transfer (RT) is depending on a large variety of input data, i.e. spectral range, state of the atmosphere (pressure, temperature, concentration of gases and aerosols), and path geometry. Furthermore, the microphysical parameters of the absorbing and scattering atmospheric constituents have to be known, that are usually taken from databases such as HITRAN, GEISA, OPAC. Thus, setting up a RT calculation can be a challenging task, and the 'input file' (job specification file etc.) of state-of-the-art RT models can easily comprise dozens or even hundreds of lines. On the other hand, the parameters controlling the execution of the widely used FASCODE line-by-line (lbl) and MODTRAN band models (developed by Phillips Laboratory, formerly Air Force Geophysics Labs, US) are given in moderately short, but formatted and un-annotated file called TAPE5 that appears rather cryptic to new users. As a compromise, the MIRART line-by-line code developed at DLR-IMF uses Fortran NAMELIST's allowing an annotated, yet terse specification of control parameters.

Graphical user interfaces (GUI) and web browser interfaces have become popular means to improve ease of use of moderately complex codes, and DLR's *Virtual Lab* provides access to several radiative transfer codes. However, although well designed GUI or web interfaces allow running RT programs even for novices or casual users, command line interfaces can be advantageous for advanced users who want to perform dozens of RT calculations, but do not want to care about the intricacies of editing a correct input file and submitting the job. Furthermore web interfaces are not available on laptop's running offline.

In the course of migrating the FASCODE and MODTRAN web interfaces (implemented in Python) from Sun-Solaris to the department's Linux cluster, command line versions of these interfaces have been developed, too. The objective has been to enable lbl or band model calculations from the Unix/Linux command line with a minimal set of mandatory parameters *(Question: What is the minimal number of parameters required to set up an atmospheric radiative transfer?)*

PFUI (Python Fascode User Interface) and CLUMP (Command Line User interface for Modtran using Python) permit atmospheric RT calculations with only the spectral range (wavenumber etc) specified. In

the following some examples of PFUI are shown, usage of CLUMP for band model calculations is largely similar. Both interfaces provide extensive help by „`pfui -h`" or „`clump -h`". For certain topics more detailed information is available, e.g. „`pfui --help geometry`". Furthermore a set of examples can be listed using the command „`pfui --help examples`" and giving

```
pfui 2150 2200
---> transmission in 2150 - 2200 cm-1 spectral range,
     vertical path between bottom and top (default ToA 100km) of atmosphere,
     default (US standard) atmosphere, 7 main molecules

pfui -a mls -g 10 2150 2200
---> transmission for a vertical path between 10km and ToA, midlatitude summer

pfui -a saw -g 10,30 -s r 2150 2200
---> radiance, observer at 10km uplooking with 30dg from zenith, subarctic winter

pfui -a saw -H 5 -C 1 -g 10,170 -s r 2150 2200
---> radiance, observer at 10km downlooking with 10dg from nadir, subarctic winter,
     urban boundary layer aerosol (haze) and cumulus cloud

pfui -g 40,95.54 -s t,r 480 510 GHz
---> transmission and radiance in the microwave region,
     limb viewing observer at 40km with zenith 95.54dg

pfui -g 40,10km -S 1 -s r,rg0.1 480 510 GHz
---> two radiance spectra: monochromatic and convolved with gaussian of HWHM=0.1cm-1
     same geometry as before: limb viewing at 40km with 10km tangent point
     stratospheric background aerosol model

end of pfui help examples
```
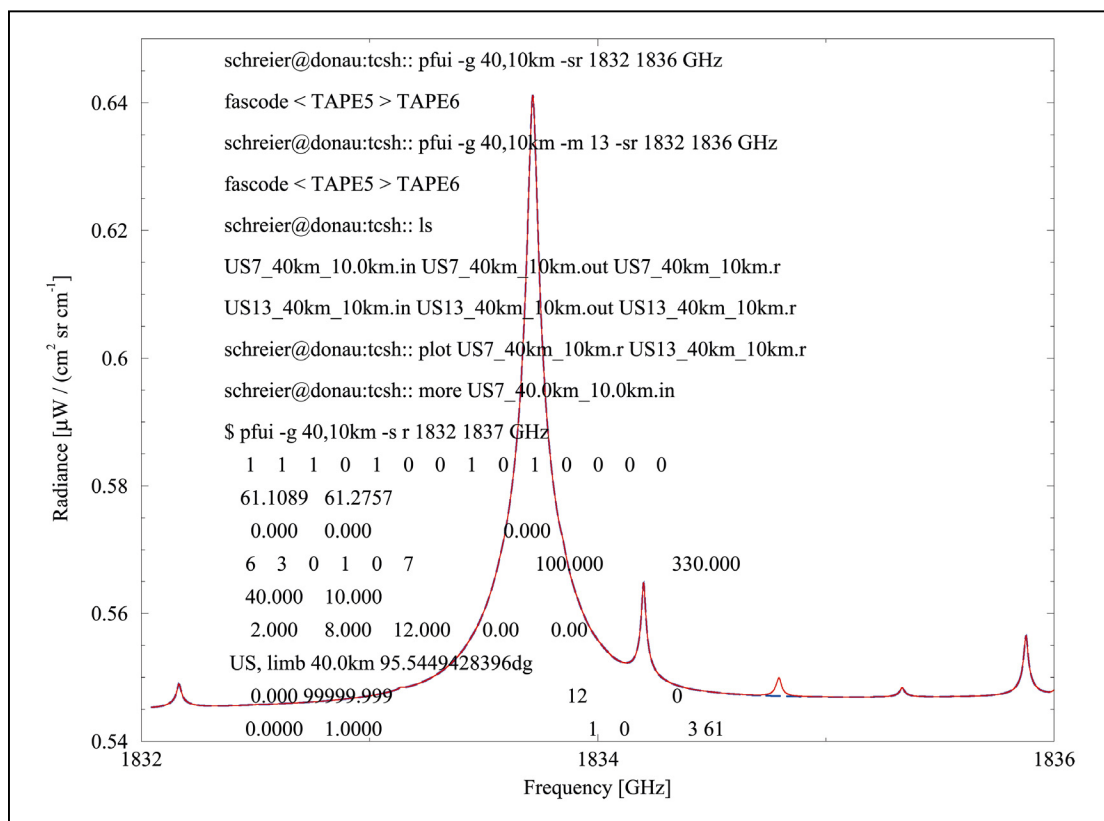

Figure 3-22: Example of two FASCODE calculations of the radiance in the TELIS OH microwindow region. The background shows a typical sample session to produce these results.

If a user wants to run a series of jobs with only a few parameters changing, e.g. computing spectra of a limb sequence, it can easily become boring to specify the common (but non-default) parameters again and again. In this case it is preferable to override some of the defaults provided by PFUI (or CLUMP) by means of an environment variable: The C-Shell command (or the equivalent bash command) `setenv PFUI 'm=28; ToA=75.0; CO2=350.'` will result in subsequent FASCODE calculations to be

performed with 28 molecules (default: the 7 main infrared absorbing molecules), a reduced top-of-atmosphere altitude, and an increased carbon dioxide concentration.

For historical reasons the input and output files required and produced by FASCODE (or MODTRAN) are named `TAPE5,` `TAPE6,` `TAPE7`, etc. In order to prevent overwriting of these files generated for each calculation, PFUI automatically renames the input, output and spectra files after successful execution of the job, i.e., the last example listed above would produce four files:

```
US7_40.0km_10.0km.in    US7_40.0km_10.0km.r
US7_40.0km_10.0km.out   US7_40.0km_10.0km.rg0.1
```

3.14   Optimization of Voigt and Complex Error Function Algorithms

F. Schreier

The convolution of a Lorentz and a Gaussian function, commonly known as the Voigt function, is important in many branches of physics, e.g., atomic and molecular spectroscopy, atmospheric radiative transfer, plasma physics, astrophysics. The Voigt function is identical to the real part of the complex error function

$$w(z) = K(x,y) + iL(x,y) = \int_{-\infty}^{\infty} \frac{e^{-t}}{z-t} \, dt$$

Unfortunately, these functions cannot be evaluated in closed analytical form and have to be computed numerically, and a large number of algorithms have been developed in the past. Rational approximations have been proven to be an efficient approach for a wide variety of functions, and have been used also for the complex error function. The complex rational approximation developed by *Hui, Armstrong, and Wray (1978)* achieves a relative accuracy of 6 digits

$$w(z) = \frac{\sum_{m=0}^{6} a_m \zeta^m}{\sum_{n=0}^{7} b_n \zeta^n} \quad for \quad \zeta = y - ix \qquad (1)$$

In many applications the Voigt or complex error function has to be evaluated for a moderate to large array of grid points x_i with $i=0,1,2,.....$ and constant y. A complex polynomial in z with real coefficients a can be written as a polynomial in x with complex coefficients depending on y. After some further re-arrangements rational approximations for $K(x,y)$ and $L(x,y)$ are obtained,

$$K(x,y) = \frac{\sum_{m=0}^{6} \rho_m x^{2m}}{\sum_{n=0}^{7} \tau_n x^{2n}} \qquad L(x,y) = \frac{\sum_{n=0}^{6} \sigma_m x^{2m+1}}{\sum_{n=0}^{7} \tau_n x^{2n}}$$

where ρ, σ, and τ are polynomials in y with coefficients depending on a_m and b_n. In contrast to the original approximation that requires complex arithmetic, the optimized approximation can be coded using real arithmetic only, resulting in more than halving the total number of floating point operations per grid point x.

For benchmark tests of these and some more versions of the *Hui-Armstrong-Wray* algorithm (implemented in Fortran) molecular absorption cross sections for high resolution 'line-by-line' atmospheric radiative transfer modelling in the microwave and infrared spectral range have been evaluated. The cross section is given by the superposition of many lines, each described by the product of a temperature dependent line strength and the Voigt line shape function describing the broadening mechanism. Cross sections of H_2O, HNO_3, and O_3 are computed in the Odin 501 GHz band for 13 pressure, temperature pairs (corresponding to atmospheric altitudes up to 120 km in 10 km steps) using

spectroscopic line parameter from the HITRAN database (note that the Sub-Millimeter Radiometer – SMR – onboard the small Swedish satellite Odin measures radiation in four spectral bands).

The computational speed up (i.e. the ratio of execution time for the new implementation to the original implementation) for the evaluation of molecular cross sections is depicted in fig. 3-23. For convenience the time required to calculate a simple Lorentzian is shown, too. The observed computational gain is in accordance with the reduced number of floating point operations. Furthermore the figure demonstrates that a continued fraction formulation is significantly worse. Comparison with the time required to calculate Lorentzian cross sections indicates that the total time is largely determined by the division. Thus, utilizing factorizations of terms independent of the grid point x and real number arithmetic results in a significant speed up, whereas further variations of the real polynomial evaluation (not discussed in detail here) gives minor changes. However, for very compute intensive applications the search for the optimum version for a given machine architecture and compiler might be important.
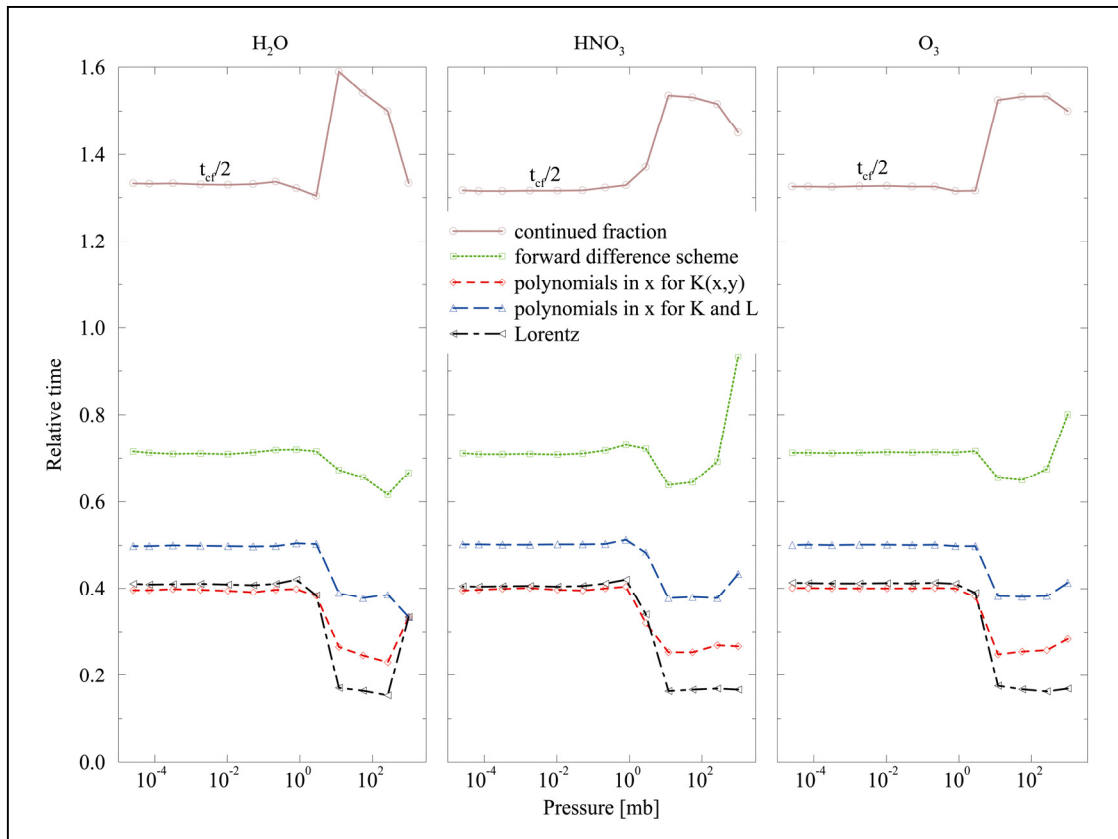
Fig. 3-23: Relative speed of implementations in units of the original algorithm equ. (1). Molecular cross sections for the range 16-17 cm^{-1}. Lines in the interval 6-27 cm^{-1} have been considered (left: H_2O - 153 lines, mid: HNO_3 - 2376 lines, right: O_3 – 21565, GNU g77 compiler, version 3.3.4). Note that the times for continued fraction have been scaled by a factor 0.5.

References:

Hui, A.K., B.H. Armstrong, and A.A. Wray: Rapid computation of the Voigt and complex error functions. J. Quant. Spectrosc. & Radiat. Transfer, 9, 509-516, 1978

3.15   Scattering Database for Spheroidal Particles

J. Wauer

Scattering of electromagnetic waves on nonspherical dielectric particles receives growing importance in remote sensing of the Earth's athmosphere as well as in technical diagnostics. Examples include e.g. the impact of dust like particles on our climate system and analyzing powder probes. An increasing number of modern measurement techniques requires to take electromagnetic wave scattering on nonspherical particles into account. However this is not a trivial task. Two aspects have to be considered:

- The numerical effort is much higher than that known for spherical particles within Mie theory. It strongly depends on the morphology of the particle and can be performed on-line only in very specific situations.
- The convergence procedures of the existing approaches are much more complex as compared to spheres. Obtaining reliable results requires the detailed knowledge of the methodology behind each approach.

The availability of a scattering database releases users from dealing with such complicated algorithmic and computational aspects. It should be noted that the total elapsed computation time to fill the scattering database to its present content amounts to more than one year on a cluster of about six double-processor Linux PCs.

This report describes the principal features of the scattering database together with giving some information on the way it can be easily accessed by users. In its first version the database will consider spheroidal particles, only. However, the general structure of this database will be used later on for other particle geometries, too. All calculations have been performed by use of the program *mieschka* described in detail in *Wauer et al. (2004)*.

Physical structure
The database contains the following scattering quantities for randomly oriented spheroidal scatterers:

- normalized phase function in the angular region (0°-180°)
- extinction efficiency
- scattering efficency
- absorption efficiency
- single scattering albedo
- back scattering efficiency (direct- and cross-polarization)
- asymmetry parameter.

The database is restricted to a size parameter of $kr_{eff} = 40$ (r_{eff} is the radius of the volume equivalent sphere). For the aspect ratio (av = a/b where a and b are semi axes with a being the semi axis along the rotation) and the refractive index (Re(n), Im(n)) the following grid was used:

n	Re(n)	1.33	1.40	1.50	1.60	1.70	1.80	
	Im(n)	0.000	0.001	0.005	0.010	0.030	0.050	0.100
av		0.67	0.77	0.87	1.00	1.15	1.30	1.50

Table 3-2: 3D-grid used in the calculations for the optical scattering database

Database access
To obtain access to our database an easy-to-use interface has been built, which allows one to retrieve the optical data either for an individual particle or for particles belonging to a certain size range. To make the access even more attractive to users, we have added the possibility to compute bulk optical properties for entire particle size distributions as a function of certain size parameters and the particle shape. As a first example the backscattering depolarization is presented in fig. 3-24. In field of remote sensing such depolarization data are important, for example, in the interpretation of lidar observations for atmospheric mineral dust particles.
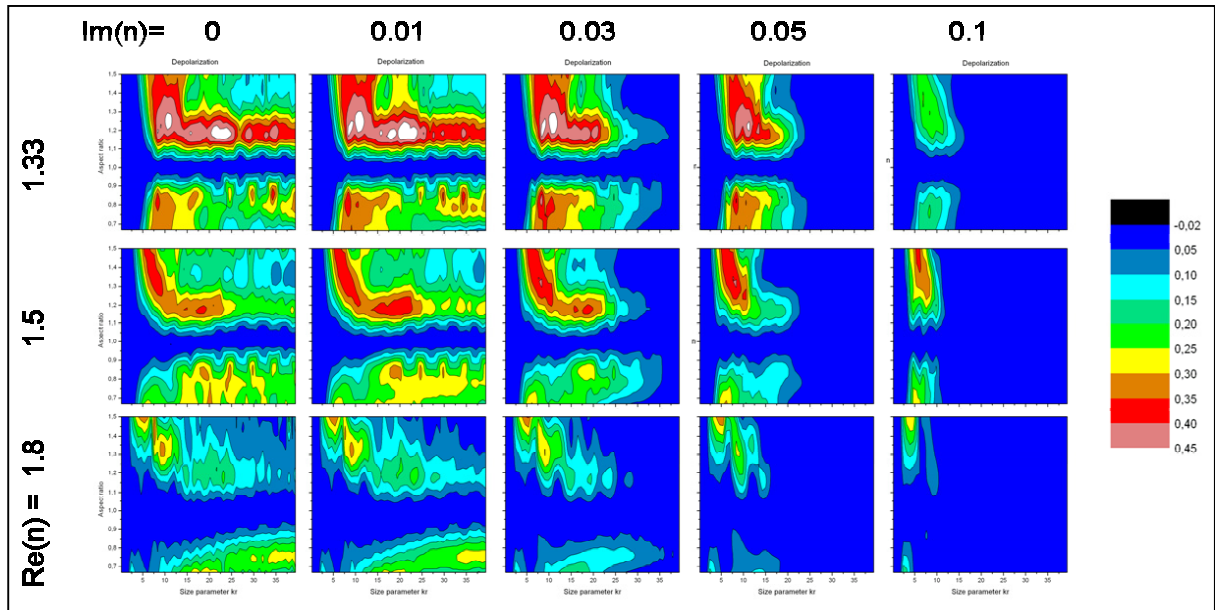
Fig. 3-24: Backscattering depolarization as a function of the size parameter and aspect ratio inside each tile and of the refractive index.

References

Wauer, J. et al.: Two software tools for plane-wave scattering on nonspherical particles in the German Aerospace Center's virtual laboratory, Applied Optics, Vol. 43 pp. 6371-6379, 2004

3.16 Green's Function for Multiple Scattering of Acoustic Waves on an Ensemble of Non-Penetrable Particles

K. Schmidt

In the past a variety of different methods have been developed to describe the scattering of acoustic and electromagnetic waves on single non-spherical and inhomogeneous particles in fixed and random orientations. Nowadays it is possible to compute the scattering functions of at least some classes of these particles within a parameter range of greater practical interest. Nevertheless the methods can only be applied to single isolated objects or to diluted systems of particles with negligible interaction between them. Therefore an increasing interest in exact multiple scattering theories is observed in the last years.

Recently, *Rother (2005,2006,2007)* has published a self-consistent Green's function formalism for acoustic and light scattering on single particles in a series of papers. It provides a basic and systematic treatment of this subject, unifies different approaches into one theoretical framework, and clarifies some of the still existing questions. This formalism has been extended to N particles. So far the case of acoustic scattering on non-penetrable objects obeying Dirichlet's condition has been considered. This is the simplest case to discuss different approaches and concepts.

Consider the acoustic scattering of an incident field $u_{inc}(x)$, generated by an arbitrary source distribution $\rho(x)$ outside the smallest sphere circumscribing all particles, on an ensemble of N non-penetrable obstacles of, in general, different size and shape. The particles are embedded in free space. We are looking for the total field $u(x)$ outside the particles. This field obeys the

- inhomogeneous Helmholtz equation
- radiation condition at infinity
- homogeneous Dirichlet condition $u(x) = 0$

on all particle surfaces $\partial\Gamma_i$, $i = 1,...,N$. In order to obtain a solution of this problem the Green's function formalism is applied. Within this formalism we are looking for the N-particle-Green-function $G(x,x')$ which has to fulfil the inhomogeneous Helmholtz equation, the radiation condition at infinity and the homogeneous Dirichlet condition $G(x,x') = 0$ on all particle surfaces, too. We have for the N-particle-Green-function

$$G(x,x') \;=\; G_0(x,x')+\sum_{i=1}^{N}\oint_{\partial\Gamma_i} G_0^>(x,\bar{x})W_i(\bar{x},x'')G_0(x'',x')dS(\bar{x})dS(x'')$$

Here, $G_0(x,x')$ and $G_0^>(x,x')$ are the free space Green's function and that one for $|x|>|x'|$. Since both functions fulfil the radiation condition $G(x,x')$ fulfils this condition, too. $W_i(\bar{x},x'')$ denotes the interaction operator of the ith particle containing the interaction between all objects. It is determined by using the system of boundary conditions

$$G(x,x')=0, x\in\partial\Gamma_i, i=1...N$$

In this way the N-particle-Green-function $G(x,x')$ fulfils automatically the required Dirichlet condition. As a result the following equation system for the matrix elements of the interaction operators is obtained.

$$\ddot{W}_i=\ddot{T}_i^t+\ddot{T}_i^t\cdot\sum_{j=1,j\neq i}^{N}\ddot{S}_1^t(a_i-a_j)\cdot\ddot{W}_j\cdot\ddot{S}_2^*(a_i-a_j)$$

$\ddot{T}_i^t$ denotes the transpose of Waterman's T-matrix $\ddot{T}_i$ for the single i^{th} particle (*Waterman, 1969*). The matrices $\ddot{S}_1$ and $\ddot{S}_2$ are transformation matrices of the normalized outgoing and incoming spherical wave functions from one coordinate system into another (see e.g. *Martin, 2006*). Their arguments (a_i, a_j) are vectors pointing from the origin of a global coordinate system outside the particles at the origins of the local coordinate systems within the ith and j^{th} particle, respectively. The above equation system represents nothing but the multiple scattering equations in terms of the matrix elements of the interaction operators. In general, this equation system has to be solved numerically. Note that the matrix $\ddot{W}_i$ is equal to the transpose of Waterman's T-matrix $\ddot{T}_i^t$ of the ith non-interacting particle only in the simplest approximation.

Knowing all $\ddot{W}_i$ and consequently the N-particle-Green-function $G(x,x')$ the total field $u(x)$ outside the particles is given by

$$u(x) \;=\; u_s(x)+u_{inc}(x) \;=\int G(x,x')\rho(x')dV(x')\,.$$

Starting with this equation and the corresponding expansions of the incident and the total scattered field $u_s(x)$, it is possible to establish a T-matrix relation between the field expansion coefficients. The resulting N-particle-T-matrix is a function of Waterman's T-matrices of all obstacles. It can be shown that this expression reduces to the two-particle-T-Matrix known from *Peterson and Ström (1974)* in the case of $N = 2$. A more detailed discussion of the whole subject is in preparation for publication.

References

Martin, P. A.: Multiple Scattering – Interaction of Time-Harmonic Waves with N Obstacles, Cambridge University Press, Cambridge, 2006

Peterson, B. and S. Ström: Matrix formulation of acoustic scattering from an arbitrary number of scatterers J. Acoust. Soc. Am. 56, 771-780, 1974

Rother, T.: Self-consistent Green's function formalism for acoustic and light scattering, Part 1: Scalar notation, Opt. Commun., 251, 254-269, 2005

Rother, T.: Self consistent Green's function formalism for acoustic and light scattering, Part 2: Dyadic notation, Opt. Commun., 251, 270-285, 2005

Rother, T.: Self-consistent Green's function formalism for acoustic and light scattering, Part 3: Unitarity and Symmetry, Opt. Commun., 266, 380-389, 2006

Rother, T.: Scalar Green's function for penetrable or dielectric scatterers, Opt. Commun., 274, 15-22, 2007

Waterman, P.C.: New formulation of acoustic scattering, J. Acoust. Soc. Am. 45, 1417-1429, 1969

3.17   Textbook on *Radiation in the Atmosphere*

T. Trautmann

In the previous year the book *Radiation in the Atmosphere. A Course in Theoretical Meteorology* (authors: *W. Zdunkowski, T. Trautmann and A. Bott*) has been published by Cambridge University Press. This book presents the theory and applications of radiative transfer in the atmosphere. It is written for graduate students and researchers in the fields of meteorology and related sciences.

Radiative transfer theory has reached a high level of development and is still a vastly expanding subject. *Kourganoff*, in the postscript of his well-known book of 1952 on radiative transfer, speaks of the three 'olympians' named *completeness*, *up-to-date-ness* and *clarity*. In our book we have not made any attempt to be complete, but we have tried to be reasonably up-to-date, if this is possible at all with the many articles on radiative transfer appearing in various monthly journals. The material is presented as a coherent and consistent development of radiative transfer theory as it applies to the atmosphere.

In the selection of topics the authors have resisted temptation to include various additional themes which traditionally belong to the fields of physical meteorology and physical climatology. Had they included these topics, the textbook, indeed, would be very bulky, and furthermore, it would not have been possible to cover these subjects in the required depth. Similarly, no attempt was made to include radiative transfer theory as it pertains to the ocean, a subject well treated 1999 by *Thomas and Stamnes* in their book *Radiative Transfer in the Atmosphere and Ocean*.

While writing the book the authors were guided by the principle to make the book as self-contained as possible. As far as space would permit, all but the most trivial mathematical steps have been included in the presentation of the theory to encourage students to follow the various developments. Nevertheless, here and there students may find it difficult to follow our reasoning. In this case, students are encouraged not to get stuck with a particular detail but to continue with the subject. Additional details given later may clarify any questions. Moreover, on a second reading everything will become much clearer.

The various chapters and topics treated in this book are:

- **Chapter 1** provides the general introduction to the book. Various important definitions such as the *radiance* and the *net flux density* are given to describe the radiation field. The interaction of radiation with matter is briefly discussed by introducing the concepts of absorption and scattering. To get an overall view of the mean global radiation budget of the system Earth–atmosphere, it is shown that the incoming and outgoing energy at the top of the atmosphere are balanced.
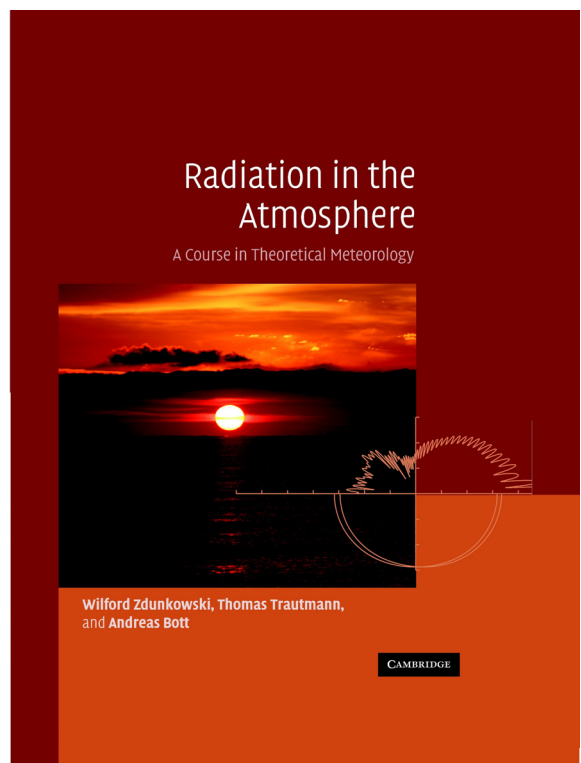
- In **chapter 2** the hydrodynamic derivation of the radiative transfer equation (RTE) is worked out; this is in fact the budget equation for photons. The radiatively induced temperature change is formulated with the help of the first law of thermodynamics. Some basic formulas from spherical harmonics, which are needed to evaluate certain transfer integrals, are presented. Various special cases are discussed.
- **Chapter 3** presents the principle of invariance which, loosely speaking, is a collection of common sense statements about the exact mathematical structure of the radiation field. At first glance the mathematical formalism looks much worse than it really is. A systematic study of the mathematical and physical principles of invariance is quite rewarding.
- Quasi-exact solutions of the RTE, such as the matrix operator method together with the doubling algorithm are presented in **chapter 4**. Various other prominent solutions such as the successive order of scattering and the Monte Carlo methods are discussed in some detail.
- **Chapter 5** presents the radiative perturbation theory. The concept of the adjoint formulation of the RTE is introduced, and it is shown that in the adjoint formulation certain radiative effects can be evaluated with much higher numerical efficiency than with the so-called forward mode methods.
- For many practical purposes in connection with numerical weather prediction it is sufficient to obtain fast approximate solutions of the RTE. These are known as two-stream methods and are treated in **chapter 6**. Partial cloudiness is introduced in the solution scheme on the basis of two differing assumptions. The method allows fairly general situations to be handled.
- In **chapter 7**, the theory of individual spectral lines and band models is treated in some detail. In those cases, in which scattering effects can be ignored, formulas are worked out to describe the mean absorption of homogeneous atmospheric layers. A technique is introduced which enables to replace the transmission through an inhomogeneous atmosphere by a nearly equivalent homogeneous layer.
- The theory of gaseous absorption is formulated in **chapter 8**. The analysis of normal vibrations of linear and nonlinear molecules is introduced. The *Schrödinger equation* is presented and the computation of transition probabilities is described, which finally leads to the mathematical formulation of spectral line intensities. Simple but instructive analytic solutions of Schrödinger's equation are obtained leading, for example, to the description of the vibration–rotation spectrum of diatomic molecules.
- Not only atmospheric gaseous absorbers influence the radiation field but also aerosol particles and cloud droplets. **Chapter 9** gives a rigorous treatment of Mie scattering which includes Rayleigh scattering as a special case. The important efficiency factors for extinction, scattering and absorption are derived. The mathematical analysis requires the mathematical skill which the graduate student has acquired in various mathematics and physics courses. The effects of non-spherical particles are not treated in this book.
- So far polarization has not been included in the RTE, which is usually satisfactory for energy considerations but may not be sufficient for optical applications. To give a complete description of the radiation field the polarization effects are introduced in **chapter 10** with the help of the *Stokes parameters*. This finally leads to the most general vector formulation of the RTE in terms of the phase matrix while the phase function is sufficient if polarization may be ignored.
- **Chapter 11** introduces remote sensing applications of radiative transfer. After the general description of some basic ideas, the RTE is presented in a form which is suitable to recover the atmospheric temperature profile by special inversion techniques. The chapter closes with a description of the way in which the atmospheric ozone profile can be retrieved using radiative perturbation theory.
- The book closes with **chapter 12** in which a simple and brief account of the influence of clouds on climate is given. The student will be exposed to concepts such as cloud forcing and cloud radiative feedback.

Problems of various degrees of difficulty are included at the end of each chapter. Some of them are almost trivial. They serve the purpose of making students familiar with new concepts and terminologies. Other problems are more demanding. Where necessary, answers to problems are given at the end of the book. One of the difficulties that any author of a physical science textbook is confronted with is the selection of proper symbols. Inspection of the book shows that many times the same symbol is used to label several quite different physical entities. It would be ideal to represent each physical quantity by a unique symbol which is not used again in some other context. Since usually confusion is unlikely, we

have tried to use standard notation even if the same symbol is used more than once. The book concludes with a list of frequently used symbols and a list of constants.

For the interested reader the authors would like to give recognition to the excellent textbooks *Radiative Transfer* by the late *S. Chandrasekhar (1960)*, to *Atmospheric Radiation* by *R.M. Goody (1964)* and the updated version of this book by *Goody and Yung (1989)*. These books have been an invaluable guidance to us in research and teaching.

3.18   Optical Constants for Mineral Dust Particles – Contribution to SAMUM

S. Otto, T. Trautmann

Mineral dust is one of the most important aerosols of the Earth's atmosphere. However, its effect on the radiation budget is still in discussion. How absorbing and scattering is the dust really? It is not just a question of the spectral behaviour of the dust complex refractive index, but the dust's radiative impact significantly depends on the particle size distribution, chemical composition/source region, particle mixing state and the particles' non-spherical shape. In this manner the microphysical properties of the individual dust particles have to be considered as starting point as was reported by *Sokolik et al. (2001)*. Comprehensive measurements were performed both at the ground as well as on aircraft during the Saharan Mineral Dust Experiment (SAMUM) in May/June 2006 in order to investigate the microphysics of mineral dust from the Sahara, i.e. size distributions, size-resolved mineralogical and chemical composition as well as size-resolved particle shapes have been measured.

In order to specify the optical input for a fine-band radiative transfer model, covering a large spectral wavelength range from 200 nm up to 40 μm, a large number of literature data for the complex refractive index had to be exploited. It turned out that most of the data were available for the longwave spectral region but not in the shortwave. This can be critical, since the shortwave optical constants are the determining factor for most of the extinction processes in which solar light is involved. Especially the silicate class was problematic with the main components orthoclase, illite, albite, kaolinite and chlorite, because either no data for the shortwave optical constants were available, or the spectral coverage and resolution in the literature data were crucial factors or the literature constants seemed to be questionable. Tab. 3-3 lists the literature data exploited for the individual constituents for calculating the mean complex refractive indices of all mineral classes presented in fig 3-25.

Constituents	References
Silicates	
illite	Egan and Hilgeman (1979)
	Glotch et al. (2007)
kaolinite	Egan and Hilgeman (1979)
	Roush et al. (1991)
	Arakawa et al. (1997)
	Glotch et al. (2007)
chlorite	Mooney and Knacke (1985)
Quartz	Popova et al. (1972)
	Ivlev and Popova (1972)
	Steyer et al. (1974)
	Shettle and Fenn (1979)
	Philipp (1985)
	Zukic et al. (1990)
	Henning and Mutschke (1997)
Carbonates	
calcite	Ivlev and Popova (1972)
	Querry et al. (1978)
	Long et al. (1993)
	Tropf (1998)
	Jarzembski et al. (2003)
Sulfates	
sulfuric acid	Palmer and Williams (1975)
ammonium sulfate	Volz (1973)
	Toon et al. (1976)
	Shettle and Fenn (1979)
	Jarzembski et al. (2003)
gypsum	Ivlev and Popova (1972)
	Aronson et al. (1983)
	Long et al. (1993)
Iron rich	
wüstite	Henning et al. (1995)
hematite	Shettle and Fenn (1979)
	Hsu and Matijevic (1985)
	Querry (1987)
	Gillespie and Lindberg (1992)
	Bedidi and Cervelle (1993)
	Marra et al. (2005)
	Glotch et al. (2007)
magnetite	Gillespie and Lindberg (1992)

References of Ensemble Data
Volz (1972), Volz (1973), Lindberg and Laude (1974), Lindberg (1975), Lindberg and Gillespie (1977), Patterson et al. (1977), Carlson and Caverly (1977), Shettle and Fenn (1979), Carlson and Benjamin (1980), Levin et al. (1980), Ivlev and Andreev (1986), Zuev and Krekov (1986), Fouquart et al. (1987), Sokolik et al. (1993), Hess et al. (1998)

Tab. 3-3: Literature references for the complex refractive indices of major constituents of mineral dust and ensembles of dust particles.

Typically Saharan mineral dust particles consist of the components:

- Silicates: illite, kaolinite, chlorite
- Quartz: quartz
- Carbonates: calcite
- Sulfates: sulfuric acid, ammonium sulfate, gypsum
- Iron rich: hematite, magnetite, wüstite.

With the help of a simple volume mixing rule the wavelength dependent complex refractive index can be computed for different particle size classes. For this the experimentally determined composition of Saharan dust must be available, i.e. the volume fraction of each particular component must be known for the dust collected from ground-based and airborne measurements. The chemical composition with regard to the volume portion is dominated by silicates, but small/large particles also can include a significant portion of sulfates/quartz. Although the portion of iron rich material usually is low compared to silicate, it nevertheless can largely contribute to the refractive index of the dust mixture. This is due to the fact that its imaginary part is by orders of magnitude larger than that of the remaining constituents (see fig. 3-25). Continuing our work *(Otto et al., 2007)* these calculated complex refractive indices will be used to estimate the radiative impact of Saharan mineral dust. Radiative transfer simulations will be performed, too, to explore non-spherical shape effects of these dust aerosols.
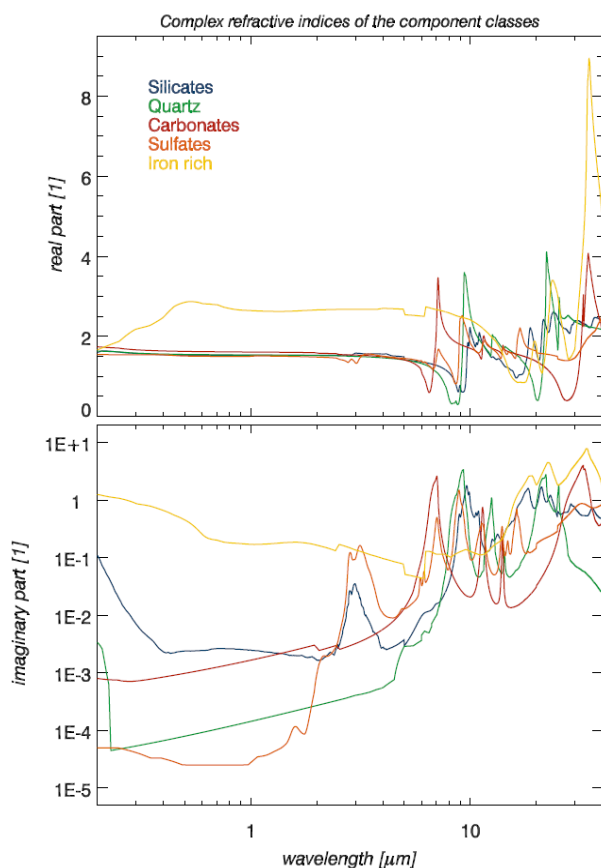
Fig. 3-25: Spectral complex refractive indices of the following material groups being representative for mineral dust mixtures: silicates, quartz, carbonates, sulfates and iron oxides. The curves were calculated using moving averages of spectral literature data cited in tab. 3-3. For any anisotropic material the ordinary complex refractive index data was simply adopted.

References:

Otto, S., M. de Reus, T. Trautmann, A. Thomas, M. Wendisch and S. Borrmann: Atmospheric radiative effects of an in situ measured Saharan dust plume and the role of large particles, Atmos. Chem. Phys., 7, 4887-4903, 2007

Sokolik, I.N., D.M. Winker, G. Bergametti, D.A. Gilette, G. Carmichael, Y.J. Kaufman, L. Gomes, L. Schütz, and J.E. Penner: Introduction to special section: Outstanding problems in quantifying the radiative impacts of mineral dust. J. Geophys. Res., 106, No. D16, 18015–18027, 2001

Remark: A complete list of references of the wavelength dependent optical constants of mineral dust components can be made available by the authors on request.

3.19 The Saharan Mineral Dust Experiment 2 – SAMUM 2

C. H. Köhler, E. Lindermeir (MF-EV), T. Trautmann

SAMUM 2 constitutes the continuation of the SAMUM 1 project (see e.g. *IMF-AP Annual Report 2006*) which aimed at the characterization of mineral dust. While SAMUM 1 gathered information about mineral dust close to its source, i.e. in the Moroccan desert, SAMUM 2 aims at investigating dust that has been transported by atmospheric currents. This aged dust differs strongly from its original constitution, as it usually underwent several cycles of changing atmospheric conditions (humidity, temperature, etc). Another process that determines the optical properties of the transported dust is the mixing with biomass burning aerosols and sea salt. This combination of mineral dust, salt and smoke has not been treated properly in satellite retrievals, yet. As the anthropogenic portion of biomass burning aerosols varies strongly with season and reaches its peak during January and February, a measurement campaign is planned for those months in 2008 on the Island of Santiago/Cap Verde, which is regularly covered by the dust-smoke-mixture originating from the African mainland. Fig. 3-26 shows a MODIS image of a dust outbreak over the Cape Verde Islands (center left) approximately 800 km off the African West Coast on February 16, 2003. The red dots (bottom right) are fires in Senegal and Gambia that have been detected by the MODIS instrument.


Fig. 3-26: On February 16, 2003, a large plume of Saharan Desert dust (light brown pixels) was blowing westward over the Cape Verde Islands in the east Atlantic Ocean. The red dots (bottom right) symbolize fires (from *NASA Visible Earth*).

IMF Contribution to SAMUM 2
In contrast to SAMUM 1, where the IMF-AP restricted its efforts to radiative transfer simulations, there will be an active participation in the 2008 field campaign: In cooperation with the IMF-EV (Experimental Methods) a team of two scientists will perform ground based measurements during a three week period in January and February 2008 on the Island of Santiago/Cap Verde. The goal is to measure downwelling radiances from the dust cloud in the near-infrared (700 to 2500 cm^{-1} or 4 to 14 μm) with a special focus on the atmospheric window region between 8 and 12 m. For this purpose a Model 102 Fourier Transform Infrared Spectrometer (FTIR) manufactured by D&P Instruments was chosen and thoroughly characterized before being shipped to Cap Verde in November 2007 (see fig. 3-27, 3-28). Besides from the standard laboratory examinations of accuracy, resolution, temperature dependence (in a temperature controlled cabinet) and field of view, the characterization included a rehearsal of the experimental set-up and measurement procedures as planned during the SAMUM 2 campaign on the Cap Verde Islands. It was conducted in July 2007 in Oberpfaffenhofen by the IMF team in cooperation with members from the SAMUM 2 consortium from the University of Mainz. Due to the absence of mineral dust in the atmosphere, the measurements focused on downwelling radiances in the near-infrared (IMF) and visible (Mainz) from cloud- and blue-sky scenarios.

The following illustrations show a comparison of our FTIR measurements with MODTRAN simulations for a standard tropical atmosphere with slightly changed humidity and temperature profile in order to fit the conditions on the day of our measurements. Fig. 3-29 (right) displays measurements of a cumulus cloud ceiling at an altitude of approximately 1000 m above ground. Fig. 3-29 (left) shows measurements that were taken earlier on the same day without cloud cover compared with a simulation of the respective conditions.

Fig. 3-27: Planned experimental set-up during the SAMUM 2 field campaign: IMF FTIR (left) and equipment from the University of Mainz (right).

Fig. 3-28: The D&P Model 102 Field FTIR.

As stated earlier the purpose of the test campaign was to estimate the instrument's performance during field conditions and to see whether it meets the estimated standards required for the 2008 field experiment on the Cap Verde Islands. Regarding the fact that the atmospheric temperature and humidity profile were not measured in situ and therefore had to be estimated, it can be stated that simulation and experiment agree very well within their respective errors. On the basis of the acquired data and under consideration of several simulations we are optimistic to contribute valuable results to the SAMUM 2 project, provided the weather creates a dust loaded atmosphere at the measurement site.
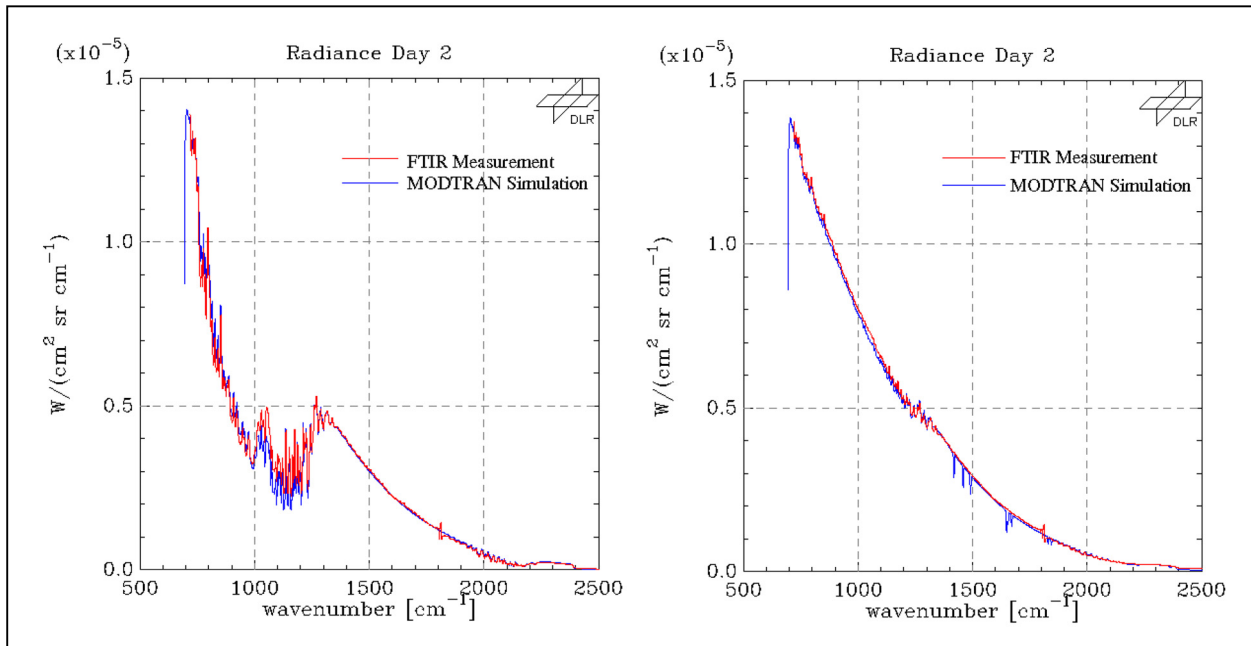

Fig. 3-29: Comparison of measured and simulated radiances for a clear sky scenario (left) and a cumulus scenario (right).

3.20   The Atmospheric Dynamic Mission – ADM Aeolus

D. Huber (DoRIT), K. Reissig (IBR)

The Atmospheric Dynamics Mission will provide profiles for raw Rayleigh and Mie data signal profile returns of the Nd-YAG laser ALADIN, which is operated at 355nm. The raw data is processed to geolocated data, the L1A products, first wind profile data, the L1B products, temperature and pressure corrected wind profiles, the L2B products, and to additional geophysical parameters, provided as L2A data products.

In preparation for the Cal/Val phase, a L1B prototype processor has been developed at IMF-AP. This processor uses as input L1A ADM products and derives wind profiles. In contrast to the operational ADM data processor, this prototype contains sophisticated algorithms under investigation. During the Cal/Val phase, selected L1A products shall be processed to test and validate the enhanced algorithms. This processor is complemented by a flexible data display tool, see fig. 3-30.
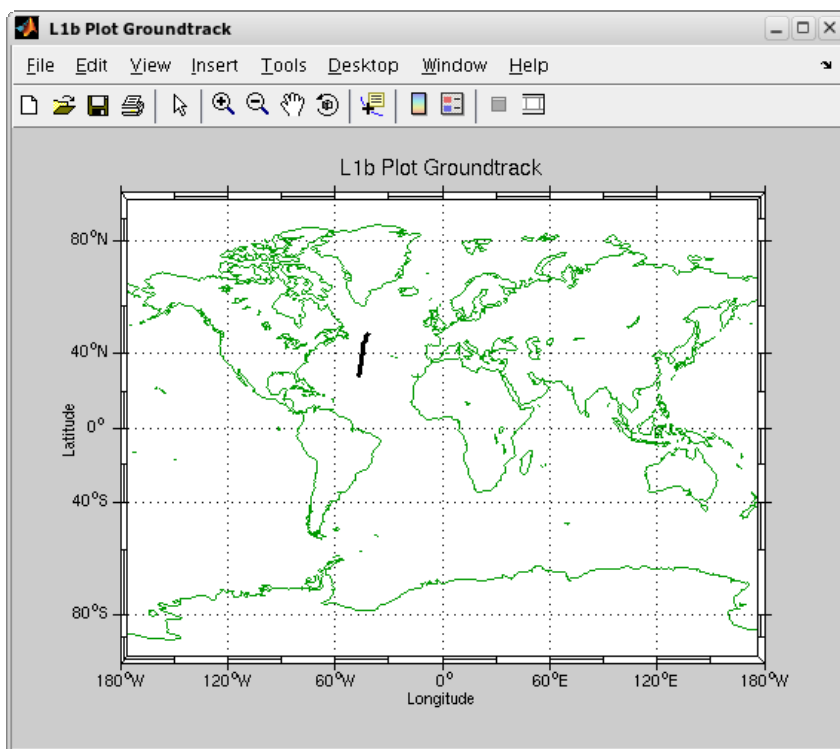

Fig. 3-30: Ground track plot of a simulated calibration scenario.

Processing of geophysical parameters

ADM L1b data will be further processed to L2a products to derive profiles of local optical depth and backscatter-to-extinction ratios. The corresponding L2a processor consists of the following four main modules.

First module: The *Synthetic Signal Calculation* predicts on the basis of an atmosphere model the expected signal return in case of a cloud free scene, using pressure and temperature profiles provided by ECMWF Met centre.

Second module: The *Cross Talk Correction* corrects the return signal on the Rayleigh channel from the Mie influence and vice versa.

Third module: The *Iterative Correct Algorithm* derives a profile of local optical depth. The algorithm is even capable to detect the position of an optically dense layer within one height bin probed by ALADIN.
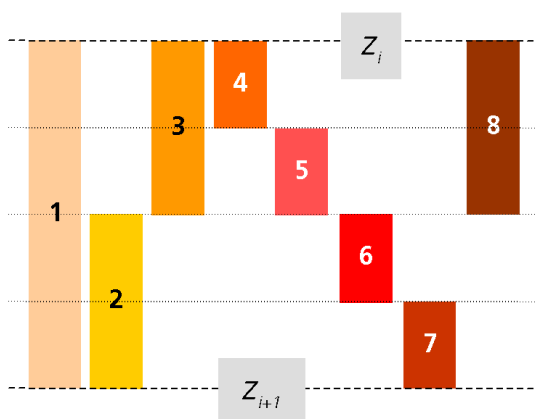
Fig. 3-31: Algorithm to determine the profile of the local optical depth within a particular height bin.

To achieve this, the processor uses a model with 8 different sub-layer cases (see fig. 3-31). In an iterative process the combination of all possible filling cases from the top to the bottom layer is tested with a depth-first search. Possible solutions are determined using a credibility criteria for every filling case, and finally the best solution providing a profile of local optical depth, scattering ratios, and filling cases is selected.

Fourth module: Mie signals processing occurs here. Signal processing is simpler for Mie channel signals, as the local optical depth and the scattering ratio may be derived directly for every bin. Probed height bins may be commanded independently for the Rayleigh and the Mie channel. But in case, the height bin commanding

matches, an additional backscatter-to-extinction ratio profile is calculated.

ALADIN optical properties retrievals together with CALIOP and ATLID data will be used then to build a long term cloud and aerosol monitoring data base.

3.21 The Retrieval Software PyReS in the VirtualLab

M. Hess (RASCIN), F. Schreier

PyReS (Prototype Retrieval System) was developed at IMF in the framework of the FOCUS and Ecofire projects, aiming at the retrieval of temperatures and gaseous composition of the plumes of vegetation fires and other *High Temperature Events (HTE)*. One major requirement for the development of the PyReS software was flexibility, allowing its use for different types of retrieval applications. Descriptions of the program and of some results can be found in previous Annual Reports of IMF-AP (2005, 2004, 2002, and 2001).

The VirtualLab (VL) contains scientific software related to scattering and atmospheric radiation *(Ernst et al., 2003)*. It can be used for scientific purposes as well for exercises in education. PyReS's flexibility also allows the easy integration of a reduced standard version into the VL. The purpose of this implementation is rather to help the researcher or student to develop a feeling for the influence of the different parameters governing the retrieval process, but in some cases, it may also be possible to get scientific first guess results.

The version currently being implemented permits the retrieval of the total column of trace gases, the surface temperature, and a baseline shift from measured (or simulated) IR spectra. The IR radiative transfer model MIRART *(Schreier et al., 2003)* is used as a forward model utilizing the Hitran spectrosocopic data base and a standard atmosphere model. Gas and temperature profiles of this model are simply scaled (shifted) to yield the minimal residual of measured and modelled IR spectra. The mathematical optimisation is done by the Port library *(Dennis et al., 1981)* in a version considering simple bounds that define an interval inside which the final result has to occur. These bounds cannot be changed by the user in the current version, but have been preselected in a way which suits all atmospheric applications.

An example input screen is shown in fig. 3-32. First, the user has to select a data file on his local computer containing the spectrum to be used for the retrieval. This file will automatically be uploaded to the VL. Two instrument types are supported, Fourier Transform IR Spectrometer and Grating Spectrometers. The user has to supply appropriate data for instrument characterization. If a synthetic (simulated) spectrum is to be used, it is possible to add noise to this spectrum, specified in terms of the *Noise Equivalent Spectral Radiance (NESR)*. In the next step, some information about the measurement geometry has to be provided. At the moment, the possible geometries are restricted to a nadir down looking view. Other geometries will be added later. Other input data concern the spectral range or the subset of the spectrum that shall be used for the retrieval.

Four parameters may be selected to be retrieved. Only the gas column is mandatory while the other parameters are optional. These are the scaling factor of the initial guess temperature profile, the surface temperature and a constant baseline which is added to the measured spectrum. With the last set of input parameters, up to four gases can be selected in addition to the gas to be retrieved, to be considered for the forward calculations.

An example result plot is shown in fig. 3-33. The results themselves are only up to four numbers, i.e. the retrieved total gas column and, if selected, the temperature profile scaling factor, the surface temperature, and the baseline shift. Therefore only the initial guess and the final spectra are plotted together with the measured spectrum.

ENTER/next   prev - *1* - *2* - *3* - *4* - *5* - current - *all*   Clear all

Input data set for: pyres-1.0 [ALL]

Quantity	VarName	Value	Unit	Remark
Measurement Data				
spectral measurement file?	spectrumFile	spectrum.dat		☐ change
instrument type	measurementType	○ FTIR ● Grating		
Noise (in case of synthetic spectra)	NESR	0.0		
slit width	slit	0.885		
Measurement Geometry				
observer height	observer_height	100.0	km	
spectral range to be used for retrieval				
begin of spectral range	wave_min	2181	cm-1	
end of spectral range	wave_max	2200	cm-1	
Retrieval Parameters				
gas column to be retrieved	gasColumn	CO		
allow shift of temperature profile ?	tempProfile	● yes ○ no		
retrieve surface temperature ?	surfTemp	● yes ○ no		
baseline fit ?	baseline	○ yes ● no		
Additional Atmospheric Gases to be used in Forward Calculation				
1. gas	gas_1	H2O		
2. gas	gas_2	--		
3. gas	gas_3	--		
4. gas	gas_4	--		

ENTER/next   prev - *1* - *2* - *3* - *4* - *5* - current - *all*   Clear all

http://vd.nz.dlr.de/VL/users/hess/my_exps/EXPS/pyres-1..../FSAPPS/pyres/1.0/doc/APP.html#VL_id_observer_height_p

Fig. 3-32: Example input screen for PyReS in the VL. The file spectrum.dat contains an AIRS spectrum from which the CO column shall be retrieved together with the surface temperature, allowing a temperature profile shift. No baseline is assumed and only H_2O is considered as additional relevant gas in the atmosphere for the selected wavelength range.
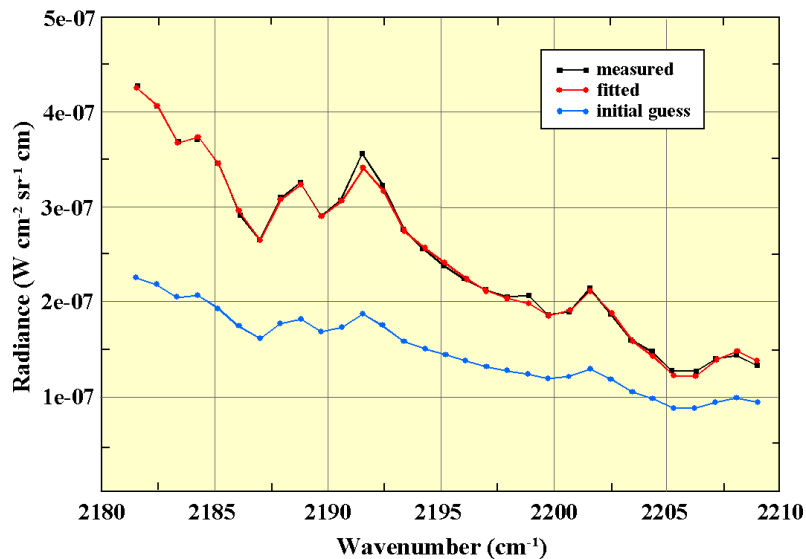
Fig. 3-33: Result plot, for the input screen from fig. 3-32.

References:

Dennis Jr., J.E., D.M. Gay, and R.E Welsch: An adaptive nonlinear least-squares algorithm, ACM Trans. Math. Soft., 7:348-368, 1981

Ernst, T., T. Rother, F. Schreier, J. Wauer, and W. Balzer: DLR's VirtualLab. Scientific software just a mouse click away, Computing in Science & Engineering, 5(1):70-79, Jan/Feb 2003

Schreier, F. and U. Böttger: MIRART, a line-by-line code for infrared atmospheric radiation computations incl. derivatives. Atmos. & Oceanic Optics, 16:262-268, 2003

3.22 The Impact of Atmospheric Variability on the Determination of the Gravity Field of the Earth

E. Fagiolini, G. Schwarz (IMF-PB), T. Trautmann

The project IDEAL-GRACE (Improved De-Aliasing for Gravity Field Modelling with GRACE) aims at determining representative error measures for atmospheric and oceanic parameters and improving the de-aliasing concept by developing an error-propagation for de-aliasing. It is funded by DFG in the frame of SPP1257: *Mass Transport and Mass Distribution in the Earth System*. The work is a collaborative effort of DLR-IMF (Oberpfaffenhofen), GFZ (Potsdam), TUM-IAPG (Munich) and UNIHH-IFM (Hamburg).
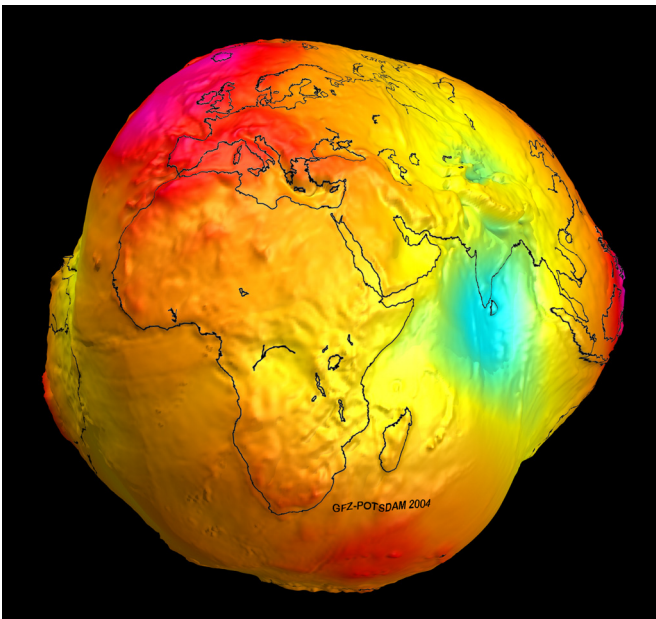

Fig. 3-34: Combined gravity field model EIGEN-GL04C complete to degree and order 360 from GRACE (Courtesy: GFZ-Potsdam).

The main current gravity missions are CHAMP (launched July 2000), GRACE (March 2002), GOCE (to be launched 2008). They deliver measures of the total sum of superimposed time varying mass signals used to derive a homogeneous time series of global gravitational field representation. As described by *Gruber et al. (2006)*, GRACE, a twin-satellite gravity mission, provides measurements of the temporal variations of the Earth's global gravitational field. The variation sources can be of two types

- high frequency: tides, atmosphere, oceans, continental water
- seasonal: atmosphere, oceans, continental water, ice mass

The expected accuracy over monthly averaged time-varying mass redistribution of the Earth is in the form of climate-sensitive signals, measured with sub-centimetre accuracy in units of column of water movement near the Earth surface with a spatial resolution of 250 km or larger and a temporal resolution of a month for a time-span of 5 years.

IDEAL-GRACE addresses one of the major remaining problems in the GRACE data analysis, i.e. the atmospheric and oceanic de-aliasing. De-aliasing means the subtraction of all short frequency phenomena from the data. For GRACE data processing only the short term variations are of importance, because with the monthly GRACE gravity field solutions it is planned to provide data for the determination of the seasonal variations. High frequency mass variations in the atmosphere have impact on all three gravity missions while high frequency mass variations in oceans are much smaller but still impact GRACE and CHAMP. Furthermore, the assumption of error free atmospheric and oceanic input parameters needs review by using independent data. If required corresponding representative error measures must be determined. The de-aliasing concept shall be improved by developing a full mathematical sampling and aliasing model applicable to the identification of homogeneous time series

and for the definition of the variability reference for the GRACE data analysis. This includes propagated errors for the high frequency atmospheric and oceanic gravitational corrections in the data processing.

The processing steps are as follows.

Step 1: Basic atmospheric input parameters, taken from meteorological data sets such as ECMWF, are spatially resolved and time-tagged maps of surface pressure, temperature profiles and specific humidity and their corresponding standard deviations are generated. ECMWF provides GRIB data archived in the following spatial coordinate systems: Gaussian grid (GG) point values as well as regular spaced latitude/longitude grid point values.
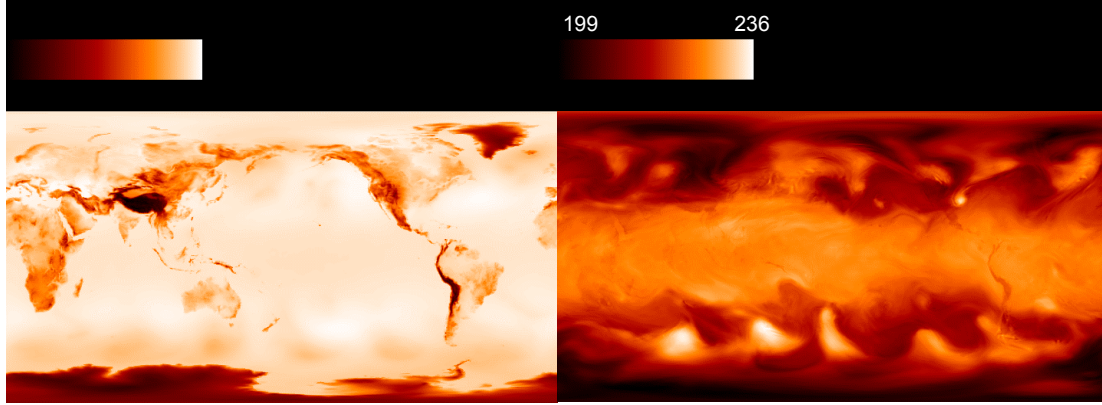

Fig. 3-35: Surface Pressure in hPa (Dec-01-2006 00:00 UT, left) and Mid-Level Temperature in K at about 180 hPa (Dec-01-2006 00:00 UT, right).

Step 2: Blockmeans covering the whole globe are calculated. We introduced weighted blockmeans based on ECMWF standard deviations which show an improvement on the quality of surface pressure, temperature and specific humidity.

Step 3: Blockmean values, plus optional noise reduction, are used as inputs in the vertical integration of atmospheric columns required by the geoid calculations. We performed some sensitivity calculations of the column integrations to show the propagated uncertainties and the diverse consequences of parameter variations. The vertical integration results depend mainly on surface pressure; temperature and specific humidity are less critical.

Step 4: Through spherical harmonic analysis *(Kaula 2000, Torge 2003)* we calculate the harmonic coefficients till degree 100 that determine in the last step the geoid height variations $\Delta N(\theta, \lambda)$, as shown in the following formulas.

$$\begin{pmatrix} C_{nm} \\ S_{nm} \end{pmatrix} = \frac{-a^2(1+k_n)}{(2n+1)M_e g_0} \iint\limits_{\theta\ \lambda} I_n(\theta, \lambda) P_{nm} \cos(\theta) \begin{Bmatrix} \cos(m\lambda) \\ \sin(m\lambda) \end{Bmatrix} \sin(\theta) d\theta d\lambda$$

$$\Delta N(\theta, \lambda) = a \sum_{n=0}^{100} \sum_{m=0}^{n} \overline{P}_{nm} \sin(\theta) \left[\Delta\overline{C}_{nm} \cos m\lambda + \Delta\overline{S}_{nm} \sin m\lambda \right]$$

As a result of introducing noise reduction in step 2 and taking into account ECMWF standard deviations, we obtain clearly visible geoid height differences.

References:

Gruber, T. et al.: Improved DE-Aliasing for Gravity Field Modelling with GRACE (IDEAL-GRACE), New Research Grant Application, 2006

Kaula, W.M.: Theory of Satellite Geodesy, 1-11, Dove Publications, Mineola, 2000

Torge, W.: Geodäsie, 2. Auflage, 245-255, Walter de Gruyter, Berlin, 2003

3.23 Venus during Transit: Illustrating Transit Spectroscopy of Extrasolar Planets

P. Hedelt (DLR-PF), F. Schreier, R. Alonso (LAM Marseille), T. Brown (LCOG Goleta, California), M. Collados-Vera (IAC Tenerife), H. Rauer (DLR-PF, ZAA Berlin), H. Schleicher, W. Schmid (both KIS Freiburg), R. Titz (DLR-PF)

Subject of a diploma thesis was the observation of the very rare event of a Venus transit in front of the the Sun on June 8, 2004. Venus transits regularly occur in pairs every 121.5 years whereby the second transit happens 8 years after the first. Observations were made on Tenerife with the Vacuum Tower Telescope (VTT) of the Kiepenheuer-Institut für Sonnenphysik (KIS), Freiburg (Germany). These measurements were used as a test case for transit spectroscopy as a means of exoplanet search; furthermore the objective was an analysis of the high CO_2 content of the Venusian atmosphere and its isotopic mixture. Transmission spectra were recorded near 1.5 µm wavelength with an Echelle grating spectrograph connected to an IR CCD detector array. The spectral resolution of the spectrograph system was approximately 200000.

Measurement slit geometry

The measurements were carried out in three wavelength intervals (1.59649-1.59729 µm, 1.59749-1.59827 µm, 1.61239-1.61319 µm) which were expected to contain several strong CO_2 absorption lines. To this end the telescope tracked the Sun, and scans over the Venusian disc were performed with the spectrograph with the Sun located behind. The slit of the spectrograph was rotated in a manner, such that the slit axis was oriented at an angle of 45.5° (anti-clockwise) with respect to the direction of Venus' north pole (V-NP). In the second phase of the measurement sequence the slit was turned by 180°, i.e. to an angle of 135.5° with respect to V-NP. The rotations of the slit enabled a scan of the Venusian disc so that images could be recorded (see fig. 3-36, left part) belonging to a particular rotation angle of the slit and covering latitudes from 0-30° and 55-85° on the Venus disc.

Image processing

The spectrograph images were processed in the following way: First, a calibration was performed, and the typical absorption lines of both the solar photosphere as well as the Earth's atmosphere were removed. This first step leads to a normalisation of the images, see fig. 3-36, right part. Second, those spectra were extracted which pertain to the limb view regions and which contain information on the light transmitted through the Venusian atmosphere including the relevant absorption lines. The spectra of the respective wavelength regions were averaged to improve the signal-to-noise ratio. The HITRAN 2004 spectroscopic database was employed to achieve a wavelength calibration. The extracted spectra clearly exhibited absorption lines of CO_2 that can be unambiguously identified with corresponding HITRAN information for CO_2, see the solid line in fig. 3-37. These lines do not overlap with the positions of solar or terrestrial absorption lines as demonstrated by the dashed line in fig. 3-37 representing a measured and scaled solar spectrum.
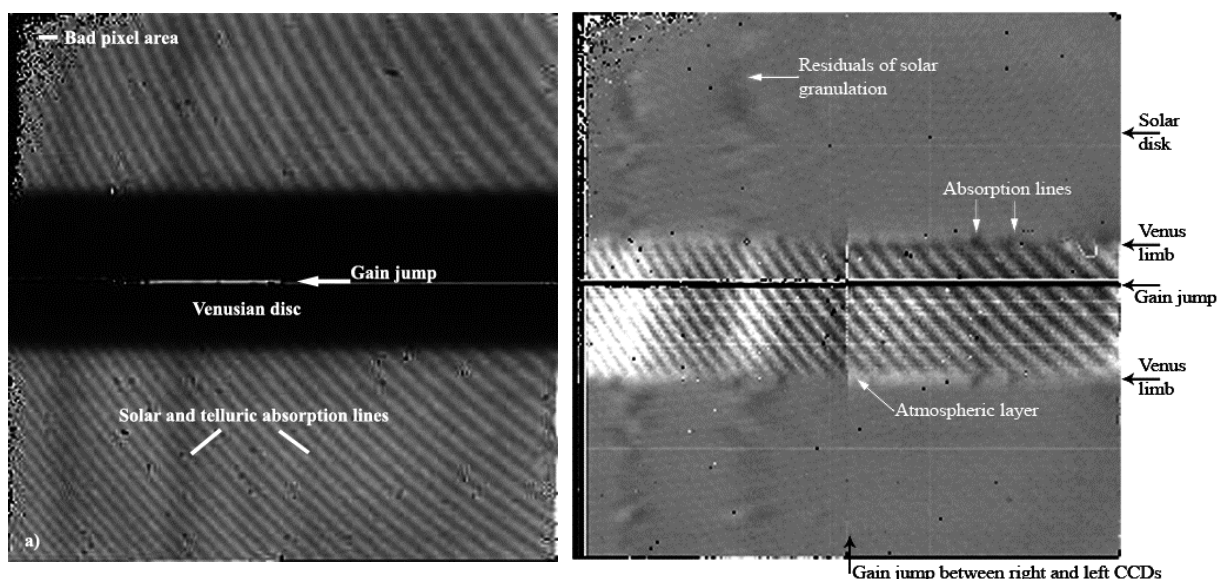

Fig. 3-36: Left: Raw image from Venus' disc visible as the horizontal dark stripe in the middle of the image. Right: Image normalised in spectral and spatial direction. The transition region between Venus' disc and the Solar disc exhibits a thin layer with absorption features.

In the analysis of the observed spectra we employed the radiative transfer module SQuIRRL, which is part of the MIRART radiative transfer package. SQuIRRL has been used to simulate the observations with the purpose to verify the Venus' spectra and to derive information on both the tangent altitude of the limb observations as well as on the temperature profile in the upper part of Venus' atmosphere well above any Venus cloud deck near 80 km altitude. A measured day-side temperature profile has been used from literature as well as the isotope ratio, normalised for Venus' atmosphere, for the three most abundant isotopes for CO_2 ($^{626}CO_2$, $^{636}CO_2$, $^{628}CO_2$). By varying the input parameters a matching of the simulated and observed spectra was achieved, see the dash-dotted curve in fig. 3-37 for the simulated spectrum. The comparison proves that the used temperature profile and the adopted isotope ratios match the measured absorption lines well.
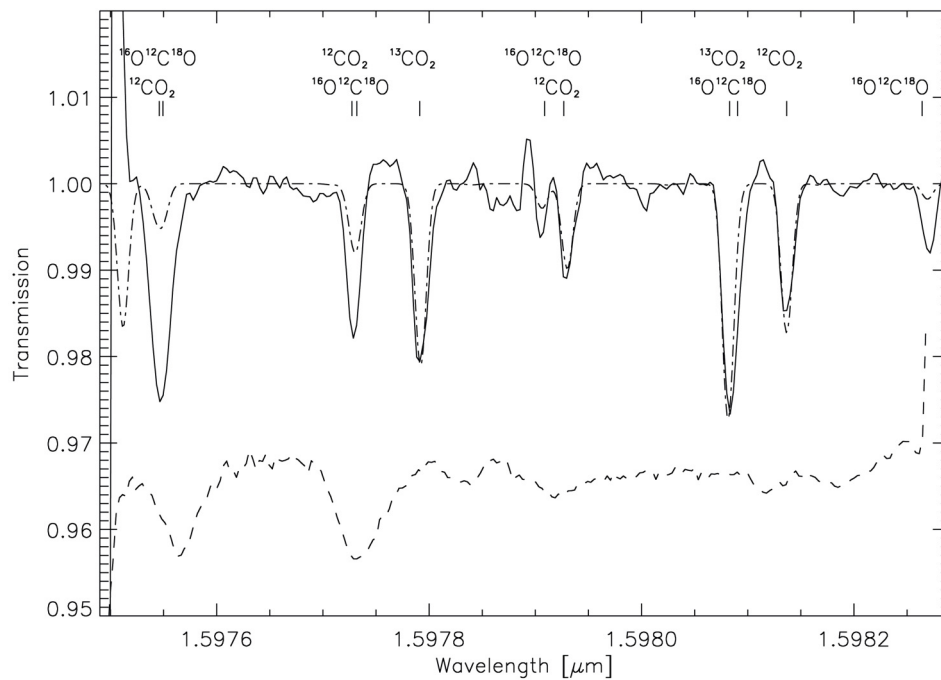

Fig. 3-37: Averaged spectrum of the left and right Venus limb. Measured spectrum (solid line), modelled spectrum (dash-dotted line), scaled spectrum of the Sun's surface in arbitrary units to show locations of the solar absorption lines (dashed line). The location of various CO_2 isotopes in Venus' atmosphere is indicated.

3.24   The EnMAP Planning Concept

M. Gottwald, S. Holzwarth (DFD-US)

The *Environmental Mapping and Analysis Programme* (EnMAP) defines, besides *TanDEM-X*, one of the two future national Earth Observation (EO) missions. EnMAP carries the *Hyperspectral Imager* (HSI) whose goal are detailed spectroscopic investigations of the Earth's surface – land and coastal areas. This is achieved by acquiring spectrally resolved images in push-broom mode in 30 km wide scenes along-track. At a spectral resolution of 5-10 nm between 420 nm and 2450 nm more than 200 spectral bands are recorded simultaneously. Within each acquired data take the spatial resolution amounts to 30 m. Because of the capabilities of the on-board memory device together with the configuration of the ground segment, i.e. a single ground station for data reception at Neustrelitz, an equivalent total length of 5000 km along-track can be observed each orbit. With the maximum possible across-track pointing of ± 30° this enables global coverage in about 4 days. EnMAP's orbit is quasi sun-synchronous with a mean altitude of 643 km and a Mean Local Solar Time (MLST) at descending node crossing of 11:00 a.m. Its launch is planned for 2011 starting a subsequent mission duration of 5 years.

The EnMAP project management rests with DLR at Bonn. Industrial contractors are OHB (platform) and Kayser-Threde (instrument and prime). The scientific lead is with the Principal Investigator H. Kaufmann from the Geoforschungszentrum Potsdam (GFZ). DLR at Oberpfaffenhofen has the responsibility for

developing and operating the ground segment (GS). It comprises mission operations at GSOC and the payload data segment at the *Applied Remote Sensing Cluster*. The payload data segment is split into the components Payload Ground Segment (PGS) and Processor, Calibration und Validation (PCV).

In 2007 the Phase B of the GS development continued. Although the goal was to use multimission functionalities from the TerraSAR-X programme to the maximum extent, some characteristics of EnMAP required to also consider mission specific items. This concerned particularly the planning chain. The HSI as a passive optical sensor does not require the strict orbit maintenance as an active microwave instrument. Therefore coverage predictions, i.e. ordering of future data products is not as straightforward as for TerraSAR-X. Another major difference between TerraSAR-X and EnMAP addresses the user communities of both missions. While TerraSAR-X has a strong commercial component with a dedicated industrial provider, EnMAP is defined as a scientific mission. Potential commercial users have to be served by the GS as well but this type of users is not regarded as the driver for the development. The scientific planning for TerraSAR-X with extensive user interfaces seems to be a more appropriate model for EnMAP.

Because IMF-AP has long-lasting experience in planning of SCIAMACHY, also a purely scientific optical mission, we participated in phase B by deriving a concept for the first part of the planning chain. It is termed *Instrument Planning* (IP) and has to be differentiated from *Mission Planning* at GSOC, a function which generates the final schedules. The concept finally proposed is depicted in fig. 3-38. IP interfaces functionally with users, Science Coordination, the Data Information and Management System (DIMS), Production Management, Mission Planning and Flight Dynamics. In general IP is the EnMAP GS function which interacts with users to collect, verify and process proposals for image acquisitions. These are the termed *Observation Requests (OR).* IP operates the OR portal, i.e. a web-based tool where all categories of users can input their proposals. The proposal content is user category dependent, e.g. requests undergoing a scientific review have to provide a scientific rationale while others may not. The OR content includes all information required for mission planning and data processing. It consists of

- administrative information
- scientific/application information: description of proposed research or application
- instrument planning information: list of parameters specifying data take
- data processing planning information: list of parameters specifying processing needs
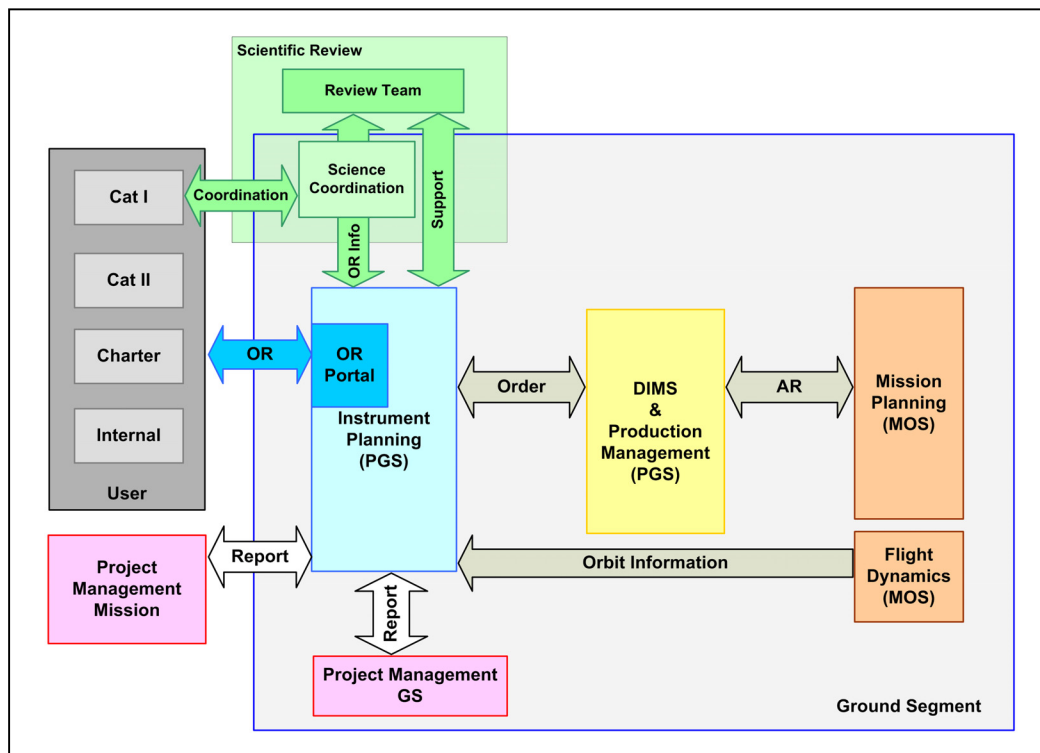
Fig. 3-38: The planning workflow in the EnMAP ground segment including Science Coordination. Instrument Planning and Science Coordination cooperate closely. Arrows in grey indicate operational interfaces.

All HSI operation activities being related to data takes (image acquisitions or calibration) shall be triggered by information passing through IP via Observation Requests. ORs are processed to generate input required for data processing (Orders) and Mission Planning (Acquisition Requests – AR). Prior to the submission of orders and ARs Instrument Planning supports scientific reviews of the ORs and checks their technical feasibility. In order to generate the planning information for distribution to the users the status of ARs and orders is received from MPS and DIMS. A further functional interface to Flight Dynamics provides orbit files used in the OR feasibility studies.

The concept described above has the advantage that users interact with the GS only once for the submission of proposal information. From the moment the proposal is accepted it is then ground segment's responsibility to accomplish data takes as requested. By properly specifying and implementing the cooperation between Instrument Planning and Science Coordination, an efficient planning front-end can be established which is a pre-requisite for successful mission execution.

4. Documentation

4.1 Books and Book Contributions

Gottwald, M.: The ENVISAT Mission - Observing our Planet from Space. In: Hiebl, Ewald; Musso, Maurizio [Hrsg.]: *Christian Doppler, Life and Work - Principle and Applications*, Living Edition, 159-176, ISBN 978-3-901585-09-8, 2007

Zdunkowski, W., T. Trautmann and A. Bott: *Radiation in the Atmosphere. A Course in Theoretical Meteorology,* Cambridge University Press, Cambridge, New York, 496 S., ISBN ISBN-13: 97805218710754, 2007

4.2 Journal Papers

Badaoui, M., F. Schreier, G. Wagner, M. Birk: Retrieval of line parameters from high resolution Fourier Transform laboratory spectra in support of atmospheric spectroscopy, *Physical and Chemical News*, 36, ISSN 1114-3800, 2007

Balis, D., J.-C. Lambert, M. Van Roozendael, R. Spurr, D. Loyola, Y. Livschitz, P. Valks, V. Amiridis, P. Gerard, J. Granville, C. Zehner: Ten years of GOME/ERS2 total ozone data. The new GOME data processor (GDP) version 4: 2. Ground-based validation and comparisons with TOMS V7/V8, *Journal of Geophysical Research*, 112 (112), DOI 10.1029/2005JD006376, 2007

Doicu, A., F. Schreier, S. Hilgers, M. Hess: Error analysis and minimum bound method for atmospheric remote sensing, *Environmental Modelling & Software*, 22 (6), Elsevier, S. 837-846, DOI 10.1016/j.envsoft.2005.08.006, 2007

Doicu, A., S. Hilgers, A. von Bargen, A. Rozanov, K.-U. Eichmann, C. von Savigny, J.P. Burrows: Information operator approach and iterative regularization methods for atmospheric remote sensing, *Journal of Quantitative Spectroscopy and Radiative Transfer*, 103, Elsevier, S. 340-350, DOI 10.1016/j.jqsrt.2006.05.002, 2007

Doicu, A., F. Schreier, S. Hilgers, A. von Bargen, S. Slijkhuis, M. Hess, B. Aberle: An efficient inversion algorithm for atmospheric remote sensing with application to UV limb observations, *Journal of Quantitative Spectroscopy and Radiative Transfer*, 103, Elsevier, S. 193-208, DOI 10.1016/j.jqsrt.2006.05.007, 2007

Flamant, P., J. Cuesta, M.-L. Denneulin, A. Dabas, D. Huber: ADM-Aeolus retrieval algorithms for aerosol and cloud products, Tellus A (OnlineEarly Articles), doi:10.1111/j.1600-0870.2007.00287.x, 2007

Gottwald, M., H. Bovensmann: SCIAMACHY – Neue Ansichten der Erdatmosphäre, *Physik in unserer Zeit* (2), WILEY-VCH Verlag GmbH & Co. KGaA Weinheim, 64-71, DOI 10.1002/piuz.200601129, 2007

Gottwald, M., E. Krieg, C. von Savigny, S. Noël, P. Reichl, A. Richter, H. Bovensmann, J.P. Burrows: SCIAMACHY's View of the Polar Atmosphere. Cooper, Alan; Raymond, Carol [Hrsg.]: *Antarctica; A keystone in a changing world* - Online proceedings for the 10th international symposium on Antarctic Earth scienes, U.S. Geological Survey Open-File Report, DOI 10.3133/of2007-1047.srp011, 2007

Hrechanyy, S., M. von Hobe, J.-U. Grooß, P. Konopka, G. Günther, R. Müller, F. Stroh: The Budget of Halogen Compounds in the tropical UTLS, *Geophys. Res. Abstr.s*, 9, 08714, 2007

Jerg, M., T. Trautmann: One-dimensional solar radiative transfer: Perturbation approach and its application to independent-pixel calculations for realistic cloud fields, *Journal of Quantitative Spectroscopy and Radiative Transfer*, 105 (1), Elsevier, S. 32-54, DOI 10.1016/j.jqsrt.2006.09.014, ISSN 0022-4073, 2007

Loyola, D., W. Thomas, Y. Livschitz, T. Ruppert, P. Albert, R. Hollmann: Cloud Properties Derived From GOME/ERS-2 Backscatter Data for Trace Gas Retrieval, *IEEE Transactions on Geoscience and Remote Sensing*, 45 (9), p. 2747-2758, DOI 10.1109/TGRS.2007.901043, 2007

Manzini, F., G. Schwarz, C. Cosmovici, C. Guaita, L. Comolli, A. Brunati, R. Crippa: Comet Ikeya-Zhang (C/2002 C1): Determination of the Rotation Period From Observations of Morphological Structures.

Earth, Moon, and Planets, 100, Springer, p. 1-16, DOI 10.1007/s11038-005-9062-6, ISSN 0167-9295, 2007

Marmer, E., B. Langmann, K. Hungershöfer, T. Trautmann: Aerosol modeling over Europe: 2. Interannual variability of aerosol shortwave direct radiative forcing, *Journal of Geophysical Research - Atmosphere*, 112 (D23S16), S. 1 - 14, DOI: 10.1029/2006JD008040, 2007

Mendrok, J., F. Schreier, M. Höpfner: Estimating cirrus cloud properties from MIPAS data, *Geophysical Research Letters*, 34 (8), American Geophysical Union, S. L08807, DOI 10.1029/2006GL028246, 2007

Otto, S., M. de Reus, T. Trautmann, A. Thomas, M. Wendisch, S. Borrmann: Atmospheric radiative effects of an in situ measured Saharan dust plume and the role of large particles, *Atmos. Chem. Phys.*, 7, 4887-4903, 2007

Rother, T.: Scalar Green's function for penetrable or dielectric scatterers, *Optics Communications*, 274, Elsevier, S. 15 - 22, DOI 10.1016/j.optcom.2007.01.071, 2007

Tan, D.G.H, E. Andersson, J. de Kloe, G.-J. Marseille, A. Stoffelen, P. Poli, M.-L. Denneulin, A. Dabas, D. Huber, O. Reitebuch, P. Flamant, O. le Rille, H. Nett: The ADM-Aeolus wind retrieval algorithms, Tellus A (OnlineEarly Articles), doi:10.1111/j.1600-0870.2007.00285.x, 2007

4.3   Conference Proceeding Papers and Presentations

Antón M., C. Zancajos, D. Loyola, B. Navascúes: Validación de la columna de ozono ghost estimada por el instrumento satelital GOME mediante ozono-sondeos, 8. Encontro Luso-Espanhol de Meteorologia, Peniche, February 2007

Badaoui, M., F. Schreier, G. Wagner, M. Birk: Instrumental Line Shapes for Molecular Line Parameter Retrieval from High Resolution Fourier Transform Spectra for Terrestrial or Planetary Atmospheric Remote Sensing, The 2007 ESO Instrument Calibration Workshop, Garching, 2007

von Bargen, A., T. Schröder, A. Doicu, K. Kretschel, C. Lerot, M. Van Roozendael, A. Kokhanovsky, M. Vountas, H. Bovensmann, M. Hess, B. Aberle, F. Schreier: SCIAMACHY Level 1b-2 Data Processing: Update of Off-line Data Processor to Version 3.0, Third Workshop on the Atmospheric Chemistry Validation of ENVISAT (ACVE-3), ESA-SP-642, Frascati, 2007

Coldewey-Egbers, M., S. Slijkhuis, B. Aberle, D. Loyola: Monitoring of the GOME/ERS-2 In-flight Calibration Parameters from GDP-4 Reprocessing. ENVISAT Symposium 2007, ESA SP-636, Montreux, 2007

Doicu, A., S. Hilgers, A. von Bargen, A. Rozanov, K.-U. Eichmann, C. von Savigny, J.P. Burrows: Information Operator Approach and Iterative Regularization Methods for Atmospheric Remote Sensing, ENVISAT Symposium 2007, ESA SP-636, Montreux, 2007

Doicu, A., F. Schreier, S. Hilgers, A. von Bargen: DRACULA – Advanced Retrieval Tool for Atmospheric Remote Sensing, ENVISAT Symposium 2007, ESA SP-636, Montreux, 2007

Doicu, A.: A regulation tool for atmospheric remote sensing, Chemnitz Symposium on Inverse Problems 2007, Chemnitz 2007

Fagiolini, E., L. Zenner, F. Flechtner, T. Gruber, G. Schwarz, T. Trautmann, J. Wickert: The Sensitivity of Satellite Gravity Field Determination to Uncertainties in Atmospheric Models, Joint GSTM/SPP Kolloquium, Potsdam, 2007

Gottwald, M., E. Krieg, S. Noël, K. Bramstedt, H. Bovensmann: SCIAMACHY Operations in an Extended Mission up to 2010, ENVISAT Symposium 2007, ESA SP-636, Montreux, 2007

Gottwald, M., E. Krieg, S. Slijkhuis, C. von Savigny, S. Noël, H. Bovensmann, K. Bramstedt: Determination of SCIAMACHY LOS Misalignments, ENVISAT Symposium 2007, ESA SP-636, Montreux, 2007

Hort, M., P. Valks and T. Erbertseder: Exupery - A Volcano Fast Response System, ESA Workshop on Global Support to Aviation Control, Meteo France, Toulouse, 2007

Kiemle, S., M. Boettcher, D. Loyola, W. Zimmer, T. Ruppert: DLR Data Services for GOME-2/METOP Atmospheric Trace Gas Monitoring, Joint 2007 EUMETSAT Meteorological Satellite Conference and the

15th Satellite Meteorology & Oceanography Conference of the American Meteorological Society, EUMETSAT Publications, P 50, Amsterdam, ISBN 92-9110-079-X, ISSN 1011-3932, 2007

Loyola, D.: Retrieval of cloud information from GOME-2/MetOp: First Results, ACCENT-TROPOSAT-2 Workshop, Bremen, 2007

Loyola, D.: Operational monitoring of the ozone hole: Transition from GOME and SCIAMACHY to GOME-2, Symposium: 20th anniversary of the Montreal Protocol, Athens, 2007

Loyola D.: GOME-2/MetOp Cloud Properties using the OCRA and ROCINN Algorithms, ACCENT-TROPOSAT-2 Report 6, 71-75, 2007

Meyer-Arnek J., L. Bock, T. Erbertseder, P. Valks, G. Gesell, D. Loyola: Tropospheric NO2: Cloud top height Intercomparison and deriving Daily Synoptic Maps of Tropospheric NO2 with Geostatistical Methods, ACCENT-TROPOSAT-2 Report 6, 231-235, 2007

Noël, S., K. Bramstedt, H. Bovensmann, J.P. Burrows, M. Gottwald, E. Krieg: SCIAMACHY Degradation Monitoring Results, ENVISAT Symposium 2007, ESA SP-636, Montreux, 2007

Otto, S., T. Trautmann, M. Wendisch, E. Bierwirth, A. Ehrlich: Radiative transfer simulations within Saharan dust atmospheres compared to measurements from the SAMUM experiment, IUGG XXIV 2007 General Assembly, Earth: our changing planet, Perugia, 2007

Pflug B., D. Loyola, P. Valks, W. Zimmer: Near-real-time estimation of spectral surface albedo- algorithm development for GOME-1/ERS-2 and GOME-2/MetOP, ENVISAT Symposium 2007, ESA SP-636, Montreux, 2007

von Savigny, C., A. Rozanov, H. Bovensmann, S. Noël, M. Gottwald, S. Slijkhuis, J.P. Burrows: Studying Envisat Attitude with SCIAMACHY Limb-scatter Measurements, ENVISAT Symposium 2007, ESA SP-636, Montreux, 2007

Schmidt, K., T. Rother, J. Wauer: Light Scattering Properties of Higher Order Chebyshev Particles and Implications for Aerosols with a Weak Surface Roughness, ACCENT-TROPOSAT-2 Workshop, Bremen, 2007

Schreier, F., S. Gimeno-Garcia, M. Hess, A. Doicu, A. von Bargen, M. Buchwitz, I. Khlystova, H. Bovensmann, J.P. Burrows: Intercomparison of vertical column densities derived from SCIAMACHY Infrared Nadir Observations, ENVISAT Symposium 2007, ESA SP-636, Montreux, 2007

Schreier, F., J. Mendrok, S. Gimeno-Garcia, A. Doicu: Automatic Differentiation of an Infrared Radiative Transfer Code for Atmospheric Remote Sensing, Sixth European Workshop on Automatic Differentiation, INRIA Sophia-Antipolis, 2007

Slijkhuis, S., R. Snel, B. Aberle, G. Lichtenberg, M. Meringer, A. von Bargen: Results of a new straylight correction for SCIAMACHY, ENVISAT Symposium 2007, ESA SP-636, Montreux, 2007

Theys, N., M. Van Roozendael, Q. Errera, S. Chabrillat, F. Daerden, F. Hendrick, D. Loyola, P. Valks: A Stratospheric BrO Climatology Based on the BASCOE 3D Chemical Transport Model, ENVISAT Symposium 2007, ESA SP-636, Montreux, 2007

Van Geffen, J., M. Van Roozendael, W. Di Nicolantonio, L. Tampellini, P. Valks, T. Erbertseder, R. Van der A: Monitoring of Volcanic Activity from Satellite as Part of GSE PROMOTE, ENVISAT Symposium 2007, ESA SP-636, Montruex, 2007

Valks, P., N. Hao, D. Loyola, W. Zimmer; First results on tropospheric NO2 from the GOME-2 instrument on MetOp, AT2 Workshop on *Tropospheric NO$_2$ measured by satellites*, KNMI, De Bilt, 2007

Valks, P., N. Hao, D. Loyola, M. Van Roozendael, W. Zimmer: First results on ozone, NO$_2$ and SO$_2$ from the GOME-2 instrument on MetOp, ACCENT-TROPOSAT 2 Workshop 2007, Bremen, 2007

Valks P., N. Hao, D. Loyola: Retrieval of Tropospheric NO2 Columns from the GOME-2 Instrument on MetOp, ACCENT-TROPOSAT-2 Report 6, 95-97, 2007

Zenner, L., E. Fagiolini, F. Flechtner, T. Gruber, G. Schwarz, T. Trautmann, J. Wickert: The Impact of Uncertainties of global Atmosphere Models on the Gravity Field Determination with GRACE, Joint GSTM / SPP Kolloquium, Potsdam, 2007

4.4   Technical Reports

Balis, D., M. Koukouli, D. Loyola, P. Valks, N. Hao: Validation of GOME-2 total ozone products (OTO/O3, NTO/O3) processed with GDP 4.2, AF/O3M/AUTH/GOME-2VAL/RP/01

Gottwald, M., E. Krieg, C. von Savigny, S. Noël, K. Bramstedt: SCIAMACHY Extra Misalignment Model, PO-TN-DLR-SH-0016, Issue 1, Rev. 0, 7 March 2007

Gottwald, M., E. Krieg, J. How, K. Reissig: SCIAMACHY Consolidated Level 0: Statistics for the Year 2007, PO-TN-DLR-SH-0015, Issue 1, Rev. 0, 21 May 2007

Gottwald, M., E. Krieg: The Impact of ENVISAT MLST Variations on SCIAMACHY Operations, PO-TN-DLR-SH-0017, Issue 1, Rev. 0, 19 July 2007

Gottwald, M., E. Krieg: Expected SCIAMACHY Instrument Performance in the Years 2010 and 2014, PO-TN-DLR-SH-0018, Issue 1, Rev. 0, 7 December 2007

Gottwald, M., E. Krieg, J. How, K. Reissig: SCIAMACHY Consolidated Level 0: Statistics for the Year 2002, PO-TN-DLR-SH-0019, Issue 1, Rev. 0, 21 December 2007

Loyola, D., P. Valks: Algorithm Theoretical Basis Document for GOME-2 Total Columns of Ozone, Minor Trace Gases, and Cloud Properties (GDP 4.2 for O3M-SAF OTO and NTO), DLR/GOME-2/ATBD/01, Iss./Rev.: 1/B, 10 October 2007

Loyola, D., P. Valks: Product User Manual for GOME Total Columns of Ozone, Minor Trace Gases, and Cloud Properties, DLR/GOME/PUM/01, Iss./Rev.: 1/D , 6 March 2007

4.5   Attended Conferences and Professional Leaves

The 2007 ESO Instrument Calibration Workshop, Garching, Germany, January 23-26, 2007

HALO Begutachtungskolloquium, SPP 1294/1, Bonn, Germany, March 18-20, 2007

SPP1257 Mass Transport and Mass Distribution in the Earth System Workshop, Gummersbach, Germany, March 21-23, 2007

ENVISAT Symposium 2007, Montreux, Schweiz, April 23-27, 2007

ACCENT-TROPOSAT-2 Workshop 2007, Bremen, Germany, June 21/22, 2007

IUGG XXIV 2007 General Assembly, Earth: our changing planet, Perugia, Italy, July 2-13, 2007

Joint 2007 EUMETSAT Meteorological Satellite Conference and the 15th Satellite Meteorology & Oceanography Conference of the American Meteorological Society, Amsterdam, The Netherlands, July 24-28, 2007

10th International Symposium on Antarctic Earth Sciences (ISAES X), Santa Barbara, California, USA, August 26-31, 2007

ACCENT-TROPOSAT-2 Workshop on *Tropospheric NO2 measured by satellites*, KNMI, Netherlands, September 10-12, 2007

Symposium: 20th Anniversary of the Montreal Protocol, Athens, Greece, September 23-26, 2007

2007 Joint EUMETSAT / AMS Conference, Amsterdam, Netherlands, September 24-28, 2007

Chemnitz Symposium on Inverse Problems, Chemnitz, Germany, September 27/28, 2007

Joint GSTM/SPP Kolloquium, Potsdam, Germany, October 15-17, 2007

Sixth European Workshop on Automatic Differentiation, INRIA, Sophia-Antipolis, France, November 15/16, 2007

ESA Workshop on Global Support to Aviation Control, MeteoFrance, Toulouse, France, November 26, 2007

4.6 Diploma and Doctoral Theses

Fagiolini, E.: The impact of atmospheric variability on the determination of the gravity field of the Earth. Dissertation, Technische Universität München. Faculty of Civil Engineering and Geodesy, Technical University of Munich. (Supervisors: Prof. Dr. Reiner Rummel, Technical University of Munich and Gottfried Schwarz)

Gimeno-García, S.: Simulation of solar radiative transfer and comparison with spectro-radiometric measurements. Dissertation, Faculty of Physics and Earth Science, University of Leipzig. (Supervisor: Prof. Dr. Thomas Trautmann)

Hiebsch, A.: Light scattering on nonspherical particles, especially Chebyshev particles. Thesis, Faculty of Physics and Earth Science, University of Leipzig. (Supervisors: Prof. Dr. Thomas Trautmann and Dr. Tom Rother)

Kniffka, A.: Influence of the inhomogeneity of clouds, aerosols and surface albedo on the three-dimensional actinic radiation field in the atmosphere. Dissertation, Faculty of Physics and Earth Science, University of Leipzig. (Supervisor: Prof. Dr. Thomas Trautmann)

Köhler, C.H.: Observation and simulation of the longwave radiative effects for Saharan mineral dust plumes. Dissertation, Faculty of Physics, Mathematics and Computer Science, Johannes Gutenberg University of Mainz. (Supervisors: Prof. Dr. Manfred Wendisch, Johannes Gutenberg University of Mainz and Prof. Dr. Thomas Trautmann)

Otto, S.: Optical properties of mineral dust and its climatic impact on radiative transfer in the Earth's atmosphere. Dissertation, Faculty of Physics, Ludwig Maximilian University of Munich. (Supervisors: Prof. Dr. Olaf Krüger, Ludwig Maximilian University of Munich and Prof. Dr. Thomas Trautmann)

Rix, M.: Observation of volcanic SO_2 plumes based on the satellite-borne GOME-2 instrument. Dissertation, Faculty of Civil Engineering and Geodesy, Technical University of Munich. (Supervisors: Prof. Dr. Richard Bamler, Technical University of Munich and Dr. Pieter Valks)

4.7 AP Seminar Talks

Aberle, B.: Wiki, die Bibliothek von allen für alle, October 31, 2007

Gottwald, M.: Die EnMAP-Mission, November 14, 2007

Hao, N.: Ground-based DOAS Measurements at Shanghai, July 11, 2007

Hedelt, P. (DLR-PF): Spektroskopische Signaturen in den Atmosphären von Venus und Exoplaneten, October 11, 2007

Hrechanyy, S.: In-Situ BrO-Messungen in der Oberen Troposphäre / Unteren Stratosphäre, July 25, 2007

Hungershöfer, K. (LISA, Paris): Optische Eigenschaften von Biomassenaerosol und Mineralstaub: Ergebnisse aus den Kampagnen EFEU und AMMA, September 26, 2007

Mendrok, J. (National Institute of Information and Communications Technology, Tokyo): Sub-mm/THz Passive Remote Sensing of (Ice) Clouds, June 14, 2007

Meringer, M.: An Introduction to Chemoinformatics. Are there Links to Aerospace Research?, November 28, 2007

Pflug, B. (IMF-GW): GOME-2 Arbeiten, October 19, 2007

Rother, T.: Die Rayleigh-Hypothese. Ein ungelöstes Problem der Lichtstreuung im neuen Gewand, December 13, 2007

Abbreviations and Acronyms

AAI	Absorbing Aerosol Index
ACVE	Atmospheric Chemistry Validation of ENVISAT
ADF	Auxiliary Data File
ADM	Atmospheric Dynamics Mission
ALADIN	Atmospheric Laser Doppler Instrument
AMF	Air Mass Factor
ANX	Ascending Node Crossing
AP	Atmospheric Processors
AR	Acquisition Request
ASM	Azimuth Scan Mechanism
ATBD	Algorithm Technical Baseline Document
ATC	Active Thermal Control
ATLID	Atmospheric Lidar
AUTH	Aristotle University of Thessaloniki
BIRA-IASB	Belgisch Instituut voor Ruimte-Aëronomie / Institut d'Aeronomie Spatiale de Belgique
BIRRA	Better InfraRed Retrieval Algorithm
BMBF	Bundesministerium für Bildung und Forschung
BOL	Begin of Life
BUFR	Binary Universal Form for the Representation of Meteorological data
CALIOP	Cloud-Aerosol Lidar with Orthogonal Polarization
CCD	Charged Coupled Device
CDI	Combined Differential-Integral
CFI	Customer Furnished Item
CGS	Carlo Gavazzi Space
CHAMP	Challenging Minisatellite Payload
CLUMP	Command Line User Interface for MODTRAN using Python
COT	Cloud Optical Thickness
CTH	Cloud Top Height
DBPM	Dead and Bad Pixel Mask
DFD	Deutsches Fernerkundungsdatenzentrum
DIMS	Data & Information Management System
DLR	Deutsches Zentrum für Luft- und Raumfahrt
DOAS	Differentielle Optische Absorptions-Spektroskopie
D-PAC	German Processing and Archiving Centre
DPQC	Data Processing and Quality Control
ECMWF	European Centre for Medium-Range Weather Forecasts
EESC	European Economic and Social Committee
EMM	Extra Misalignment Model
EnMAP	Environmental Mapping Programme
ENVISAT	Environmental Satellite
EO	Earth Observation
EOL	End of Life
EOWEB	Earth Observation on the Web
EPS	EUMETSAT Polar System
ERS	European Remote Sensing Satellite
ESA	European Space Agency
ESM	Elevation Scan Mechanism
ESOC	European Space Operation Centre
ESRIN	European Space Research Institute
ESTEC	European Space Technology Centre
EU	European Union
EUMETSAT	European Organisation for the Exploitation of Meteorological Satellites

EUMETCast	EUMETSAT broadcast system for environmental data
FASCODE	Fast Atmospheric Signature Code
FAT	Factory Acceptance Test
FTIR	Fourier Transform Infrared Spectrometer
GADS	Global Annotation Data Set
GDP	GOME Data Processor
GEISA	Gestion et Etude des Informations Spectroscopiques Atmosphériques
GFZ	GeoForschungszentrum
GG	Gaussian Grid
GMES	Global Monitoring for Environment and Security
GOCE	Gravity Field and Steady-state Ocean Circulation Explorer
GOME	Global Ozone Monitoring Experiment
GRACE	Gravity Recovery and Climate Experiment
GS	Ground Segment
GUI	Graphical User Interface
HITRAN	High Resolution Transmission Molecular Absorption
HSI	Hyperspectral Imager
HTE	High Temperature Events
IDEAL-GRACE	Improved De-Aliasing for Gravity Field Modelling with GRACE
IECF	Instrument Engineering & Calibration Facility
IMF	Institut für Methodik der Fernerkundung
IO3C	International Ozone Commission
IP	Instrument Planning
IUP/IFE	Institut für Umweltphysik / Institut für Fernerkundung
IR	Infrared
KNMI	Koninklijk Nederlands Meteorologisch Instituut
LIDORT	Linearized Discrete Ordinate Radiative Transfer
LLI	Life Limited Item
LRAC	Low Rate Reference Archive Centre
MetOp	Meteorological Operational Polar Satellites of EUMETSAT
MIRART	Modular Infrared Atmospheric Radiative Transfer
MLST	Mean Local Solar Time
MO&C	Moon Occultation & Calibration
MODIS	Moderate Resolution Imaging Spectrometer
MODTRAN	Moderate Transmittance Code
MPH	Main product Header
NCWM	Nadir Calibration Window Mechanism
NESR	Noise Equivalent Spectral Radiance
NRT	Near Realtime
O3M	Ozone Monitoring
OBM	Optical Bench Module
OPAC	Optical Properties of Aerosols and Clouds
OCM	Orbit Control Manoeuvre
OCR	Operation Change Request
OCRA	Optical Cloud Retrieval Algorithm
OR	Observation Request
PCV	Processor, Calibration and Validation
PDU	Product Dissemination Unit
PFUI	Python Fascode User Interface
PGS	Payload Ground Segment
PROMOTE	Protocol Monitoring for the GMES Service Element
PyReS	Prototype Retrieval System
ROCINN	Retrieval of Cloud Information using Neural Networks
RT	Radiative Transfer
RTE	Radiative Transfer Equation
SAA	South Atlantic Anomaly

SAF	Satellite Application Facility
SAMUM	Sahara Mineral Dust Experiment
SCIAMACHY	Scanning Imaging Absorption Spectrometer for Atmospheric Chartography
SCD	Slant Column Density
SCR	Software Change Request
SF	Sun Follower
SEU	Single Event Upset
SM	Service Module
SMR	Sub-Millimeter Radiometer
SO&C	Sun Occultation & Calibration
SODAP	Switch-on and Data Acquisition Phase
SOST	SCIAMACHY Operations Support Team
SPH	Specific Product Header
SPR	Software Problem Report
SQWG	SCIAMACHY Quality Working Group
SRON	Netherlands Institute for Space Research
SSAG	SCIAMACHY Science Advisory Group
TC	Thermal Control
TCFoV	Total Clear Field of View
TN	Technical Note
UMARF	Unified Meteorological Archive and Retrieval Facility
UNEP	United Nations Environment Programme
UPAS	Universal Processor for Atmospheric Spectrometers
UV	Ultraviolet
VL	Virtual Laboratory
V-NP	Venus North Pole
VTT	Vacuum Tower Telescope
WFM-DOAS	Weighting Function Modified DOAS
WDC-RSAT	World Data Center for Remote Sensing of the Atmosphere
WMO	World Meteorological Organization

DLR at a Glance

DLR is Germany's national research center for aeronautics and space. Its extensive research and development work is integrated into national and international cooperative ventures. As Germany's space agency, DLR has been given responsibility for the forward planning and the implementation of the German space program by the German federal government as well as for the international representation of German interests. Furthermore, Germany's largest project-management agency is also part of DLR.

Approximately 5,100 people are employed in DLR's 27 institutes and facilities at eight locations in Germany: Köln-Porz (headquarters), Berlin-Adlershof, Bonn-Oberkassel, Braunschweig, Göttingen, Lampoldshausen, Oberpfaffenhofen, and Stuttgart. DLR also operates offices in Brussels, Paris, and Washington, D.C.

Remote Sensing Technology Institute
Institut für Methodik der Fernerkundung

DLR's Remote Sensing Technology Institute (IMF) is located in Oberpfaffenhofen, Berlin-Adlershof, and Neustrelitz.

IMF carries out research and development for retrieving geo-information from remote sensing data. It conducts basic research on physical principles of remote sensing and develops algorithms, techniques, and operational processing systems for synthetic aperture radar, optical remote sensing, and spectrometric sounding of the atmosphere. The processing systems are in operational use for national, European, and international Earth observation missions.

For preparation and in support of spaceborne missions IMF operates a suite of multi- and hyperspectral optical airborne sensors. The institute contributes its expertise to novel sensor and mission concepts.

The German Remote Sensing Data Center (DFD) and IMF form DLR's Applied Remote Sensing Cluster (C-AF).

Deutsches Zentrum
für Luft- und Raumfahrt e.V.
in der Helmholtz-Gemeinschaft

Institut für Methodik der Fernerkundung
Oberpfaffenhofen
82234 Weßling

www.dlr.de/caf